Final Report

FDOT Contract No.: BD-545, RPWO # 76
UF Project No. 00066303

Modification of LRFD Resistance Factors Based on Site Variability

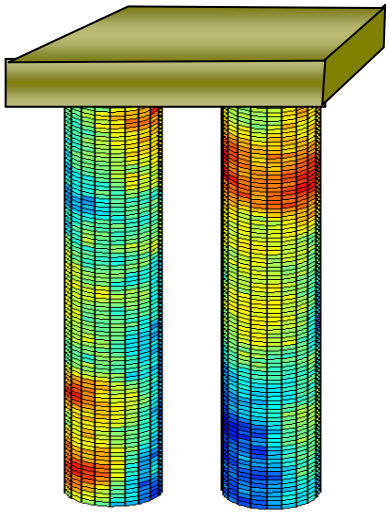

Principal Investigator: Michael McVay, PhD
Primary Researcher: Harald Klammler, PhD
Co-Principal Investigator: David Bloomquist, PhD, PE
Graduate Students: Johanna Otero and Michael Farone

Department of Civil and Coastal Engineering
University of Florida
Gainesville, Florida 32611-6580

Developed for the

David Horhota, Ph.D., P.E., and Peter Lai, P.E., Project Managers

November 2009

DISCLAIMER

"The opinions, findings, and conclusions expressed in this publication are those of the authors and not necessarily those of the State of Florida Department of Transportation or the U.S. Department of Transportation.

Prepared in cooperation with the State of Florida Department of Transportation and the U.S. Department of Transportation."

SI (MODERN METRIC) CONVERSION FACTORS (from FHWA)

APPROXIMATE CONVERSIONS TO SI UNITS

SYMBOL	WHEN YOU KNOW	MULTIPLY BY	TO FIND	SYMBOL
LENGTH				
in	inches	25.4	millimeters	mm
ft	feet	0.305	meters	m
yd	yards	0.914	meters	m
mi	miles	1.61	kilometers	km

SYMBOL	WHEN YOU KNOW	MULTIPLY BY	TO FIND	SYMBOL
AREA				
in^2	square inches	645.2	square millimeters	mm^2
ft^2	square feet	0.093	square meters	m^2
yd^2	square yard	0.836	square meters	m^2
ac	acres	0.405	hectares	ha
mi^2	square miles	2.59	square kilometers	km^2

SYMBOL	WHEN YOU KNOW	MULTIPLY BY	TO FIND	SYMBOL
VOLUME				
fl oz	fluid ounces	29.57	milliliters	mL
gal	gallons	3.785	liters	L
ft^3	cubic feet	0.028	cubic meters	m^3
yd^3	cubic yards	0.765	cubic meters	m^3
NOTE: volumes greater than 1000 L shall be shown in m^3				

SYMBOL	WHEN YOU KNOW	MULTIPLY BY	TO FIND	SYMBOL
MASS				
oz	ounces	28.35	grams	g
lb	pounds	0.454	kilograms	kg
T	short tons (2000 lb)	0.907	megagrams (or "metric ton")	Mg (or "t")

SYMBOL	WHEN YOU KNOW	MULTIPLY BY	TO FIND	SYMBOL
TEMPERATURE (exact degrees)				
^oF	Fahrenheit	5 (F-32)/9 or (F-32)/1.8	Celsius	^oC

SYMBOL	WHEN YOU KNOW	MULTIPLY BY	TO FIND	SYMBOL
ILLUMINATION				
fc	foot-candles	10.76	lux	lx
fl	foot-Lamberts	3.426	candela/m^2	cd/m^2

SYMBOL	WHEN YOU KNOW	MULTIPLY BY	TO FIND	SYMBOL
FORCE and PRESSURE or STRESS				
lbf	pound force	4.45	newtons	N
lbf/in^2	pound force per square inch	6.89	kilopascals	kPa

APPROXIMATE CONVERSIONS TO SI UNITS

SYMBOL	WHEN YOU KNOW	MULTIPLY BY	TO FIND	SYMBOL
		LENGTH		
mm	millimeters	0.039	inches	in
m	meters	3.28	feet	ft
m	meters	1.09	yards	yd
km	kilometers	0.621	miles	mi

SYMBOL	WHEN YOU KNOW	MULTIPLY BY	TO FIND	SYMBOL
		AREA		
mm^2	square millimeters	0.0016	square inches	in^2
m^2	square meters	10.764	square feet	ft^2
m^2	square meters	1.195	square yards	yd^2
ha	hectares	2.47	acres	ac
km^2	square kilometers	0.386	square miles	mi^2

SYMBOL	WHEN YOU KNOW	MULTIPLY BY	TO FIND	SYMBOL
		VOLUME		
mL	milliliters	0.034	fluid ounces	fl oz
L	liters	0.264	gallons	gal
m^3	cubic meters	35.314	cubic feet	ft^3
m^3	cubic meters	1.307	cubic yards	yd^3

SYMBOL	WHEN YOU KNOW	MULTIPLY BY	TO FIND	SYMBOL
		MASS		
g	grams	0.035	ounces	oz
kg	kilograms	2.202	pounds	lb
Mg (or "t")	megagrams (or "metric ton")	1.103	short tons (2000 lb)	T

SYMBOL	WHEN YOU KNOW	MULTIPLY BY	TO FIND	SYMBOL
		TEMPERATURE (exact degrees)		
^oC	Celsius	1.8C+32	Fahrenheit	^oF

SYMBOL	WHEN YOU KNOW	MULTIPLY BY	TO FIND	SYMBOL
		ILLUMINATION		
lx	lux	0.0929	foot-candles	fc
cd/m^2	candela/m^2	0.2919	foot-Lamberts	fl

SYMBOL	WHEN YOU KNOW	MULTIPLY BY	TO FIND	SYMBOL
		FORCE and PRESSURE or STRESS		
N	newtons	0.225	pound force	lbf
kPa	kilopascals	0.145	pound force per square inch	lbf/in^2

*SI is the symbol for International System of Units. Appropriate rounding should be made to comply with Section 4 of ASTM E380.
(Revised March 2003)

TECHNICAL REPORT DOCUMENTATION PAGE

1. Report No.	2. Government Accession No.	3. Recipient's Catalog No.

4. Title and Subtitle	5. Report Date
Modification of LRFD Resistance Factors Based on Site Variability	November 2009
	6. Performing Organization Code

7. Author(s)	8. Performing Organization Report No.
Michael McVay, Harald Klammler, David Bloomquist, Johanna Otero and Michael Farone	

9. Performing Organization Name and Address	10. Work Unit No. (TRAIS)
Department of Civil and Coastal Engineering 365 Weil Hall – P.O. Box 116580 University of Florida Gainesville, FL 32611-6580	11. Contract or Grant No. BD-545 #76

12. Sponsoring Agency Name and Address	13. Type of Report and Period Covered
Florida Department of Transportation 605 Suwannee Street, MS 30 Tallahassee, FL 32399	Draft Final Report 03/04/07 – 12/01/09
	14. Sponsoring Agency Code

15. Supplementary Notes

16. Abstract

Current practice by the Florida Department of Transportation (FDOT), Federal Highway Administration (FHWA), and American Association of State Highway Transportation Officials (AASHTO) for deep foundation design is to use a constant load and resistance factored design (LRFD) Φ depending on redundancy, but independent of pile/shaft dimension. Unfortunately, soil/rock properties vary from point-to-point (CV_q: coefficient of variation) and are typically spatially correlated. Since both the skin friction and end bearing involve spatial averaging of soil/rock properties over the shaft surface, the resulting total shaft resistance variability (CV_R) will not share the same point variability (CV_q). Moreover, the total shaft variability (CV_R) will also vary with different degrees of spatial correlation, typically represented with a covariance function and a correlation length a.

This work employs well established geostatistical principles to establish both the covariance function (e.g., variogram) and expected total pile/shaft variability (CV_R) using borehole data. Consideration is given to the number of borings, the location of borings relative to each other, and to the design foundation (e.g., if the borings are within the footprint of the design pile/shaft). Since the resulting pile/shaft variability CV_R is a function of pile/shaft dimensions, soil/rock variability CV_q, and its spatial correlation, the resulting LRFD Φ is not constant for any site. To help the designer, four quadrant iterative design charts are developed for single and group pile/shaft layouts, which consider side and tip resistances, as well as layered systems. To better define the total pile/shaft variability CV_R, the practice of load testing is also incorporated into the proposed approach. The work includes multiple design examples and data from existing FDOT bridge sites (e.g., 17th Street, Fuller Warren, and Jewfish Creek bridges).

17. Key Words	18. Distribution Statement
Deep Foundations, LRFD Φ, Spatial Variability, Load Testing, and Design Examples	No restrictions.

19. Security Classif. (of this report)	20. Security Classif. (of this page)	21. No. of Pages	22. Price
Unclassified	Unclassified	146	

Form DOT F 1700.7 (8-72) Reproduction of completed page authorized

ACKNOWLEDGMENTS

The researchers would first like to thank the Florida Department of Transportation (FDOT) for the financial support to carry out this research as well as the guidance of the project managers for its successful outcome. In addition, this research could not have been completed without the aid of the State Materials Office (SMO) and Central Office Geotechnical/Structures Groups. Specifically, SMO was instrumental in conducting additional laboratory/field testing at a number of bridge sites (17th Street and Fuller Warren), and the Central Office collected data (spread-sheets, load test reports, and borings) for the Jewfish Creek site discussed in this report. Also, the districts were of great help in locating and ensuring that the field testing occurred near the identified load test shaft plans.

EXECUTIVE SUMMARY

During the past five to ten years, the Florida Department of Transportation (FDOT) and the Federal Highway Administration (FHWA) have moved away from allowable stress design (ASD) to probability based load and resistance factored design (LRFD) for deep foundations. Using their extensive databases of load test data in combination with insitu boring/laboratory data, the FDOT has selected LRFD Φ from a low of 0.45 (inclusion of end bearing) to a high of 0.75 when done in conjunction with a field load test. In general, the LRFD resistance factors for drilled shafts were developed for reliability values of 2.5 to 3.0 using expected pile/shaft coefficient of variation (CV_R) ranging from 0.25 to 0.30. For typical design (e.g., no end bearing), a designer would use Φ of 0.5 (non-redundant) or 0.6 (redundant) with one rock strength for all shafts on a given site.

Unfortunately, typical rock strengths (unconfined and split tension) vary from site to site in Florida resulting in a range of coefficient of variation of rock strengths CV_q. In addition, since the axial shaft resistance is the sum, or average, of rock strength over its surface, its coefficient of variation of shaft resistance, i.e., CV_R, will be a function of the shaft's dimension (i.e., length/ diameter (L/D)), and the rock's strength variability CV_q. For instance, shorter shafts will result in less averaging and should result in larger shaft variability CV_R, which should lead to smaller LRFD Φ. In addition, Florida soil/rock data are correlated spatially. When correlated rock/soil properties are averaged, e.g., shaft resistance, the resulting variability CV_R is a function of the correlation length. Finally, the number and locations of borings relative to the design shaft (e.g., in or out of footprint) contributes to shaft resistance uncertainty CV_R.

Using sound geostatistical theory, this work develops analytical methods for assessing CV_R and the ensuing LRFD Φ for shaft design based on boring data. The work considers

multiple types of boring scenarios: inside or outside footprint; as well as number of borings; and location of borings relative to each other and with respect to the design shaft. The report cumulates in the development of four quadrant charts, which the designer may employ for side resistance alone or side and tip resistance together, as well as layered systems. The charts are entered with the known design load, the shaft diameter, the site or zone's soil/rock variability CV_q, and reliability of interest, from which the shaft length is assessed for single or multiple shafts (i.e., group) design.

To improve predictions, the work also focuses on incorporating load testing in the design (i.e., LRFD Φ assessment) process. In current design, the bias (λ_R) is a proportionality constant between the measured shaft resistance (e.g., skin and tip) and the borehole's estimate of resistance, is predefined (e.g., American Association of State Highway Transportation Officials' (AASHTO's) $\lambda R = 1.06$). To incorporate both site specific borehole and load testing into the design process, the relationships between expected production shaft variance σ^2_L and borehole predicted resistance variance σ^{*2}_B is established, which includes a variance of a random residual σ^2_ε, accounting for uncertainty in the shaft construction. Note, the earlier work on borehole variability, i.e., σ^{*2}_B applies. Also, the design unit side friction is represented as $-f_{des} = \Phi_u m^*_L$, where Φ_u is defined as Φ from AASHTO's First Order Second Moment (FOSM) equation with $\lambda_R = 1$, CV_R includes the combined borehole and load test variability (σ^{*2}_B and σ^2_ε), and m^*_L is the mean predicted load shaft resistance from the borehole data. Finally, the report gives multiple examples of design using data from existing FDOT sites incorporating just borehole, or combined borehole and load test data, for the proposed approach.

TABLE OF CONTENTS

APPENDIX

LIST OF TABLES

LIST OF FIGURES

CHAPTER 1
INTRODUCTION

1.1 Background

The support of structures (i.e., bridges, elevated roadways, buildings, etc.) in Florida has gone from small diameter piles (e.g., 14″) and drilled shafts (e.g., 48″) in the 1980s to very large diameter piles (e.g., 66″ cylinders) and drilled shafts (e.g., 108″) in the twenty-first century. The larger piles/shafts have greatly diminished the footprint of pier caps, reducing cost and right-of-way issues. Unfortunately, the newer foundations have become both non-redundant as well as highly susceptible to soil/rock variability. In the case of the latter, the use of fewer larger shafts/piles results in higher pile/shaft volume-to-surface-area ratios which will result in higher variance of axial pile/shaft resistances and even the possibility of collapse (e.g., Lee Roy Selmon Crosstown Expressway bridge, Tampa) due to the higher variance of soil/rock strength over the finite pile/shaft zones. Compounding this problem is the fact that the insitu/laboratory testing is generally carried out at a fixed spacing (e.g., 100 ft to 500 ft), which may be hundreds of feet away from the final constructed foundations. Recently in 2003 however, the Florida Department of Transportation (FDOT) has mandated the use of borings and laboratory testing of samples recovered in the footprint of non-redundant foundations as well as load test drilled shafts.

During the past five to ten years, the FDOT as well as other state departments of transportation (DOTs) and the Federal Highway Administration (FHWA), have gradually moved away from allowable stress design (ASD) to load and resistance factored design (LRFD) for deep foundations. Since LRFD models both the loads and the resistances acting on a shaft/pile as random variables, the resistance factors (Φ) are assessed based on the probability of failure (i.e., load is greater than resistance). Using their extensive database of load tests with adjacent

borings/laboratory tests in Florida, the FDOT established LRFD resistance factors based on assumed reliability index. For example, shown in Figure 1-1 are recommended LRFD resistance factors (Φ) for drilled shafts founded in Florida limestone for reliability index of 2.5 to 3.0 and an expected pile/shaft coefficient of variability ($CV_{R[H1]}$) of 0.25 to 0.30. In addition, all limestone is generally treated uniformly and constantly over a site, i.e., it is not broken into zones.

3.6.3 Resistance Factors [10.5.5] ***(01/06)***»

Delete ***LRFD*** Table 10.5.5-3 and substitute ***SDG*** Table 3.5 for drilled shafts.

Table 3.5 Resistance Factors for Drilled Shafts (Bridge Foundations)

Loading	Design Method	Construction QC Method	Resistance Factor, Φ	
			Redundant	Non-redundant[6]
Compression	For soil: FHWA alpha or beta method[1]	Std Specifications	0.60	0.50
	For rock socket: McVay's method[2] neglecting end bearing	Standard Specifications	0.60	0.50
	For rock socket: McVay's method[2] including 1/3 end bearing	Standard Specifications	0.55	0.45
	For rock socket: McVay's method[2]	Statnamic Load Testing	0.70	0.60
	For rock socket: McVay's method[2]	Static Load Testing	0.75	0.65
Uplift	For soil: FHWA alpha or beta method[1]	Std Specifications	Varies[1]	Varies[1]
	For rock socket: McVay's method[2]	Std Specifications	0.50	0.40
Lateral[3]	FBPier[4]	Std Specifications Or Lateral Load Test[5]	1.00	0.90

1. Refer to FHWA-IF-99-025, soils with N<15 correction suggested by O'Neill.
2. Refer to ***FDOT*** ***Soils and Foundation Handbook***.
3. Extreme event.
4. Or comparable lateral analysis program.
5. When uncertain conditions are encountered.
6. As defined in SDG 3.6.9.

Commentary: LRFD resistance factors are based on the probability of failure (Pf) of an element or group of elements resisting structural loads. When resistance factors were calibrated, the state of practice utilized redundant drilled shaft

Figure 1-1. *FDOT Structural Design Manual* table of resistance factors for drilled shaft socket in limestone.

Unfortunately, the strength characteristics of Florida's soil/rock are highly variable. For instance, in Figures 1-2 and 1-3 are the unconfined compressive strengths recorded at the

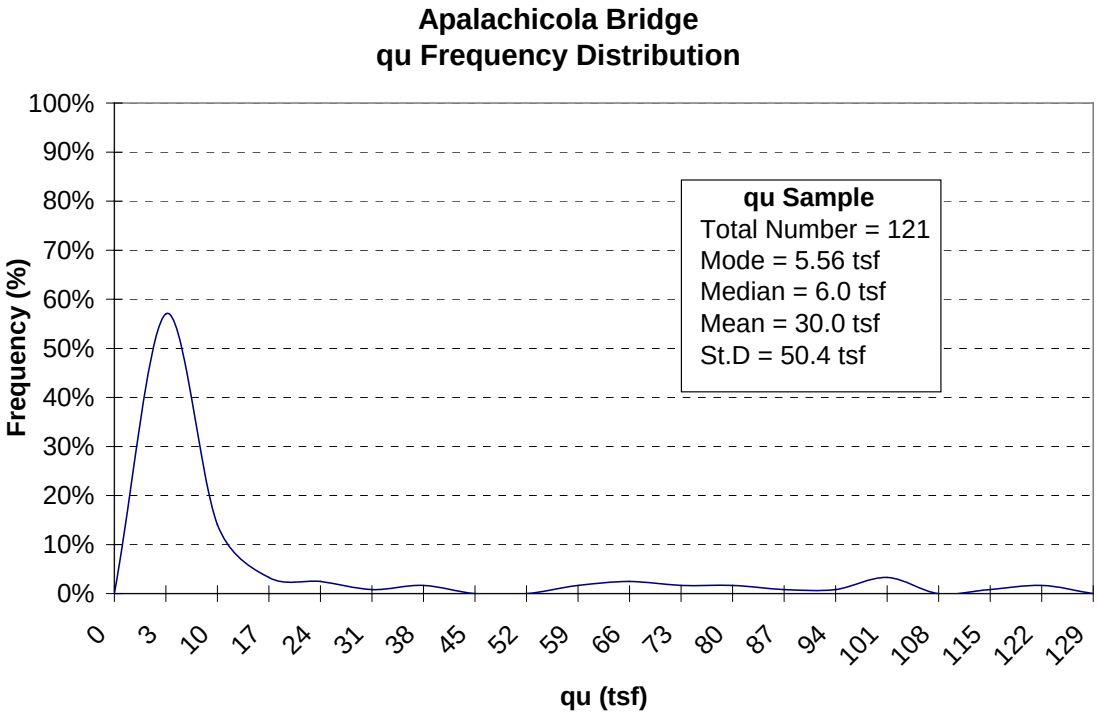

Figure 1-2. Apalachicola Bridge site – q_u frequency distribution.

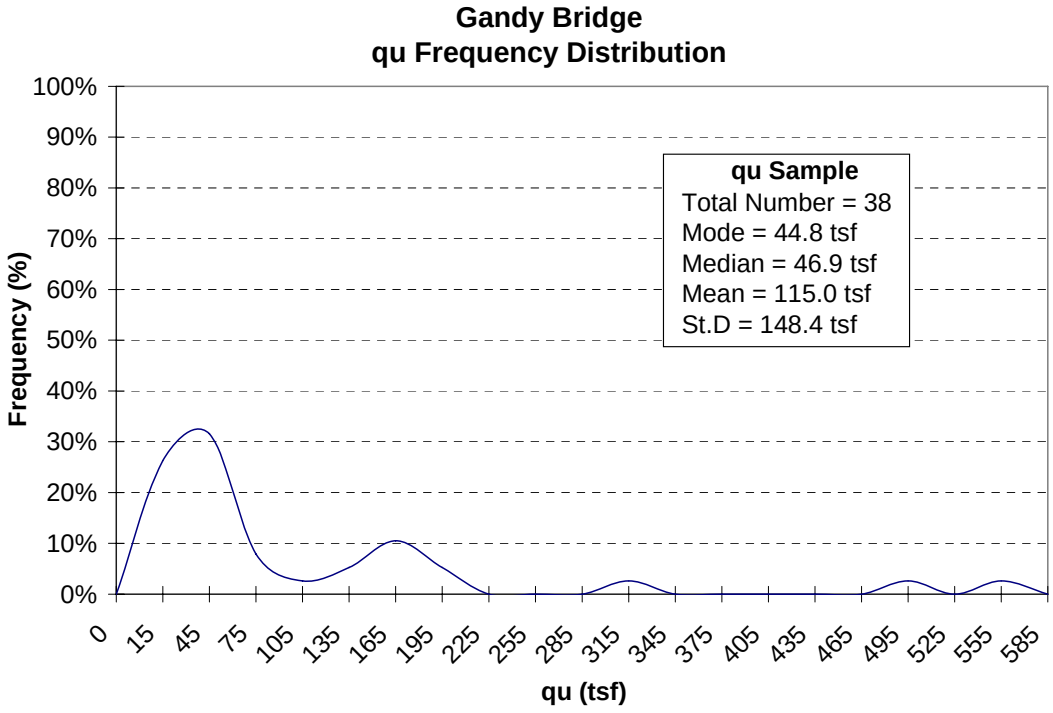

Figure 1-3. Gandy Bridge site – q_u frequency distribution.

Apalachicola and Gandy bridges, respectively. The coefficients of variation CV_q (standard deviation/mean) vary from 1.2 to 1.7 for these sites, which should result in a different coefficient of variation of shaft resistance (CV_R) and different LRFD Φ values (versus Figure 1-1) for each site. In addition, the frequency distribution for the Gandy Bridge (Figure 1-3) has a bimodal distribution suggesting the existence of zones of different strength over the site.

Also, not addressed in the current practice, is the possibility of correlation of soil/rock strength data from point-to-point within the ground. Shown in Figure 1-4 is the simulated rock strength for two drilled shafts located at the 17th Street Bridge in South Florida. The red represents high strength values and blue is the lowest strength, in between are medium strengths which are yellow and green. Evident from the figure, the rock strengths are correlated (i.e., transition from red to blue) over each shaft. The latter is significant, since it will result in higher variation in pile/shaft resistances than if the strength was uncorrelated (i.e., red values next to blue, etc.). Of interest is that there is a way of introducing soil/rock spatial correlation into LRFD Φ values for a site.

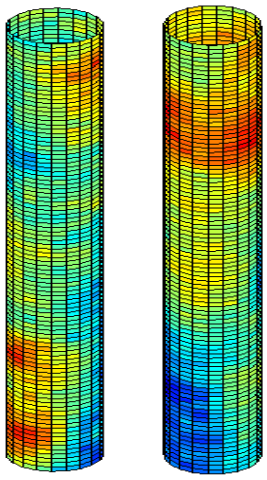

Figure 1-4. Variation of rock strength at the 17th Street Bridge.

Finally, of major concern, is the influence of load testing on the recommended LRFD Φ values for design. Recently in 2009, the American Association of State Highway Transportation

Officials (AASHTO) recommended a range of LRFD Φ values based on the number of load tests and the variability of soil/rock properties on the site (see Figure 1-5). Unfortunately, use of higher LRFD Φ values with load testing (e.g., Lee Roy Selmon Crosstown Expressway bridge, Tampa), as suggested in Figure 1-5, has resulted in pier failure. Of interest is the use of load testing to improve bias assessment (e.g., measured versus predicted capacity) along with borehole data to quantify spatial variability for development of LRFD Φ for an individual site.

Table 10.5.5.2.3-2 Relationship between Number of Static Load Tests Conducted per Site and φ (after *Paikowsky et al., 2004*).

Number of Static Load Tests per Site	Resistance Factor, φ		
	Site Variability[a]		
	Low[a]	Medium[a]	High[a]
1	0.80	0.70	0.55
2	0.90	0.75	0.65
3	0.90	0.85	0.75
≥4	0.90	0.90	0.80

a See commentary.

Figure 1-5. AASHTO LRFD Φ based on number of load tests and site variability.

1.2 Objectives and Supporting Tasks

The primary objective of this project is to account for spatial variability and load testing in assigning LRFD resistance factors (Φ) for drilled shafts socketed in Florida limestone at FDOT bridge sites. The resistance factors should be a function of geometry, i.e., shaft diameter and embedment (length/diameter (L/D)), rock/soil strength variability (i.e., CV_q) and spatial correlation length (a), at a site. To assist in assessing typical spatial correlation lengths (a), the review of FDOT database as well as site visits should be carried out to evaluate expected ranges of values, since it has never been undertaken before. In assessing the influence of load testing on LRFD Φ, the data from prior sites, which had soil/rock borings in the foot print of the load tests, are employed. Finally, the work includes a number of case studies to identify how the proposed

design compares with current practice. The research was accomplished through five tasks as outlined below.

1.2.1 Task I – Collecting Shaft/Pile Capacities and Rock/Soil Variability

The FDOT Geotechnical Internet Based Database maintained by the Florida Bridge Software Institute (BSI) has multiple bridge sites, which contain both insitu and laboratory (i.e., rock q_u, q_t, etc.) data and field load test data. The insitu and laboratory data for each site were collected to establish the rock/soil strength variability (i.e., CV_q) and study of spatial correlation length (a). Existing project sites, which included detailed insitu/laboratory testing near the piers with load testing, were identified and a few were revisited to obtain borehole/laboratory data at closer horizontal spacing (i.e., 5 to 10 ft). Sites evaluated were Fuller Warren and 17th Street Bridges, which covered the expected range of rock strength variability in Florida. The study included identification of correlation both vertically and horizontally. In the case of vertical correlation, boreholes spaced quite far apart might be used to identify zonal anisotropy, as well.

Since the work must differentiate between spatial variability influences and the design approach bias, a site was needed which had load testing with boring and laboratory data within the footprint, as well as the pier footings. The Jewfish Creek Bridge site was selected due to its two load tests and extensive boring/laboratory data within the footprint of load test, as well as at individual piers.

1.2.2 Task II – Drilled Shaft Axial Coefficient of Variation (CV_R) as a Function of Rock Point Statistics (Mean CV_q) and Spatial Correlation Length (a)

The focus of Task II is the upscaling of rock point characteristics (e.g., rock strength) recorded in a boring/laboratory test to the whole shaft. Specifically, the point-to-point variability of rock strengths acting on the shaft's surface result in similar shaft and rock mean capacities,

but reduced coefficient of variation (CV_R) of shaft capacities versus the rock coefficient of variation (CV_q). The latter is due to the averaging of rock strength along the surface of the shaft. Also impacting the coefficient of variation of shaft resistance (CV_R) is any rock strengths that are correlated from point-to-point, e.g., Figure 1-4. For instance, having a correlation range larger than the embedded length of the shaft may result in a shaft located in all weak or strong rock that would result in large variations in shaft resistances. However, shafts embedded in low correlation length rock will have both high and low rock strengths along their length, resulting in smaller variation in shaft resistance from shaft to shaft (i.e., different piers).

Consequently, the focus of Task II is the development of expected coefficient of variation (CV_R) of drilled shaft axial capacities as a function of shaft dimensions (i.e., length L and diameter D); the rock strength coefficient of variation (CV_q); and its correlation length (a). Initial work assumed that the correlation length is known in both the vertical (a_v) and horizontal (a_h) direction. However, since the establishment of horizontal correlation length (a_h) requires boreholes at close spacing (i.e., 5 to 10 ft), a conservative assumption of averaging the rock's variance only in the vertical direction (i.e., line shaft approximation) is also considered. Finally, in this task, LRFD Φ factors are developed as a function of shaft CV_R and resistance bias (λ_R) equal to one using the First Order Second Moment (FOSM) approach suggested by AASHTO.

1.2.3 Task III – Development of LRFD Φ Values from Pre-Design Borehole Data

The focus of Task III is the development of LRFD Φ values when limited borehole/laboratory information is available. Specifically for the case of pre-design borehole/laboratory data (obtained during the Planning Design and Engineering, PD&E, study), the design piers may be quite far away from the borehole locations, and the number of boreholes/laboratory tests may be limited. Consequently, the coefficient of variation of the shafts should include uncertainty

associated with the number of borings, as well as a conservative assumption on horizontal correlation. In the case of the latter, the least reduction in CV_R is to assume that the horizontal correlation is much larger than the radius of the shaft (i.e., no reduction due to averaging in the horizontal direction). All of the boreholes in a region/zone are treated together to identify mean borehole strength and CV_q.

Also of concern with pre-design borehole data is the existence of rock variability (i.e., variance) which is greater for the zone/region than exhibited in any given borehole. The latter is referred to as random areal trend (which is a type of zonal anisotropy), and it identifies variability that is not reduced by vertical averaging. Such additional variability must be considered for any shaft design within the zone or region.

1.2.4 Task IV – LRFD Φ Values for Borehole Data in the Footprint of Shaft/Piers

The use of borehole/laboratory data in the footprint of the shaft or pier results in significant improvement in the LRFD Φ values for design. Specifically, the increased number of borings allows the designer to use individual mean borehole strength for the pier shaft design, i.e., eliminating the uncertainty between mean borehole strength (i.e., average over a zone) and an individual shaft resistance. However, the approach typically does not allow inference of the horizontal correlation length and some worst case scenario must be assumed to be conservative under all circumstances. If the designer chooses to obtain a sufficient number of borings in the vicinity of the pier/shaft, the horizontal correlation may be established to improve on this worst case scenario. The LRFD Φ values developed from borehole/laboratory data in the footprint of the pier/shaft are higher than the values developed for Task III due to the reduction in the uncertainty of shaft axial resistance.

1.2.5 Task V – LRFD Φ Values for Sites which Include Field Load Testing

Borehole/laboratory strength data may not be a perfect estimate of drilled shaft resistance. Uncertainties associated with the design method, as well as construction issues (e.g., drilling fluids, casings, etc.), allow the development of site specific correction to the borehole/laboratory design approach from field load testing. The use of borehole data within the footprint of the load tests allows a direct assessment of a design method bias, as well as prediction error variance. In addition, if the load test and production shafts have similar diameters, the upscaling relationship between test/production shaft and borehole is exactly accounted for. In addition, the prediction error variance established between the load test and borehole design approach may be used in combination with the uncertainties associated with borehole/laboratory data, i.e., the approach outlined in Task III (boreholes far away from design shafts) and Task IV (boreholes within their footprint of the design pier/shaft). The combined uncertainties associated with borehole/laboratory data along with prediction error variance of the design approach are used to assess the total shaft axial resistance variance (CV_R) and the associated LRFD Φ value for the designed shaft. Again, it is expected the use of boreholes within the footprint of the design shaft/pier will have the smallest uncertainty or variance (CV_R) and result in the highest LRFD Φ values. Guidelines for the number of load tests, as well as pairs of predicted versus measured shaft resistance values are given to ensure accurate bias and error variance assessment.

CHAPTER 2
GEOSTATISTICAL PRINCIPLES

2.1 Introduction

While classical statistics deal with single (univariate statistics) or a finite number of possibly correlated random variables (multivariate statistics), geostatistics represent an extension to spatially distributed random functions, which are also called regionalized variables. Random functions consist of an infinite number of random variables defined at every point in a one or higher dimensional space, which are correlated according to their relative spatial arrangement, and a spatial correlation structure transforming spatial closeness into statistical closeness, i.e., correlation. As opposed to purely deterministic (i.e., no random component) functions, random functions are capable of describing spatially distributed parameters in probabilistic terms at every location, while preserving a certain degree of smoothness in space as typically observed in nature (parameter values at two close-by locations are more likely to be similar than at two distant locations).

Geostatistics originated during the 1950s in the mining industry and have ever since experienced strong theoretical and practical development. Since the 1980s, applications have expanded to include many fields such as petroleum engineering, agriculture, meteorology, and hydrology, for example. As an introductory text for practice oriented engineers, the book by Isaaks and Srivastava (1989) is recommended. Among the large variety of literature available on the topic, Journel and Huijbregts (1978), Deutsch and Journel (1992), Goovaerts (1997), Kitanidis (1997) and Deutsch (2002) represent textbooks for further reading. In the present study, geostatistics was applied to model the uncertain, yet in some way spatially continuous, distribution of rock/soil strength over a site, with the goal of estimating nominal resistances and uncertainties of drilled shafts to subsequently quantify LRFD resistance (Φ) factors incorporating spatial variabil-

ity of local strength. For this purpose, the remainder of this chapter is dedicated to introducing the most fundamental geostatistical principles, operations, and tools applied in this report.

2.2 Random and Deterministic Components – Stationarity

As stated above, random functions consist of an infinite number of random (and generally correlated) variables defined at every point within a spatial domain of interest. To fully define a random function, hence, it is required to know the univariate distribution (probability density function or PDF) of the random variable at each location and the correlation between each pair of locations inside the domain. This represents a large amount of information, which is simplified by the concept of stationarity assuming that univariate PDFs are the same throughout the domain, and spatial correlations are the same for equal separation distances, i.e., independent of the actual location. Thus, stationarity somehow implies a concept of statistical homogeneity over a domain, which is also fundamental for practical implementation as it allows inference of a single PDF and spatial correlation structure describing a random function from a limited amount of data acquired at a site. That is by grouping all observations (although they conceptually correspond to different random variables at different locations), the PDF of the random function may be determined (this is also known as the principle of ergodicity). In the same way, by grouping all observations separated by (approximately) equal distances, which the spatial correlation structure may be inferred as a function of spatial separation. This process is discussed in further detail below.

Most common deviations from stationarity occur due to deterministic trend components or discontinuities (e.g., layering), i.e., locally varying mean values. In general, a random function RF(x) where x represents a spatial coordinate, may be written as the sum of a deterministic component D(x) and a random component R(x) fluctuating about D(x).

$$RF(x) = D(x) + R(x) \tag{2-1}$$

Figure 2-1 graphically illustrates the meaning of Equation 2-1 for (a) a linear deterministic trend component and (b) a discontinuous trend. In both cases, all geostatistical operations are performed on the random component R, i.e., after subtracting D from observed values of RF. Component D is added back into final results only after geostatistical analysis has been concluded. In the latter example, RF may alternatively be divided into two separate sub-domains, A and B, which are both stationary by themselves, however, not together. The decision about stationarity or not must be carefully considered and is often scale dependent, i.e., what appears to be a deterministic trend at a local scale may become part of a random fluctuation component at a larger scale. Inspection of location maps or depth profiles with data values is most helpful in identify overall trends or discontinuities. Data histograms (see next section) may also indicate the presence of more than a single homogeneous sub-domain if more than one

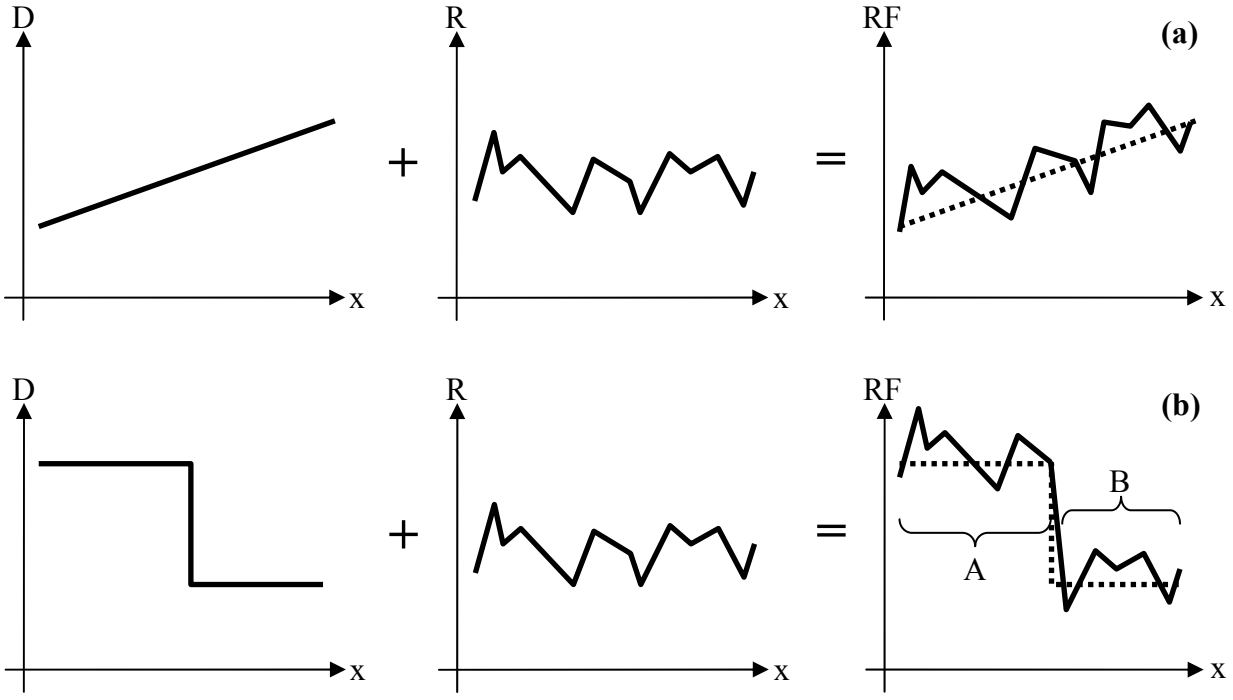

Figure 2-1. Deterministic (D) and random (R) components of non-stationary random functions (RF): (a) Linear deterministic trend; and (b) Discontinuous deterministic trend (two stationary sub-domains A and B).

mode (peak) is identified. There are, however, no hard rules available for the decision about stationarity and some practical guidelines are given in the course of case studies below.

2.3 Histogram, Scatterplot, and Variogram

As stated above, an intermediate goal is to describe the spatially variable distribution of rock/soil strength at a given site as a random function (defined by PDF and spatial correlation structure) based on local strength data (e.g., core samples, SPT, CPT, etc.) collected at that site. Data are hereby assumed to be stationary, i.e., deterministic trend components have previously been subtracted or division into sub-domains (e.g., layers, zones, etc.) has been performed. The PDF expresses the probability (frequency) of occurrence of a data value at a site and is inferred through a data histogram. Hereby, the data range between minimum and maximum data values is divided into a number of equal intervals in which the numbers of occurrence (frequency) of data values are counted (i.e., histogram). For each data interval on the x-axis, respective frequencies are plotted as bars in y-direction to obtain the histogram. Different PDFs, e.g., normal, log-normal, etc., may be tried out to best fit the data histogram (Figure 2-2). Location maps, depth profiles, and histograms are easily generated through basic Microsoft Excel functions.

Important parameters of the data histogram are the mean (m) and variance (σ^2) defined by

$$m = \frac{1}{n}\sum_{i=1}^{n} q_i \tag{2-2}$$

$$\sigma^2 = \frac{1}{n-1}\sum_{i=1}^{n} (q_i - m)^2 \tag{2-3}$$

where n is the number of q_i data collected. From this, the coefficient of variation is obtained as

$$CV = \frac{\sigma}{m} \tag{2-4}$$

where σ (square root of variance) is called the standard deviation. Large values of CV indicate a

large relative spread of data values about the mean. Note that no strict rules exist for the choice of number of bin classes in a histogram.

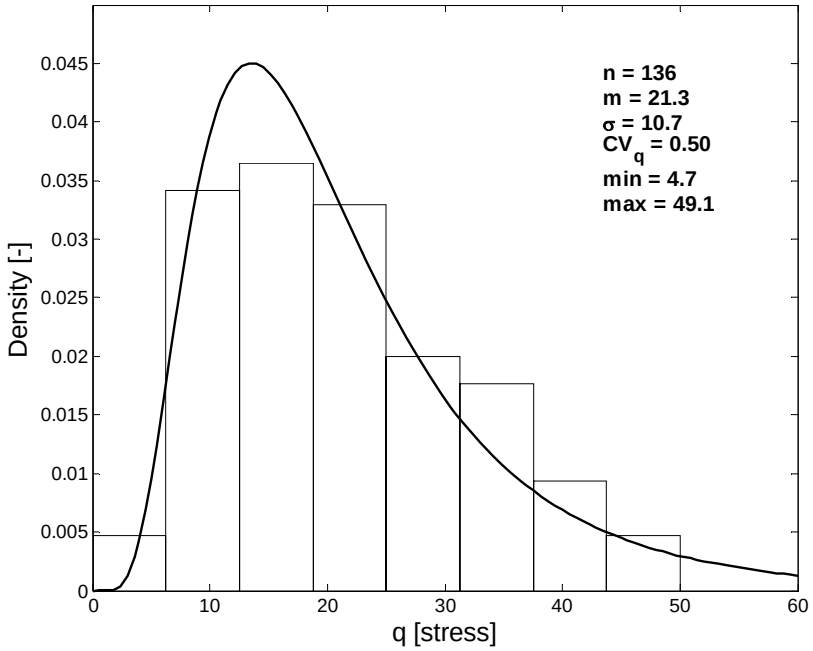

Figure 2-2. Example of local strength q histogram (bars) and log-normal PDF fit (continuous line).

It is good practice to experiment with several numbers of bin classes to get an impression of the sensitivity of the histogram shape. Among many different approximate formulas, Scott's rule recommends a number of bin intervals equal to $3.49\sigma(n)^{-1/3}$, which can be used as a starting point. The probability distribution function (i.e., PDF) is obtained from the histogram by dividing the number of occurrences in each bin by the total number of occurrences recorded to give the probability of each event with the summation equal to one (i.e., area under PDF). The cumulative distribution function (CDF) is the summation of probabilities of each bin up to the current bin and is plotted on the y-axis.

In order to infer the spatial correlation structure from available data at a site, it is required to determine the correlations between data pairs that are separated by different distances. As

opposed to histogram inference, where data are grouped into intervals of data values, e.g., strength, data are now grouped into intervals of data separation distance (referred to as lag distance). For example, all data pairs are selected, which are separated between 3 and 4 meters from each other and plotted in a scatterplot, i.e., in a chart where one data value q_i of the pair is on the x-axis and the other data value q_j (located from q_i value by lag distance h) of the pair on the y-axis. Figure 2-3 (a through c) depicts examples of scatterplots for increasing separation (lag) distances and decreasing degree of correlation, i.e., larger spread of data points about the 45° line. Perfect correlation would be indicated by all data points falling onto the 45° line, which is the case for $q_i = q_j$, i.e., when the spatial separation distance is zero (data points are paired with themselves).

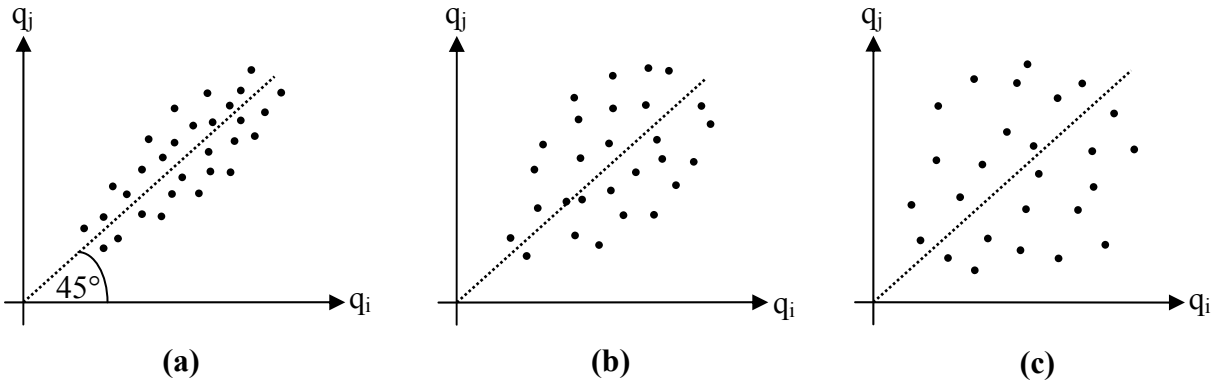

Figure 2-3. Data scatterplots for different separation (lag) distances of data pairs (q_i, q_j): Sequence of (a), (b), and (c) represents increasing separation distance and decreasing correlation. Dashed line is 45° and represents perfect correlation ($q_i - q_j$ or zero separation distance).

A fundamental parameter contained in the scatterplots is the covariance $Cov(q_i,q_j)$ between data values q_i and q_j, which are separated by a certain lag distance h (or an interval around h),

$$Cov(q_i, q_j) = \frac{1}{n_h - 1} \sum_{n_h} (q_i - m)(q_j - m) \tag{2-5}$$

where n_h is the number of data pairs in the interval (also called lag class) around separation distance h. For zero lag distances, $q_i = q_j$ and Equation 2-5 reduces to the variance of Equation 2-3. The covariance is directly linked to the dimensionless correlation coefficient r by

$$r = \frac{Cov(q_i, q_j)}{\sigma^2} \tag{2-6}$$

Note that Equations 2-5 and 2-6 are based on the stationarity assumption, which implies that the means and variances of q_i and q_j are the same and equal to m and σ^2. By evaluating Equations 2-5 and 2-6 for a series of lag distance intervals (e.g., 0 – 2 m, 2 – 4 m, 4 – 6 m, etc.), points of the spatial covariance function C(h), and the spatial correlation function r(h), respectively, are obtained. Another measure of spread of the data points in Figure 2-3 about the 45° line as a function of lag distance h is the semi-variogram (or frequently abbreviated to variogram) $\gamma(h)$ defined as

$$\gamma(h) = \frac{1}{2n_h} \sum_{n_h} \left(q_i - q_j\right)^2 \tag{2-7}$$

which is related to the spatial covariance function C(h) by

$$\gamma(h) = \sigma^2 - C(h) \tag{2-8}$$

Figure 2-4 gives graphical examples of C(h), r(h), and $\gamma(h)$, where it is illustrated that spatial correlation, i.e., C(h) and r(h) in Figure 2-4 (a) and (b) typically reaches zero after a distance denominated as range or correlation length. In turn, h = a, $\gamma(h)$ in Figure 2-4(c) reaches its so-called sill (dotted line) equal to the variance σ^2 according to Equation 2-8. Similar to fitting a PDF model to a data histogram (Figure 2-2), Figure 2-4 further shows how one of a series of theoretical variogram models (e.g., exponential or spherical model; dashed lines) must be fitted to the experimental variogram points (dots) for subsequent use in geostatistical analysis. Care must be taken that each experimental variogram point is based on a sufficient amount of

data pairs to be representative. No strict guidelines are available, but by widening the lag distance intervals, if necessary (e.g., 0 – 4 m instead of 0 – 2 m), more than 30 data pairs should be used in each variogram point. It is good practice to inspect experimental variograms of different lag separation intervals to evaluate the sensitivity of the outcome to this choice. Many commercially available or free-to-download programs exist for variogram analysis, which however, is also emendable to implementation in Microsoft Excel.

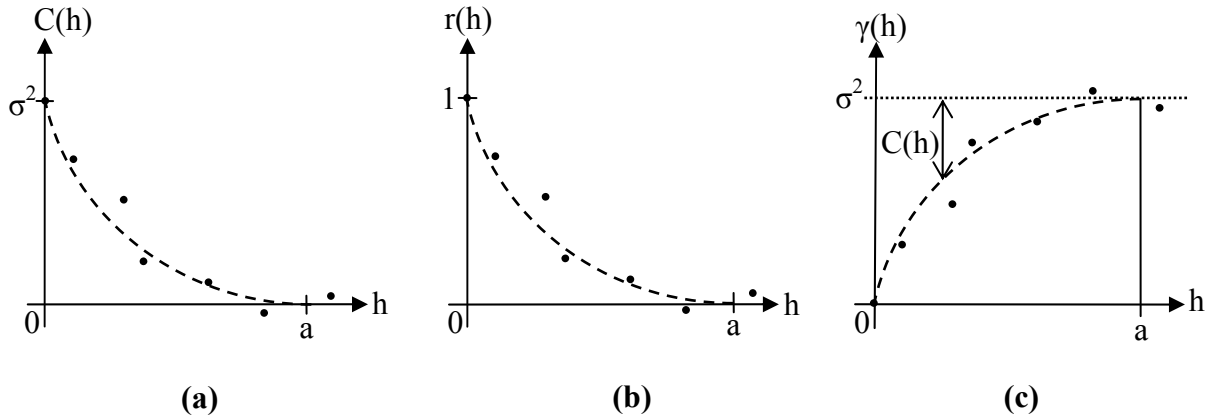

Figure 2-4. Graphical examples: (a) Spatial covariance function C(h); (b) Spatial correlation function r(h); and (c) Variogram γ(h). Dots represent experimental values derived from site data and Equations 2-5, 2-6 and 2-7, respectively, while dashed lines represent variogram model fits of range a.

Different independent random functions can be added to better describe a variable of interest. Just as the variances for each random function may be added, the individual variograms may be added to obtain the total variogram representing the sum of the random functions. Variograms composed of more than one basic structure are called nested variograms and examples are given in Figure 2-5. Most important is the case of Figure 2-5(c), where the range a_1 of one variogram component is zero (i.e., smaller than the shortest data separation distance in practice). This variogram component is called nugget or nugget effect and it represents small scale

variability and measurement errors, for example. It causes the composite variogram (continuous line) to intersect the y-axis at the nugget variance C_0.

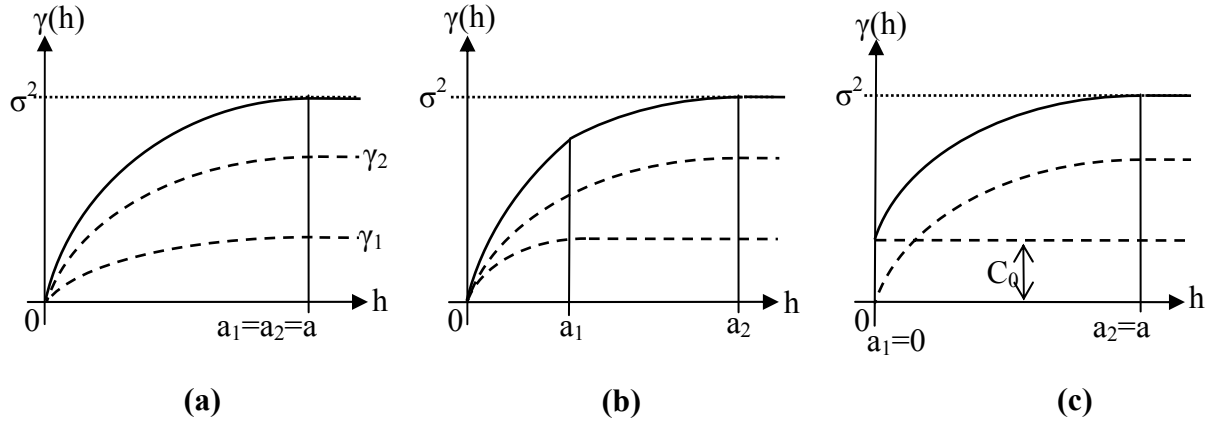

Figure 2-5. Examples of nested (composite) variograms: (a) Equal ranges $a_1 = a_2 = a$; (b) $a_1 < a_2$; and (c) $a_1 = 0$ representing a nugget effect of variance C_0.

In more than one dimension, variograms may not be a function of separation distance h only, but also the direction in which the separation vector points. For example, a process studied over a certain portion of the earth's surface may possess a larger spatial continuity (i.e., correlation length) in the north-south direction than in the east-west direction. Similarly, it is very common in geological settings to observe a different correlation length in both horizontal directions than in the vertical direction (e.g., short scale depositional variability in vertical direction with larger spatial continuity in horizontal directions). This represents an example of a phenomenon, which is called anisotropy of the variogram and which may be investigated by not only grouping data pairs into separation distance intervals only (as in Figure 2-4), but also by grouping data pairs according to their direction of alignment. Thus, experimental variogram points are obtained for different spatial directions and may be compared to see whether anisotropy is present or not. By differentiating horizontal and vertical direction, Figure 2-6 represents different types of anisotropy that may occur. The case of Figure 2-6(a) is called

geometric anisotropy and corresponds to the situation discussed above, where horizontal and vertical ranges are different whereas both horizontal and vertical variogram reach the same sill, i.e., contain the same amount of variability. Figure 2-6(b) gives an example of a so-called zonal anisotropy, where horizontal and vertical ranges are the same, but the variances (sills) σ^2_h and σ^2_v are different. This means that more spatial variability is contained in one direction and reflects random layering if $\sigma^2_h < \sigma^2_v$ or random areal trends in the horizontal plane if $\sigma^2_h > \sigma^2_v$. To illustrate an extreme case of zonal anisotropy in the case of random layering, would be if $\sigma^2_h = 0$ corresponding to a vertical sequence of layers of random and possibly vertically correlated strengths, which are, however, constant in the horizontal direction, i.e., within layers. Finally, Figure 2-6(c) shows that geometric and zonal anisotropies may occur simultaneously to different individual extents.

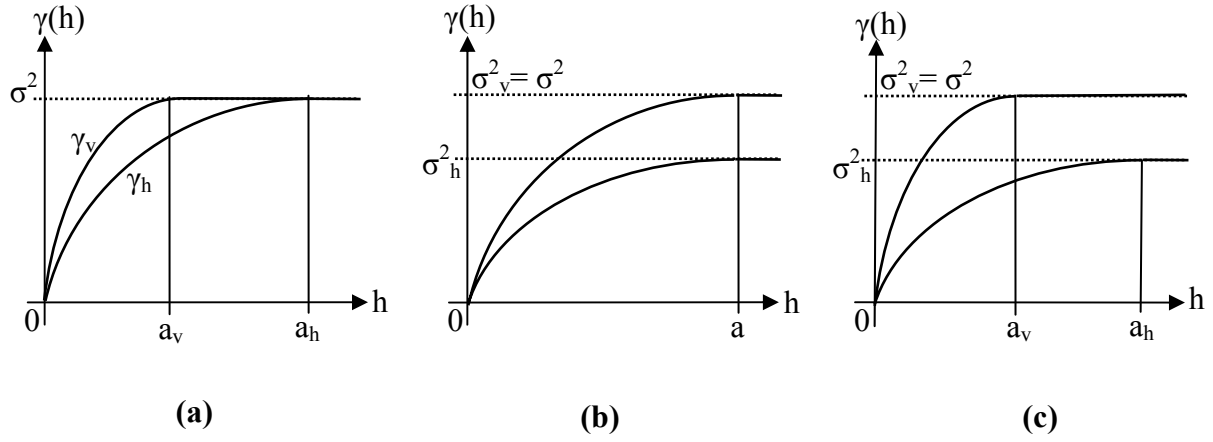

Figure 2-6. Examples of anisotropic variograms: (a) Geometric anisotropy with $a_h > a_v$; (b) Zonal anisotropy with $\sigma^2_h < \sigma^2_v$; and (c) Mix of geometric and zonal anisotropies with $a_h > a_v$ and $\sigma^2_h < \sigma^2_v$.

2.4 Upscaling, Kriging, and Stochastic Simulation

In all of the above, the issue of scale is of fundamental importance. That is, histograms, scatterplots, and variograms are only valid for a certain support size of the data collected (i.e., sample size). All data used should be of the same support size (e.g., inches, centimeter scale) and may be treated as point values if observed correlation lengths are at a larger (e.g., ft or meter) scale. It is well known in statistics that averaging of random variables has a variance reducing effect on the outcome. Of interest to the present work is the spatial averaging of local strength values over the cylindrical outside surface of a drilled shaft in order to obtain an average design strength value for the whole shaft. The variance reduction principle may hereby be thought of as the compensating effect of large and small local strength values on the shaft surface, which leads to some intermediate strength value when averaged. Thus, it is less likely for mean strengths over a whole shaft to take as extreme values as local or point-to-point strength does. The branch of geostatistics dealing with this kind of phenomenon is called change of support or upscaling (if change of support is from small to large). For n independent (i.e., uncorrelated) random variables of variance σ^2, it is well known from classical statistics that the variance σ^2_m of the mean is

$$\sigma_m^2 = \frac{\sigma^2}{n} \tag{2-9}$$

This relationship may be generalized to correlated random variables and spatially correlated random functions where averaging is over certain spatial domains (e.g., shaft surface). For this purpose, a dimensionless variance reduction factor α is introduced such that

$$\sigma_m^2 = \alpha\sigma^2 \tag{2-10}$$

$$\alpha = \frac{1}{A^2}\int_A\int_A r(x_1 - x_2)dx_1dx_2 \tag{2-11}$$

where A is a spatial domain (e.g., line, area or volume) over which averaging occurs due to $r(1 \leq r \leq 0)$; x_1 and x_2 are coordinates. Despite the complex aspect of Equation 2-11, its intuitive interpretation is straightforward as the mean value of the correlation function r(h) over all possible combinations of location pairs within A. If A is reduced to a finite number of n uncorrelated locations, Equation 2-10 becomes equal to Equation 2-9 with $\alpha = 1/n$. As r(h), decreases with h, and becomes zero for distances beyond the variogram range (Figure 2-4(b)), Equation 2-11 illustrates that variance reduction becomes stronger (i.e., α smaller) as the spatial averaging domain A grows. If A is reduced to a single point (no upscaling), then $\alpha = 1$ and $\sigma^2_m = \sigma^2$.

Upscaling is the geostatistical operation which determines the variance (uncertainty) of the total shaft resistance from well known PDF and variogram of local strength, while the expected or mean shaft resistance remains unaffected and equal to the mean local strength at a site (i.e., upscaling does not affect the mean of a distribution). No specific location is hereby associated with a shaft, i.e., the upscaled variance corresponds to the variability of the resistances of many shafts arbitrarily located over a site or zone defined by the same variogram. In practice, local strength data are never perfectly well known due to limited sampling and explicit shaft locations must be defined during the design process. While the former represents an additional component of uncertainty, the latter may lead to a reduction in uncertainly of shaft resistance, if local strength data are available in the vicinity (within the correlation length) of a shaft. Spatial correlation between local strength data and the shaft surface then allows for an improved estimate of shaft resistance and variance. The geostatistical tool provided for this task is called ordinary kriging or best linear unbiased estimation (BLUE). Denoting all n local strength data at a site with q_i, kriging estimates the unknown average local strength (average unit side friction) f over a lateral shaft surface A as the weighted average of all q_i,

$$f = \frac{R}{A} = \sum_{i=1}^{n} \lambda_i q_i \tag{2-12}$$

where R is the shaft resistance and λ_i represents the weights associated with each data value that add up to one $\left(\sum_{i=1}^{n} \lambda_i = 1 \right)$. The error variance σ_f^2 associated with this estimate is called ordinary kriging variance and given by

$$\sigma_f^2 = \sigma_m^2 + \sigma_q^2 - 2C(m,q) \tag{2-13}$$

σ_m^2 hereby is the upscaled shaft resistance variance from Equation 2-10 and σ_q^2 is the variance of the estimator in Equation 2-12,

$$\sigma_q^2 = \sum_{i=1}^{n} \sum_{j=1}^{n} \lambda_i \lambda_j C(x_i - x_j) \tag{2-14}$$

which is simply the mean weighted covariance between all possible combinations of data pairs. The last term in Equation 2-13 represents the covariance between the shaft resistance to be estimated and the estimator of Equation 2-12 and is equal to the mean weighted covariance between all combinations of a data point and a point on the shaft surface A.

$$C(m,q) = \frac{1}{A} \sum_{i=1}^{n} \int_A \lambda_i C(x_i - x) dx \tag{2-15}$$

Ordinary kriging uses Equation 2-13 to find the values of the weights λ_i required in Equation 2-12 by minimizing the error variance σ_f^2. Error variance σ_f^2 and, hence λ_i, depend on both the data locations and shaft location through the spatial covariance function in Equations 2-14 and 2-15. Data closer to the shaft receive larger weights such that C(m,q) in Equation 2-15 increases and σ_f^2 decreases. The ordinary kriging estimator is also known to account for data redundancy, i.e., correlated data close to each other (data clusters) are assigned smaller weights than isolated data points. In taking A in Equations 2-11 and 2-15 very large (e.g., whole site rather than shaft surface), Equation 2-12 becomes an estimator of the mean strength at a site and

$\sigma_f^2 = \sigma_q^2$ as Equations 2-11 and 2-15 approach zero. If, in addition, all available data are uncorrelated, then Equation 2-12 reduces to Equation 2-2 (i.e., $\lambda_i = 1/n$) and σ_f^2 becomes equal to σ_m^2 from Equation 2-9. For more than one spatially distributed parameter involved in a problem, the above kriging approach may be generalized to co-kriging of several random functions. In addition to spatial correlation of each random function (auto-correlation), it is also hereby accounting for spatial correlation between different random functions (cross-correlation).

Kriging provides an estimate of average unit side friction over a shaft surface and a respective measure of uncertainty in terms of a variance. In order to translate this information into a probability of failure for a given load, it is required to make assumptions about the distribution of the kriging error around the kriging estimate (e.g., normal, log-normal). Moreover, if the shaft failure mechanism is not a simple linear function (i.e., spatial average) of local strength values (e.g., function of modulus or stress), as in the case of ultimate limit state based on side friction only (no end bearing), then upscaling or kriging may no longer provide a direct estimate of shaft resistance and uncertainty. In those cases, failure is typically simulated by numerical finite difference/element models (Figure 2-7), which require the spatial distribution of local strength values at each grid point of the model as input. As the exact spatial distribution of local strength q at a site is never known, the geostatistical method called stochastic simulation is used to generate a number of q fields (called realizations), which honor PDF and variogram of q at that site. Each realization is a possible scenario for the real spatial distribution of q based on the geostatistical site characteristics and is equally likely to occur in reality (examples of two-dimensional realizations of q are given in Figure 2-8). With this, shaft failure may be simulated through numerical models for every realization of q resulting in a distribution (histogram) of shaft resistance for a specified displacement of limit state.

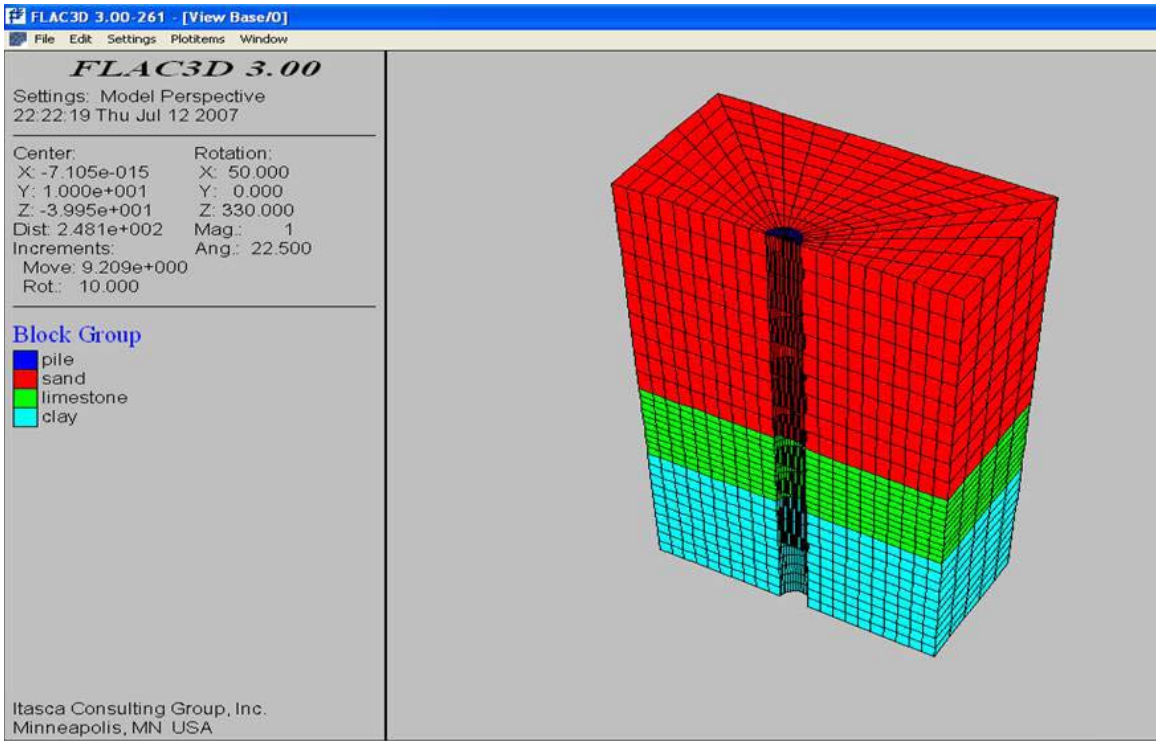

Figure 2-7. Example of three-dimensional grid for finite element model to simulate shaft resistance.

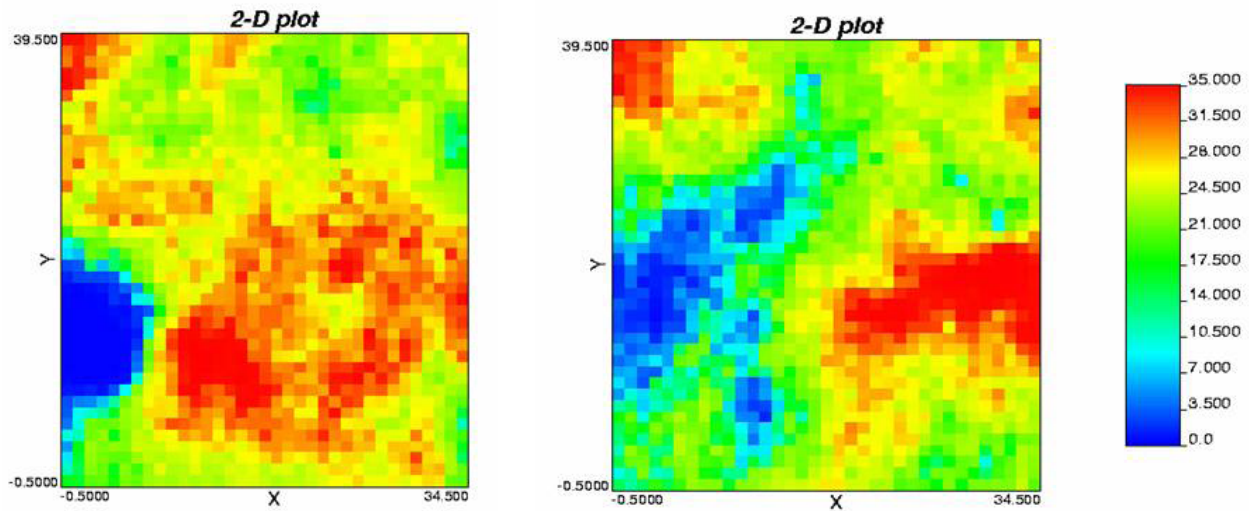

Figure 2-8. Examples of two 2-dimensional unconditional realizations of local strength generated by sequential Gaussian simulation (SGS) of 17th Street Bridge data.

In contrast to kriging, no assumptions are required about the shape of the shaft resistance distribution, but a very large number of realizations and numerical model runs may be necessary to obtain reliable information in the tails of the shaft resistance distribution, which is of actual interest. Realizations that are generated by using stochastic simulations, which possess a given PDF and variogram, are called unconditional, while realizations that also honor (i.e., reproduce) local data values are called conditional. From a large number of realizations, a histogram of simulated q values may be constructed for each location. The means and variances of those histograms coincide with those predicted by respective kriging. Many algorithms and programs exist to perform stochastic simulation. Most common in geosciences are methods based on Gaussian (normal) fields (e.g., sequential Gaussian simulation (SGS), LU-simulation, etc.), which are generated first to honor a given variogram and, subsequently, transformed to honor a given PDF.

2.5 Case Studies

Appendix A contains local strength data from core sample analysis with respective spatial coordinates for two bridge sites (17^{th} Street and Fuller Warren). This section uses these data to discuss the problem of stationarity as well as to give examples of location maps, depth profiles with subsequent histogram, and variogram inference. This is what is called basic data analysis or structural analysis (when including the variogram) and is a fundamental task at the beginning of every geostatistical analysis. The principles of variance reduction, upscaling, and kriging will be further developed and illustrated in the next chapter.

2.5.1 17th Street Bridge

Figure 2-9 represents a location map and depth profiles from six borings (136 local strength values) near Pier 10, where x and y are coordinates in the horizontal direction and z is

an elevation above some arbitrary datum (all in feet). The location map also contains values of means and standard deviations (in parentheses) of local strength values q per boring (both in tsf). This representation is useful for deciding whether a discontinuity or a deterministic trend is present in the horizontal direction. A review of the mean values reveals no gradual (smooth) tendency to increase or decrease in any directions of the horizontal plane. Moreover, the maximum difference in borehole mean values is 20.2 – 11.8 = 8.4 tsf, which is very similar to the average standard deviation per boring, reflecting the fact that all depth profiles in Figure 2-9(b) overlap each other to some extent.

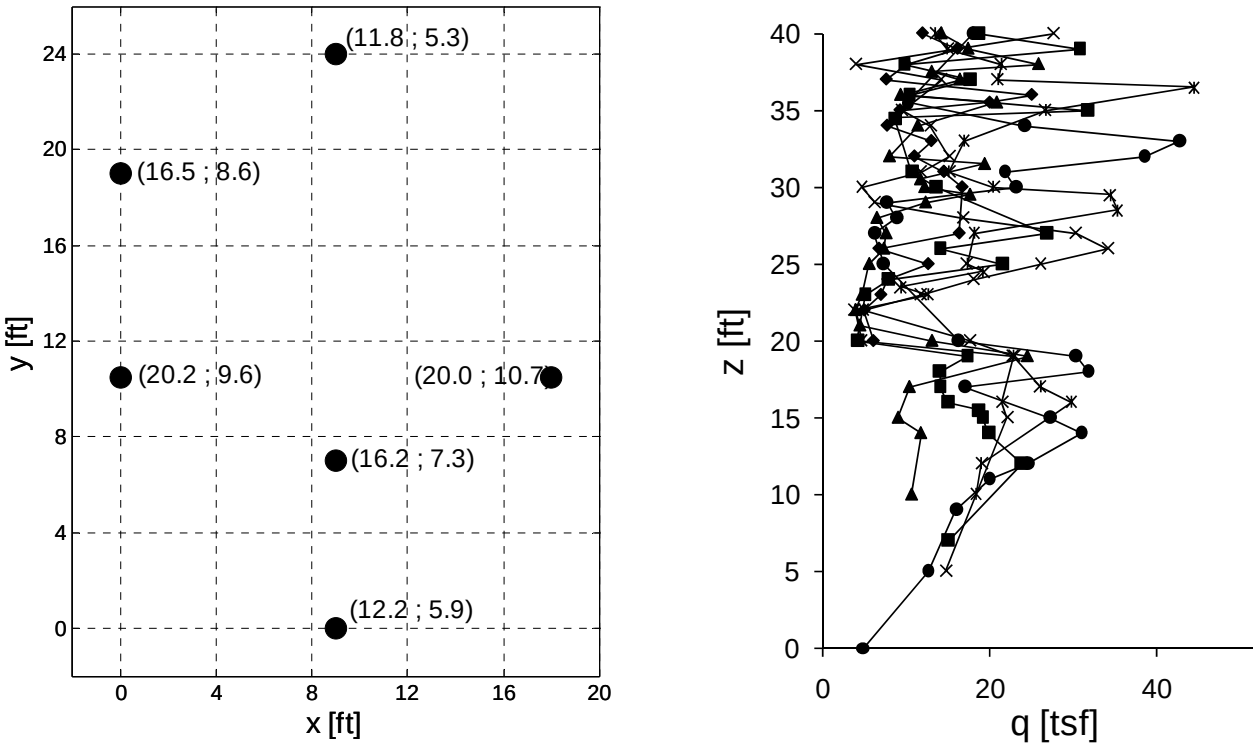

Figure 2-9. Site near Pier 10: (a) Location map with means and standard deviations (both in tsf) per boring (dots) in parentheses; and (b) Depth profiles of six borings.

This overlap further manifests in the histograms of Figure 2-10, which possess a single mode (peak) and may be approximated by a log-normal PDF as indicated by the continuous line. Figures 2-10(a) and 2-10(b) are based on the same data but different choices of data intervals for grouping into bin classes (number of vertical bars in the histogram). They illustrate that the overall aspect of the data distribution is relatively robust to this choice of bin class number (nine bins are shown in 2-10(a); and six are shown in 2-10(b)). Note also that the log-normal PDF fit does not depend on the number of bin classes in the histogram, but solely on the mean and variance of the data indicated in Figure 2-10(a). Non-overlapping depth profiles (either between different borings or within a single boring with layering) would lead to a multi-modal (more than a single peak) histogram and strongly suggest considering division into statistically homogeneous

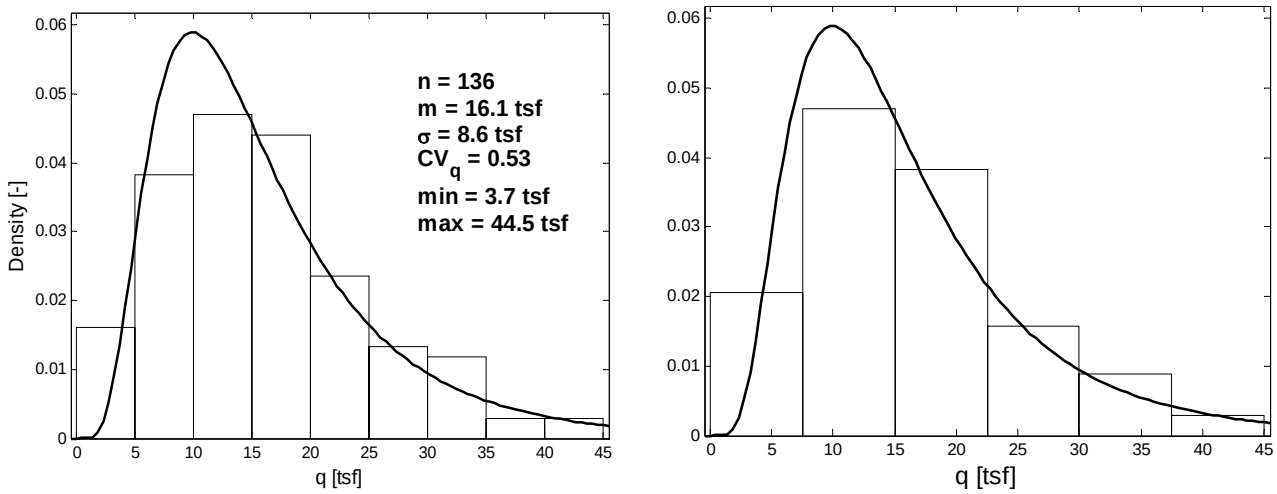

Figure 2-10. Data histograms with fundamental parameters and log-normal fit of PDF: (a) Nine bin classes (data intervals or bars) used; and (b) Six bin classes used.

sub-domains. This division is straightforward if each histogram mode may be attributed to data from distinct regions or layers of a site, and the inclusion of geological information from core samples is fundamental (e.g., changing rock type vertically or horizontally). However, if data from different modes are intermingled over the whole site, such homogeneous sub-domains may not exist (at the scale of the study), and the discrepancy in local strength values between different borings or different layers will manifest as a zonal anisotropy in the variogram (Figure 2-6). Based on Figures 2-9 and 2-10, the present data are treated as statistically homogeneous (stationary).

Figure 2-11 shows different outcomes of the variogram analysis, where sub-figures (a) and (b) are based on a 1-foot lag interval and sub-figures (c) and (d) on a 2-foot lag interval. Not necessarily all lag classes contain data, but the overall picture of Figure 2-11 indicates a vertical range between 4 and 5 feet (dashed lines) and a horizontal range between 10 and 12 feet (continuous lines). The short range behavior of the experimental variogram points does not clearly indicate whether a nugget effect is present as assumed in the model fits of Figure 2-11(b) and 2-11(d) or not as in 2-11(a) and 2-11(c). For spatial averaging, however, it will be seen that it is conservative to assume zero nugget variance such that the models 2-11(a) and 2-11(c) would be considered in this case. Figure 2-11 nicely illustrates the situation of a geometric anisotropy, where both horizontal and vertical variograms reach the same sill equal to the data variance (or one, if the variogram is normalized to the data variance as in the present case, i.e., all variogram values are divided by the data variance).

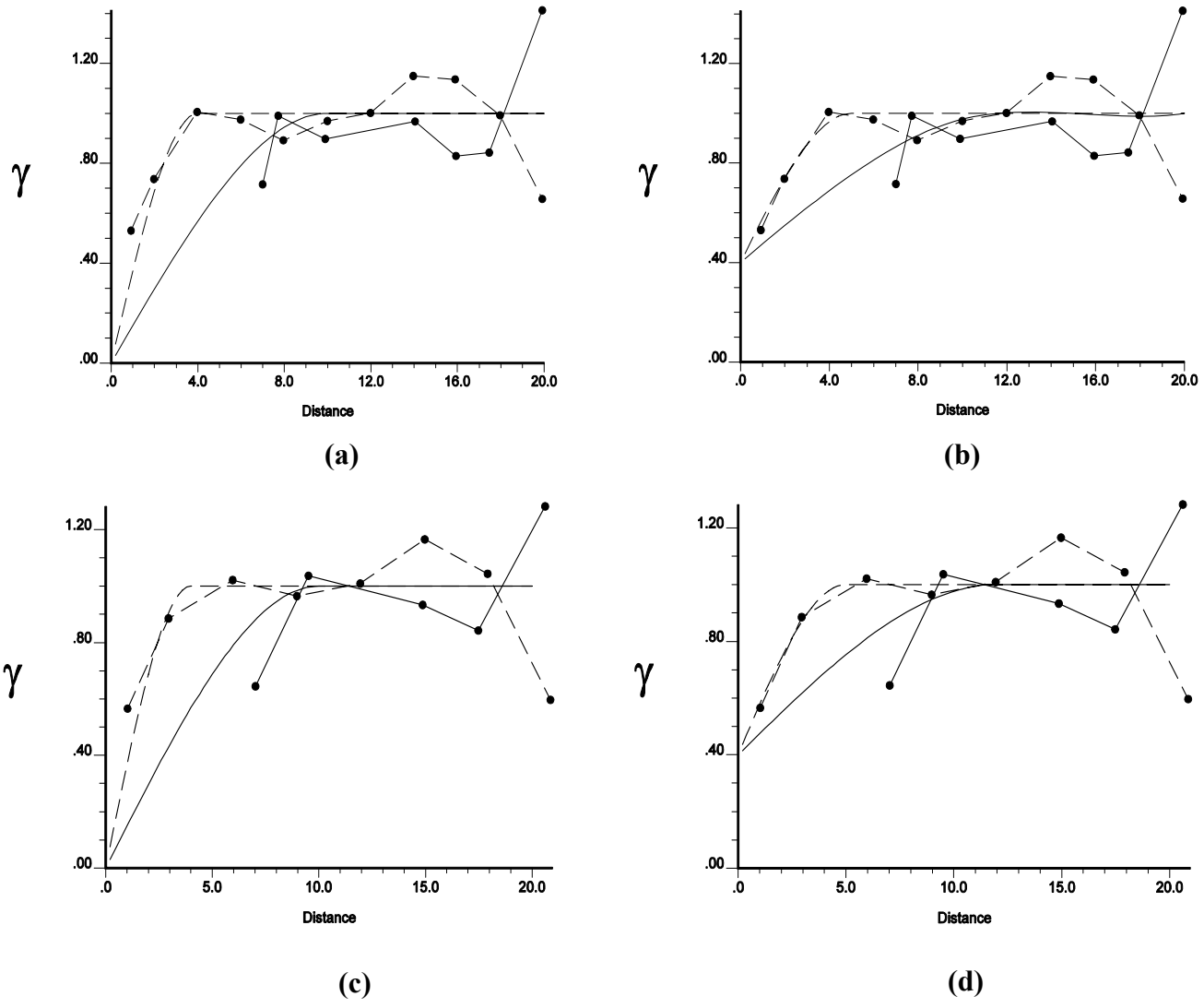

Figure 2-11. Vertical (dashed) and horizontal (continuous) variograms normalized to unit sill. Dots are experimental variogram point from data and smooth lines are variogram model fits: (a) and (b) use constant 1-foot lag interval; while (c) and (d) use constant 2-foot lag interval.

2.5.2 Fuller Warren Bridge

The location map and depth profiles of the 57 core sample data collected in three borings near the Load Test Shaft 4 (west side of bridge) are depicted in Figure 2-12. The depth profiles immediately reveal a strong discontinuity in measured strength values at an elevation of approximately 16 ft, which is consistent for all three borings. Visual core sample inspection may underline this by observing a distinct change in rock/soil type and quality. As a consequence, the

data set is divided into two sub-domains, i.e., two horizontal layers, a *top* and a *bottom* one. The numbers in parentheses next to each boring in Figure 2-12(a) represent means and standard deviations for all data in a boring (top line), for data in the top layer only (center line) and for data in the bottom layer only (bottom line). In agreement with the depth profiles, no significant trend or discontinuity may be observed in the horizontal direction. However, the differences in means and standard deviations between the two layers in each boring confirm the previous division of the site into the two layers. It may also be observed that the ratio of means between the layers is approximately equal to the ratio of respective standard deviation (i.e., approximately constant CV). This is typical for log-normal variables and is known as proportional effect in geostatistics reflecting the fact that variability increases with strength, as may be visually confirmed in Figure 2-12(b).

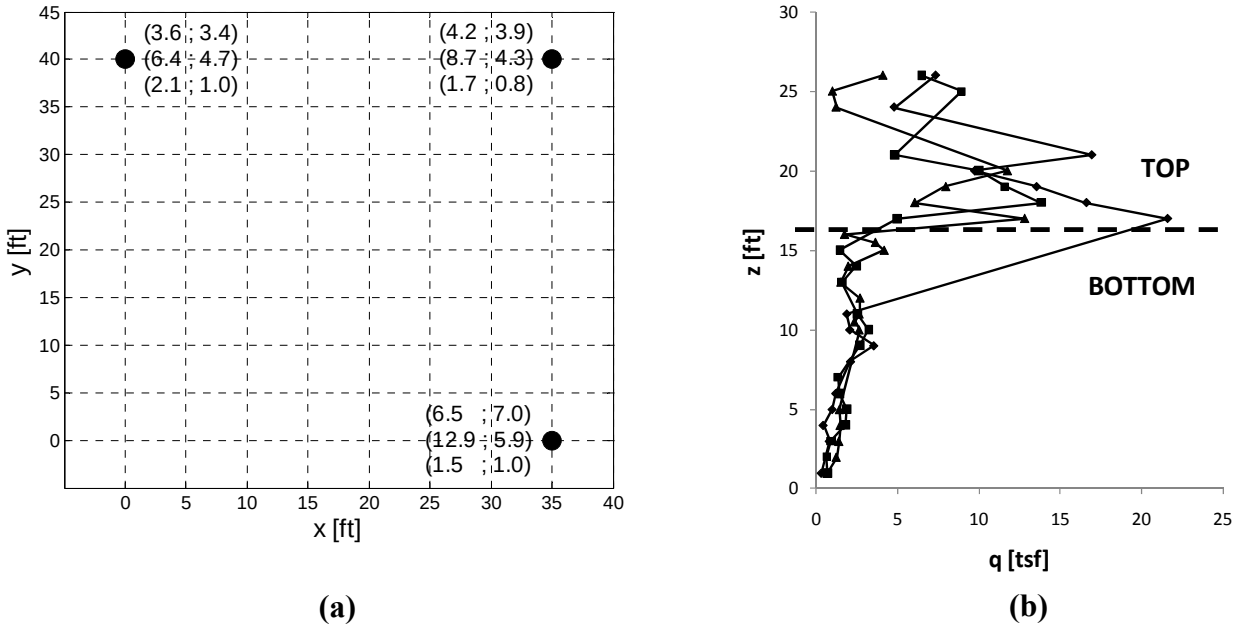

Figure 2-12. Core sample data from three borings: (a) Location map with means and standard deviations (both in tsf) per boring (dots) in parentheses, Top line – All data; Center line – Top layer; and Bottom line – Bottom layer; and (b) Depth profiles of all three borings indicating top and bottom layer.

Figure 2-13 gives the data histograms for (a) all data, (b) the bottom layer only, and (c) the top layer only. From the combined histogram in Figure 2-13(a), the presence of two distinct layers is not obvious as the data values of both layers slightly overlap and, most importantly, as the number of data in the top layer is smaller than that in the bottom layer, thus the bottom layer dominates the histogram and the second histogram peak of the top layer is not pronounced. When inspecting the histograms of the bottom and top layers in Figures 2-13(b) and 2-13(c) separately, however, the different strength distributions become evident. Fundamentally related

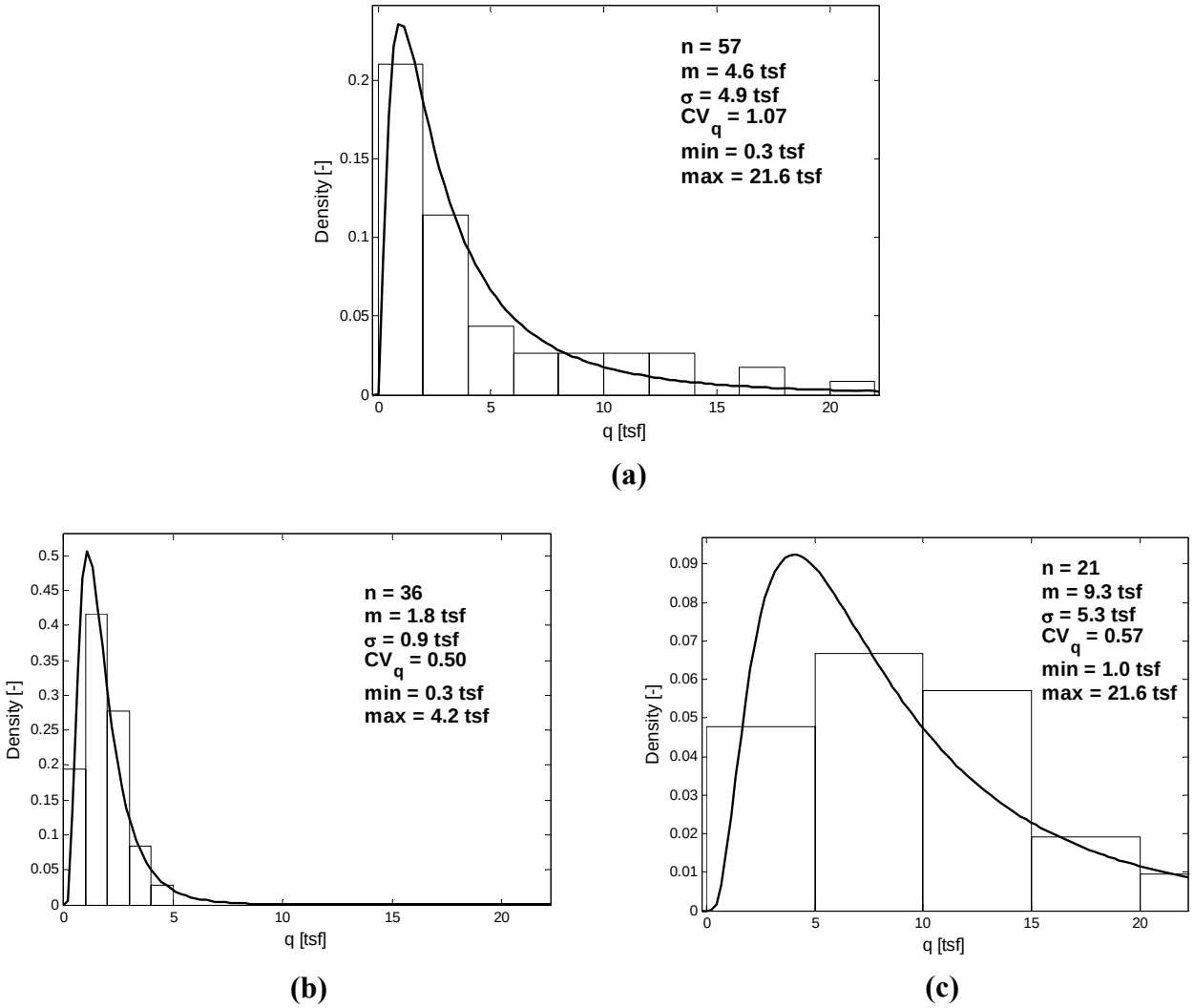

Figure 2-13. Data histograms with fundamental parameters and log-normal fits of PDF: (a) Compound histogram of all data; (b) Bottom layer only; and (c) Top layer only.

to the division into statistically homogeneous sub-domains is the principle of finding spatial regions within which variability (i.e., variance) is a minimum, while differences (i.e., variance) between data means of different spatial regions is a maximum. By taking the coefficient of variation CV_q given in Figure 2-13 as a measure of variability, it is seen that division into layers achieved a reduction of CV_q from 1.07 to approximately 0.5. The fact that CV_q in both layers is approximately equal is, again, an indicator of the proportional effect. Figure 2-13 also illustrates how the choice of the number of histogram bars depends on the number of data available.

In addition to layering, Figure 2-12(b) suggests the presence of linear deterministic trends in each layer. Figure 2-14(a) shows linear regression fits and equations to the data of each layer, where it is important to note that the strength q is the dependent variable (y-axis in regression) for which the regression over the elevation z (x-axis in regression model) is performed (i.e., the opposite as depicted in Figure 2-14). Figure 2-14(b) shows the so-called regression residuals, which are the actual data values minus the regression values at their respective elevations (i.e., horizontal distances between data points and regression lines in Figure 2-14(a). The residuals are seen to possess a mean of zero and different variances of 0.45 and 18.4 tsf^2 for the bottom and top layer, respectively. The identification and subtraction of these linear trends represent an additional reduction of variability from standard deviations of 0.9 and 5.3 tsf for bottom and top layers, respectively (Figure 2-13(b) and 2-13(c)), to 0.67 and 4.3 tsf (i.e., $CV_q = 0.37$ and 0.46 when used with mean q for each layer). The latter standard deviations correspond to those of the residuals depicted in Figure 2-14(b).

Based on the residuals (Figure 2-14(b)) variogram analyses are performed with results shown in Figures 2-15(a) and 2-15(b) using dashed lines for the vertical and continuous lines for the horizontal direction. Evident from this and the location map of Figure 2-12(a) is that the

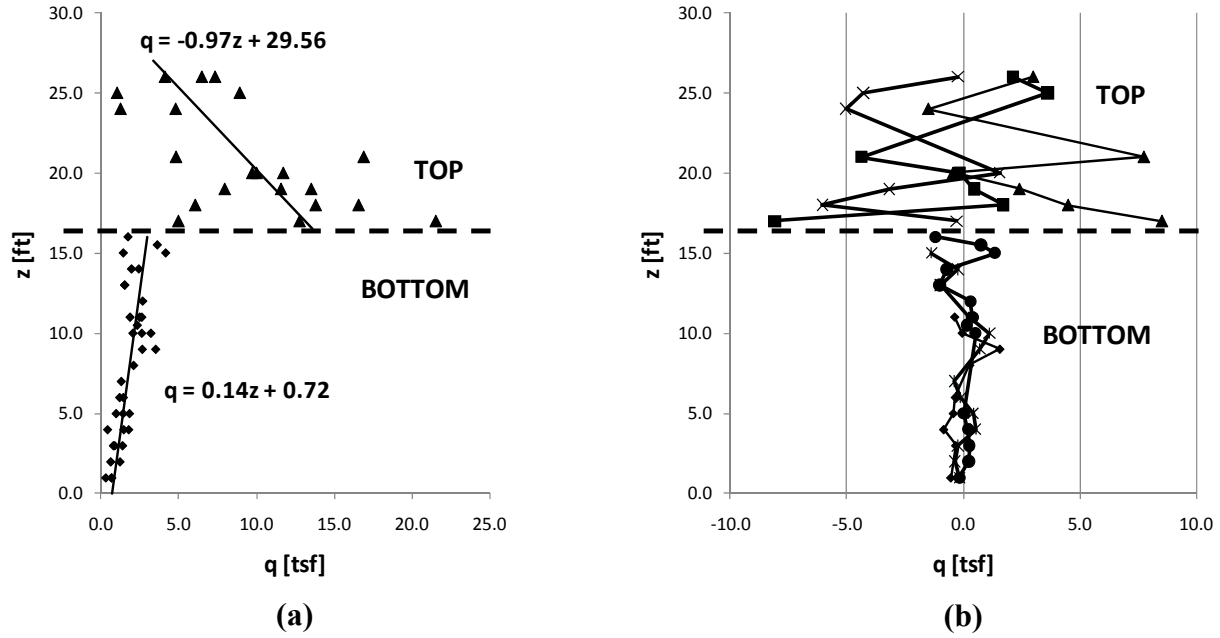

Figure 2-14. Depth profiles: (a) With linear regression lines fitted to data from all borings in each layer; and (b) Residuals (= data values – regression values).

horizontal spacing between the borings is very large and that experimental variogram points may only be found for three distinct lag distances (namely the distances between the borings). With this, it may not be expected to be able to infer a reliable horizontal variogram. In the vertical direction, the amount of data and resolution are better, especially in the bottom layer; however, no spatial correlation is observed, i.e., no consistent decrease in experimental variogram points towards the origin. In the top layer, fewer data are available and the inference of a reliable vertical variogram is additionally limited by a small number of data pairs contributing to each experimental variogram point. Figure 2-15(c) and 2-15(d) are for comparison and depict experimental variograms for the raw data (i.e., before subtracting trends; Figure 2-12(b)) for the bottom and top layer, respectively. As the trends are taken out only in the vertical direction, no significant changes occur in the shape of the horizontal variograms between Figure 2-15(a) and 2.15(b) versus 2-15(c) and 2-15(d) (except for different scaling). In the vertical direction, results

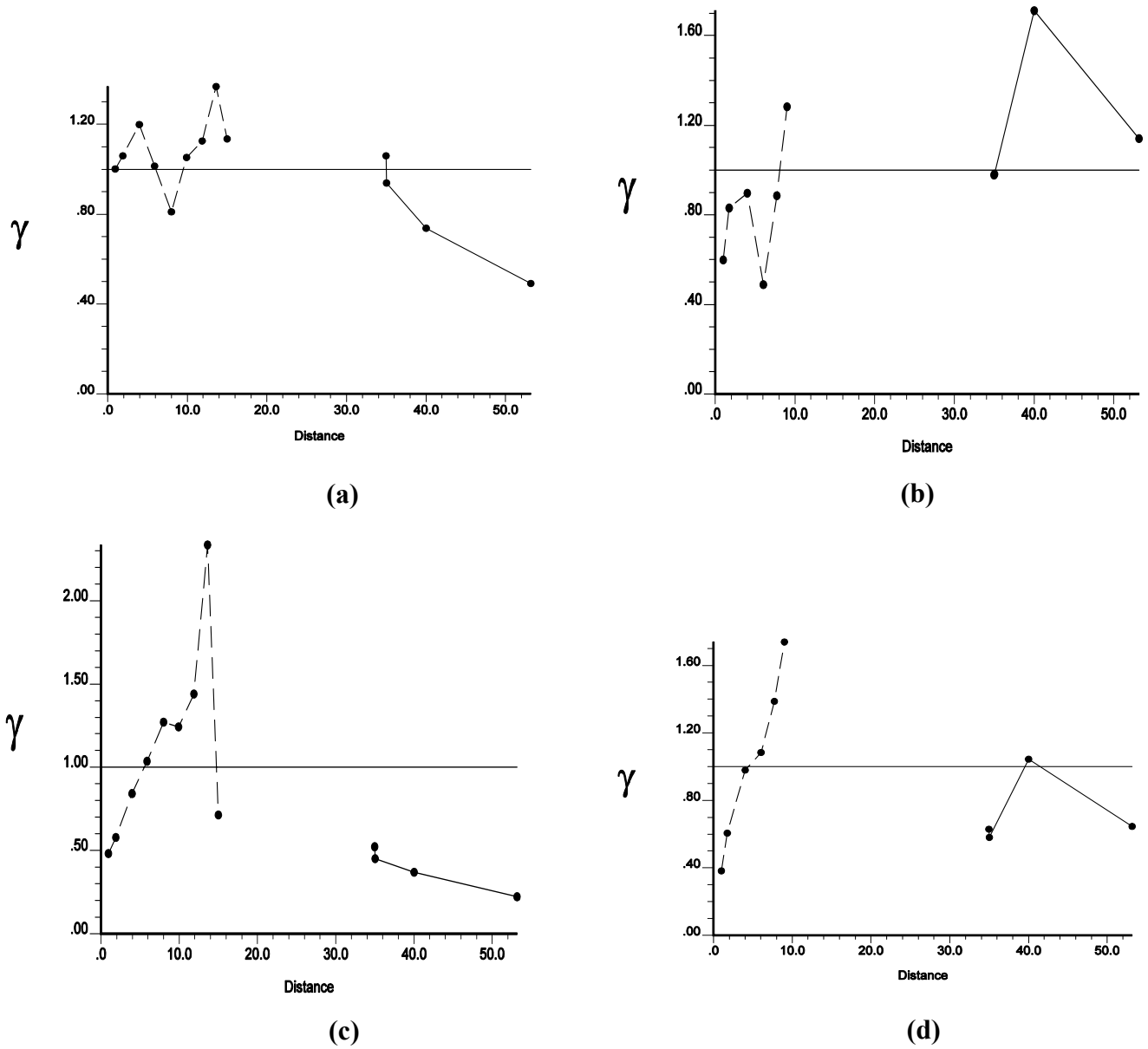

Figure 2-15. Experimental variograms in horizontal (continuous) and vertical (dashed) directions normalized to unit sill: (a) Detrended data (Figure 2-14(b)) – Bottom layer; (b) Detrended data (Figure 2-14(b)) – Top layer; (c) Raw data (Figure 2-12(b)) – Bottom layer; and (d) Raw data (Figure 2-12(b)) – Top layer.

are quite different thus nicely reflecting the effect of a trend. The vertical variogram points in Figure 2-15(c) and 2-15(d) indicate a more or less linear variogram, which does not level off at the sill value of one. Linear variograms belong to the category of non-stationary variogram types

and their identification may motivate a search for deterministic trends in the data. Obviously, in the presence of a monotonous trend function, the variogram cannot become horizontal as the expected difference in data values (Equation 2-7) keeps increasing with distance. An important note in connection with deterministic trend functions is that they are never to be used for extrapolation beyond the spatial domain of where data are available for their inference.

CHAPTER 3
ASSESSMENT OF SHAFT RESISTANCE (UPSCALING) AND LRFD Φ FROM EXHAUSTIVE BOREHOLE/LABORATORY DATA

3.1 Description of the Approach

Based on the geostatistical fundamentals of Chapter 2, this chapter investigates the variability of shaft resistance for known site conditions (e.g., from exhaustive core sampling), but yet unknown (i.e., in some sense arbitrary) shaft location. Section 3.2 develops a variance reduction factor for side friction and a formula to combine it with uncertainty in end bearing, which is developed in Section 3.3. Section 3.4 translates results into terms of LRFD Φ values with an approach for practical implementation in Section 3.5. Section 3.6 finally demonstrates the practical application by continuation of the case studies from Chapter 2.

Shaft resistance R, due to side friction for axial loads at ultimate limit state, is assessed from the local ultimate unit side friction q of the rock (or soil) matrix times the unit surface area dA summed (i.e., integrated) over the lateral shaft surface. While the lateral shaft surface area A_s is typically known from the shaft geometry chosen, the local values of q on A_s are associated with significant uncertainty due to geospatial variability and limited sampling. For instance, in the case of rock, the measured local values of q at a site may be available from core sampling and laboratory testing as $q = \varepsilon\sqrt{q_u q_t}/2$, where q_u is the unconfined compression strength, q_t the split tension strength, and ε the local recovery. Similarly for soil, the cone penetrometer (CPT) tip resistance at a given depth may be used to assess local side friction by multiplying a soil and installation method factor. In the case of cylindrical shafts of length L and diameter D, which is independent of the variability in local ground stiffness (i.e., ultimate, not mobilized), R may be determined from the product of the shaft's lateral surface area $A_s = \pi DL$ and the mean ultimate unit side friction f_s over A_s as

$$R = A_s f_s \tag{3-1}$$

where

$$f_s = \frac{1}{A_s} \int_{A_s} q \cdot dA \tag{3-2}$$

Note that the subscript "s" is used to distinguish variables related to the shaft from variables defined on a (quasi) point support such as q (without subscript). Variable q may be regarded as a spatially random ("regionalized") variable of a certain continuous distribution (e.g., log-normal) and spatial correlation structure (variogram). Its parameters are assumed to be given in terms of expectation m, variance σ^2, and covariance function C(h). As discussed in more detail in the previous chapter, C(h) is a measure of spatial correlation between values of a variable, which are separated by a distance h, and is directly related to the variogram γ(h), i.e., $\sigma^2 - C(h)$; furthermore, by definition, it is known that $C(0) = \sigma^2$. In practice, the above assumption of known parameters m, σ^2, and C(h) corresponds to situations where the geostatistical properties of q at a site are known with high confidence (e.g., from exhaustive core sample testing), and the shaft is located at a random location on the site. Different situations may arise when, (1) core sampling is limited such that m is also associated with some uncertainty; and (2) core sample data are available in the vicinity of a known shaft location for conditioning. While (1) increases the uncertainty in f_s and R, (2) tends to decrease it. Both aspects are investigated in Chapters 4 and 5, respectively.

3.2 Variance Reduction Factor α for Side Friction

Due to Equations 3-1 and 3-2, f_s and R are also random variables in space whose properties depend on those of q and A_s. In the present work, A_s is considered to be deterministic, i.e., the uncertainty in shaft surface area is neglected with respect to uncertainty in rock/soil strength.

Since, for this case, the relationship between f_s and R in Equation 3-1 is very simple, the following discussion is based on f_s and the propagation of uncertainty through Equation 3-2. Variable f_s is described to second order by its expectation m_s and its variance σ_s^2. Due to the simple linear relationship of the arithmetic averaging process in Equation 3-2,

$$m_s = m \tag{3-3}$$

may be immediately found by taking the expectation on both sides. Equation 3-3 states that the expected values of q and f_s are identical. On the other hand, the variability in f_s is reduced with respect to q as a result of the spatial averaging over the shaft surface resulting in $\sigma_s^2 < \sigma^2$. This is introduced in Chapter 2 as "upscaling." In the present case, q may be considered as defined on a point support (cores sample dimensions much smaller than spatial correlation ranges) as opposed to f_s, which is defined on a support equal to the shaft's lateral surface A_s. Factor α can be introduced as the factor of variance reduction between q and f_s and is determined by the relationship

$$\alpha = \frac{\sigma_s^2}{\sigma^2} = \frac{1}{A_s^2} \int_{A_s} \int_{A_s} C'(h) dA_1 A_2 \tag{3-4}$$

where $C'(h) = C(h)/\sigma^2$ is the correlation function or the covariance function normalized to unit variance. While Equation 3-4 implies the assumption of geostatistical stationarity, it is general in that $C'(h)$ can be anisotropic (h is then a directed magnitude) of any permissible type and $A_s = \int_{A_s} dA$ can be any joint or disjoint domain in one or more dimensions. It expresses that α is nothing but the arithmetic average of the normalized covariance values that correspond to all possible combinations of two points in the averaging domain A_s. If A_s consists of a discrete number of n points with statistically independent observations of some random variable, then Equation 3-4 reduces to the well known formula of the standard error $\sigma_s^2 = \sigma^2/n$, i.e., $\alpha = 1/n$.

On the other hand, for perfect correlation over A_s, i.e., $C'(h) \equiv 1$, Equation 3-4 shows $\sigma_s^2 = \sigma^2$ or $\alpha = 1$. These observations indicate a fundamental qualitative relationship: **The larger the averaging domain with respect to the spatial correlation length, i.e., the more independent data included in the averaging process, the larger is the variance reduction from σ^2 to σ_s^2 and the smaller is α.** It may be worthwhile noting that Equations 3-3 and 3-4 are valid independent of the actual distribution type of q, i.e., they are independent of higher order statistical moments, such as skewness or kurtosis.

3.2.1 Single Shaft Foundations

For single shaft foundations, $A_s = \int_0^L \int_0^{2\pi} \frac{D}{2} d\varphi dz = \pi DL$ is the lateral surface area of a cylinder of diameter D and length L, and Equation 3-4 becomes

$$\alpha = \frac{1}{(2\pi L)^2} \int_0^L \int_0^L \int_0^{2\pi} \int_0^{2\pi} C'(h_i) d\varphi_1 d\varphi_2 dz_1 dz_2 \tag{3-5}$$

where $C'(h_i)$ is the normalized covariance function with unit variance, isotropic correlation structure and unit range. By limiting the further analysis to cases of "vertical anisotropy" (i.e., isotropic range in horizontal plane different from range in vertical direction) $h_i = \sqrt{(h_h/a_h)^2 + (h_v/a_v)^2}$ is used as the isotropic lag distance normalized to unit range with $h_h = D\sin[(\varphi_1-\varphi_2)/2]$ and $h_v = z_1 - z_2$ being the horizontal and vertical lag distance components, respectively. Variable a_h is introduced as the isotropic correlation length in all directions of the horizontal plane, while a_v denotes the correlation length in the vertical direction (for $a_h \neq a_v$ this is introduced as geometric anisotropy in Figure 2-6(a)). $C'(h_i)$ is determined from an experi-

mental variogram in practice and is here assumed to be of the spherical (Equation 3-6) or exponential (Equation 3-7) type as depicted in Figure 3-1.

$$C'(h_i) = \begin{cases} 1 - 1.5h_i + 0.5h_i^3 & \text{for } h_i < 1 \\ 0 & \text{for } h_i \geq 1 \end{cases} \tag{3-6}$$

$$C'(h_i) = \exp(-3h_i) \tag{3-7}$$

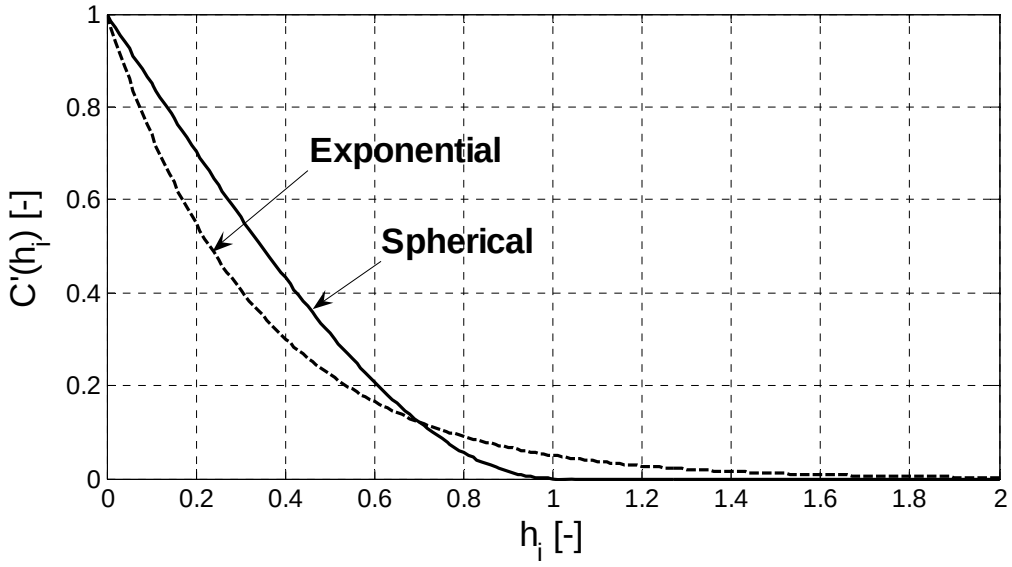

Figure 3-1. Normalized spherical and exponential covariance functions of unit variance and unit isotropic correlation range from Equations 3-6 and 3-7, respectively.

From Equation 3-5, it is evident that the variance reduction factor α depends on both the spatial correlation structure of q as well as the shaft geometry and may be assessed by using $C'(h_i)$ from Equation 3-6 or 3-7 and a set of respective parameters L, D, a_v, and a_h. Results from numerical integration in terms of $\alpha^{1/2}$ (using the square root for better graphical representation and later convenience) as a function of the dimensionless variables L/a_v and D/a_h are represented in Figure 3-2(a) (spherical) and Figure 3-2(b) (exponential). In agreement with the observation discussed earlier, α decreases as L/a_v and D/a_h increases, i.e., as averaging occurs over a larger number of correlation ranges and, thus, independent data. In the extreme case of either L/a_v or

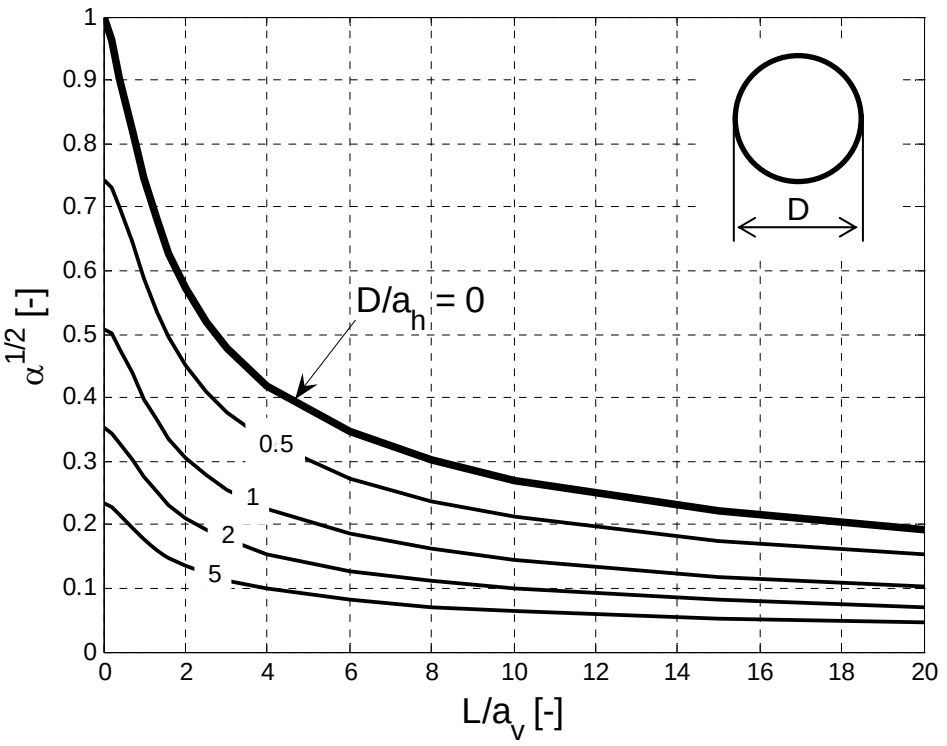

(a)

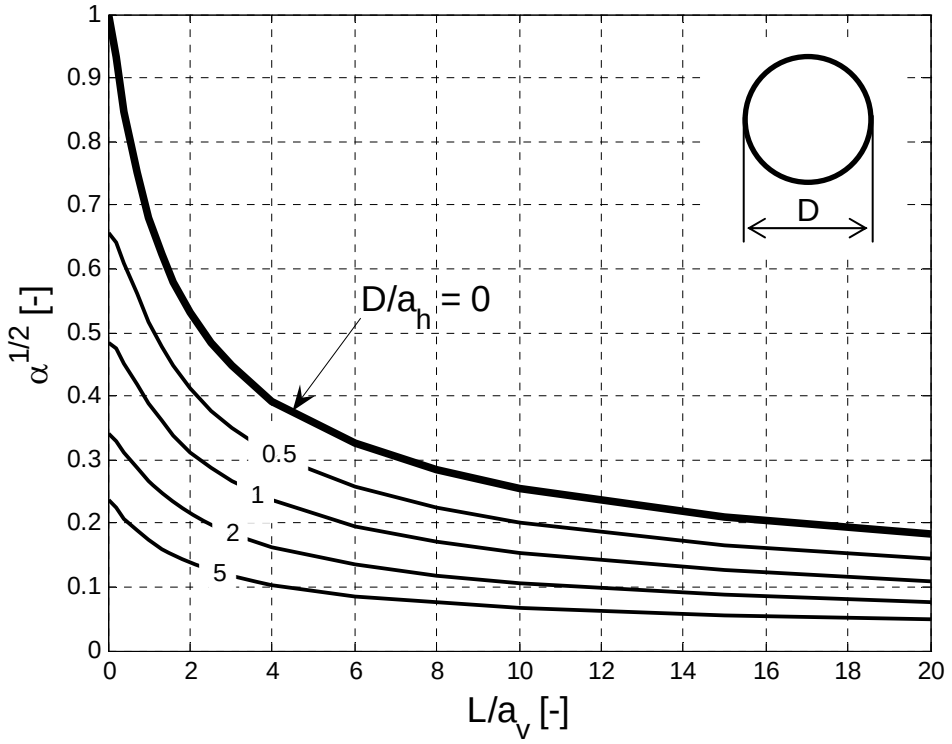

(b)

Figure 3-2. Integration $\alpha^{1/2} = \sigma s/\sigma$ as a function of L/a_v and D/a_h for single shafts: (a) spherical; and (b) exponential covariance model (Equations 3-6 and 3-7, respectively).

D/a_h being very large (e.g., nugget variogram with very short range), α approaches zero. In the opposite case of L/a_v and D/a_h equaling zero, no effective averaging and variance reduction occur leading to $\alpha = 1$. Comparing values of α from Figure 3-2(a) for the spherical covariance model and Figure 3-2(b) for the exponential covariance model reveals both qualitative and quantitative similarity. The most significant differences occur where both L/a_v and D/a_h are smaller than approximately one and the exponential model shows smaller α values. This behavior is easily understood by inspection of Figure 3-1 illustrating a faster decay of correlation for the exponential model over short distances, hence, more effective averaging and lower α. For larger distances, the exponential model is seen to preserve more correlation than the spherical model and, after integration, both effects balance out leading to insubstantial differences in α between the spherical and exponential covariance model. For an analytical derivation and validation of α for the spherical model with $D/a_h = 0$, see Appendix B giving the simple expression $\alpha = 0.75(a_v/L) - 0.2(a_v/L)^2$ for this case and $L/a_v \geq 1$, which will frequently be required in the sequel and denominated by α_0. It may be further observed from Figure 3-2 that minimum (optimized) values for α with given a_h and a_v are only achieved in the impractical cases of either L or D approaching infinity (α going to zero). Similarly, maximum (worst case) values for α, given shaft dimensions L and D, are obtained for the trivial condition of both a_h and a_v approaching infinity, in which case no effective averaging and variance reduction takes place (α going to one).

3.2.2 Multiple Shaft Foundations

In case more than a single shaft (pile) is deployed in a foundation (i.e., under a single cap) then A_s in Equation 3-4 becomes the conjunction (sum) of all lateral surface areas of the shafts involved. That is, the covariance function is not only averaged over all possible location

pairs on each shaft, but also between shafts. An equivalent interpretation is to imagine each individual shaft's resistance as a random variable (of upscaled variance from Equation 3-5) with known covariances to all the other shafts (these upscaled covariances are simply the means of all covariances between location pairs, where one location is on one pile and the other location on a different pile at a certain distance). As separation distances between shafts are typically regular (e.g., 3D between shaft centers), the latter interpretation is more efficient for mathematical implementation. The upscaled variance of a multiple shaft foundation is then nothing but the variance of the mean of a number of correlated variables, which is known to be equal to the mean of all the elements of the variance-covariance matrix of the individual shafts.

With this, variance reduction charts analogous to Figure 3-2 for arbitrary number of shafts and arranged in arbitrary geometries under a pile cap, may be generated. Figures 3-3 and 3-4 represent two examples for triple and quadruple shafts, respectively. It may be seen that the qualitative aspect is not significantly different between single, triple, and quadruple shafts, however, variance reduction for equal L/a_v and D/a_h is the larger (i.e., α smaller), the more individual shafts are deployed. This is again due to the larger horizontal spreading of the foundation's elements causing a more effective horizontal averaging. In practice, however, single and different types of multiple shaft foundations typically possess different shaft design diameters and length (e.g., individual shaft of multiple shaft foundation are thinner as a single shaft), which will affect this comparison. Note, on the other hand, that the thick continuous lines of $D/a_h = 0$ in Figures 3-2(a), 3-3, and 3-4 are identical as they correspond to a very large horizontal correlation length, for which horizontal averaging becomes zero and, as a consequence, the geometry of the foundation in the horizontal plane does not matter anymore. In other words, spatial averaging only occurs in the vertical direction and the foundation may be conceptually reduced to a vertical line of length L for computation of variance reduction.

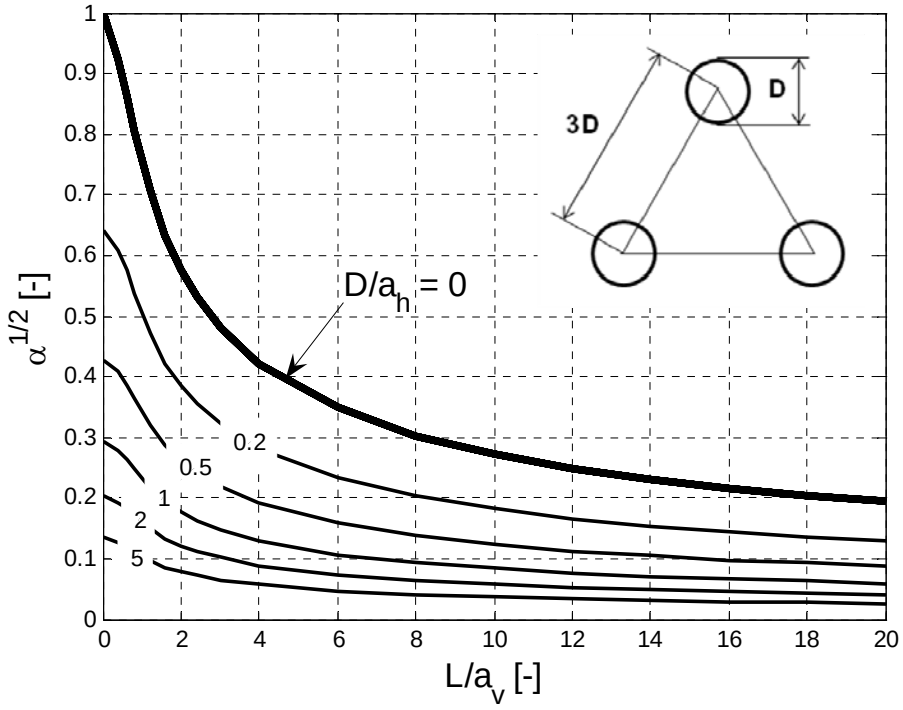

Figure 3-3. Integration $\alpha^{1/2}$ for a triple shaft foundation (isosceles triangle) as a function of L/a_v and D/a_h (3D shaft separation; spherical covariance model).

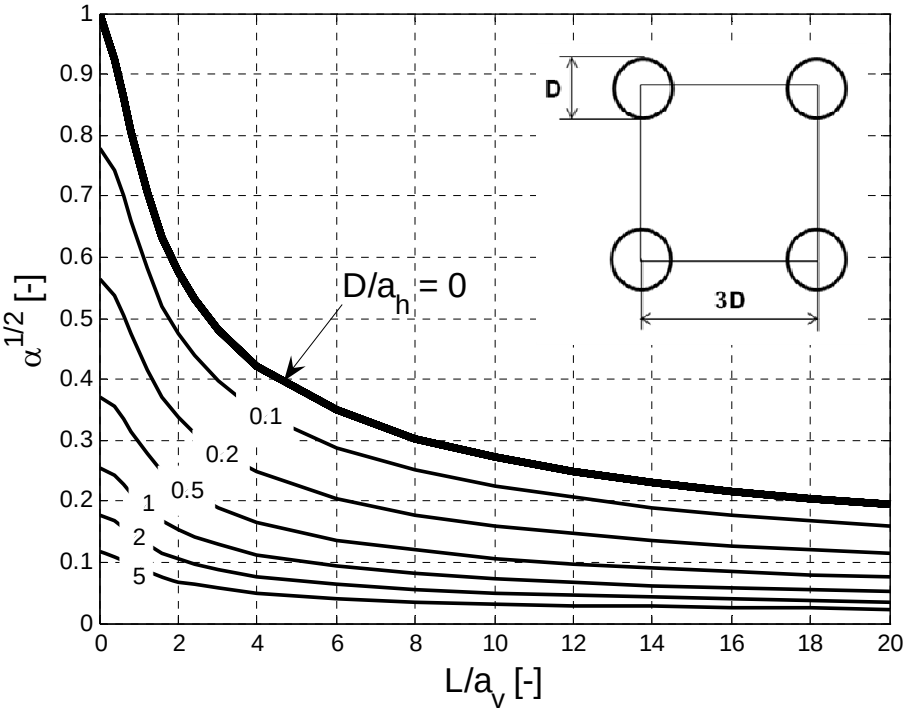

Figure 3-4. Integration $\alpha^{1/2}$ for a quadruple shaft foundation (square) as a function of L/a_v and D/a_h (3D shaft separation; spherical covariance model).

3.2.3 Line Shaft Approximation for Unknown Horizontal Correlation Range

Since variogram inference in practice will be based on core sample data from a limited number of borings, a_h may not always be known. However, knowing a_v from the vertical resolution of the core samples, Figures 3-2, 3-3, and 3-4 indicate conservative (worst case) values for α by assuming very large a_h. As stated above, this is equivalent to not considering any effective averaging on A_s in the horizontal direction or the reduction of the shaft to a vertical line of length L ("line shaft approximation"). Note that the outcome of this line shaft approximation in terms of variance reduction is the same for single and any kind of multiple shaft foundations. If, however, site conditions and characterization are such that a_h is not known, but yet a maximum value can be stipulated, then this value may be used as the worst case scenario and the foundation type will become relevant again for variance reduction.

3.2.4 Nested Variograms and Zonal Anisotropies

In the case of a nested variogram as discussed in conjunction with Figure 2-5, i.e., the sum of n_v variogram structures, the variogram may be divided into a number of independent structures to which Figures 3-2, 3-3, or 3-4 can be applied individually to find an α_i ($i = 1, 2, \ldots, n_v$) for each structure. Each structure corresponds to a certain portion σ_i^2 of the total variability $\sigma^2 = \sum_{i=1}^{n_v} \sigma_i^2$ in q, and α for the compound (nested) variogram is determined as the weighted sum

$$\alpha = \frac{1}{\sigma^2} \sum_{i=1}^{n_v} \alpha_i \sigma_i^2 \tag{3-8}$$

A typical example of nested variograms occurs in the presence of zonal anisotropy components discussed in Figure 2-6(b), which lead to different sill values s_h and s_v of the variogram in the horizontal and vertical directions, respectively. For $s_h < s_v$ more variability is contained in the vertical direction, thus indicating random layering in the spatial distribution of q, which,

however, is too erratic to be captured by a vertical deterministic trend or layer model. In the opposite case of $s_v < s_h$, a random areal trend in q may be present in the horizontal direction between different borings. Both can be regarded as extreme cases of geometric anisotropy, where either a particular variogram component of a_h approaches infinity (as in the case of random layering) or a_v approaches infinity (as in the case of random areal trend). Accordingly, for a variogram component corresponding to random layering, a respective α_i is obtained from the thick continuous line for $D/a_h = 0$, while α_i for a random areal trend component is obtained from the ordinate ($L/a_v = 0$) of Figures 3-2, 3-3, or 3-4.

Even though a_h may not be reasonably inferred from site data, the possible presence of random areal trend components is easily recognized by observing a vertical variogram sill s_v that is smaller than the site variance σ^2. Random areal trend components represent variability in q, which is not contained in the vertical direction, and, hence, does not suffer any variance reduction with the line shaft approximation. In Equation 3-8, this is reflected by a respective value of $\alpha_i = 1$, i.e., the magnitude (variance) of a random areal trend component, is directly propagated into the variance in shaft resistance. Intuitively speaking, this represents a situation of increased uncertainty, since an entire shaft may be located in a zone of either high or low strength, which persists over the whole depth of the site investigated. An analogous reasoning can be followed for the opposite situation (but rather irrelevant in practice) of unknown a_v, known a_h, and a random layering component in the variogram. Finally, as pointed out in the previous chapter (Figures 2-1 and 2-14), it should be noted that possible deterministic trend components in q need to be removed before variogram analysis and application of Figures 3-2, 3-3, 3-4 or equivalent figures for other multiple shaft configurations, and subsequently added back in.

3.2.5 Deterministic Layering and Effect of End Bearing

Chapter 2 lays out the principle of stationarity and explains the effect of dividing a site into statistically homogeneous sub-domains if necessary (e.g., Figures 2-1 and 2-14). Most relevant in this aspect is division into sub-domains, which are either horizontally or vertically separated. While it is rather unlikely (and to be avoided if happening) that a foundation is partially located on more than a single sub-domain in the horizontal direction, it frequently occurs that a foundation penetrates more than one distinct geological layer in the vertical direction. Moreover, the above results are obtained for resistance due to side friction only, i.e., not considering possible contributions of end bearing. Defining the nominal resistances R_n as the expected value of shaft resistance, Equations 3-1 and 3-3 immediately lead to $R_n = A_s m$, if the foundation (single or multiple shaft) is confined in a single stratigraphic layer. Due to the proportionality between f_s and R in Equation 3-1, the foundation coefficient of variation $CV_R = \sigma_s/m_s$ may be rewritten by Equations 3-3 and 3-4 as

$$CV_R = \frac{\sqrt{\alpha\sigma^2}}{m} = \sqrt{\alpha} CV_q \tag{3-9}$$

Here $CV_q = \sigma/m$ is the coefficient of variation in the core sample data q. However, Equation 3-1 assumes that the properties of q are statistically homogenous over the depth of the foundation (single layer) and that end bearing resistance is neglected. In order to include the possibility of stratigraphic layering over the depth of a foundation and the contribution of end bearing, Equation 3-1 is generalized to

$$R = \pi D \sum_{j=1}^{n_L} L_{Lj} f_{sLj} + R_{EB} \tag{3-10}$$

where L_{Lj} are the known (deterministic) length intervals of the shaft, and f_{sLj} the respective uncertain spatial averages of side friction over the shaft surface in each of n_L layers; R_{EB} is the

uncertain end bearing resistance. By taking the expectation of R in Equation 3-10 and using Equation 3-3, one obtains a more general form of the nominal resistance R_n as

$$R_n = \pi D \sum_{j=1}^{n_L} L_{Lj} m_{Lj} + m_{EB} \tag{3-11}$$

where m_{Lj} are the expected values of f_{sLj} (and hence q) in each layer and m_{EB} is the expected value of end bearing resistance. By considering all f_{sLj} (j = 1, 2, …, n_L) and R_{EB} as independent random variables in Equation 3-10 (reasonable in view of discontinuous layering and ultimate limit state), the variance σ_R^2 of R can be written as

$$\sigma_R^2 = \pi^2 D^2 \sum_{j=1}^{n_L} L_{Lj}^2 \sigma_{sLj}^2 + \sigma_{EB}^2 \tag{3-12}$$

where σ_{sLj}^2 are the variances of f_{sLj} in each layer and σ_{EB}^2 is the variance in end bearing resistance. From Equation 3-4 $\sigma_{sLj}^2 = \alpha_{Lj}\sigma_{Lj}^2$ is known, where α_{Lj} is obtained from Equation 3-8 for each layer and σ_{Lj}^2 is the variance in q for each layer. A generalized expression for CV_R from Equations 3-11 and 3-12 is

$$CV_R = \frac{\sigma_R}{R_n} = \frac{\sqrt{\pi^2 D^2 \sum_{j=1}^{n_L} L_{Lj}^2 \alpha_{Lj} \sigma_{Lj}^2 + \sigma_{EB}^2}}{\pi D \sum_{j=1}^{n_L} L_{Lj} m_{Lj} + m_{EB}} \tag{3-13}$$

which reduces to Equation 3-9 for $n_L = 1$ (single layer) and $m_{EB} = \sigma_{EB}^2 = 0$ (no end bearing). Note that Equation 3-13 is also general in the sense that contributions to R_n from previously subtracted deterministic trend components in one or more layers may be simply added to the denominator, while the numerator remains unaffected. In summary, Equations 3-11 and 3-13 are obtained by considering the contributions of side friction in each layer and end bearing to total shaft resistance R as independent random variables with different expected values and variances that can be added up to arrive at R_n and CV_R of the whole shaft. While respective parameters for

side friction resistance may be obtained for each individual layer as described above, the determination of m_{EB} and σ_{EB}^2 for end bearing is discussed in the following section.

3.3 End Bearing Resistance and Uncertainty for Single Shafts

The shaft's tip resistance Q_{tip} is found by multiplying the mobilized unit tip stress q_b by the tip's cross-section area. The mobilized unit tip resistance of the shaft is a function of the shaft's displacement (FHWA: FB-DEEP) as

$$q_b = \Lambda W_t^{0.67} \tag{3-14}$$

where Λ = Elastic compressibility parameter of the shaft; and

W_t = Displacement at top of shaft.

The settlement of the bottom of the shaft W_b is computed from the elastic shortening of the shaft as follows:

$$W_b = W_t - \left[\frac{2\left(Q_{top} + Q_{tip}\right)L}{\pi\, E_c\, D^2}\right] \tag{3-15}$$

where E_c = Young's modulus of the concrete shaft;

Q_{top} = Force at top of shaft; and

Q_{tip} = Force at bottom of shaft ($q_b\, A_{shaft}$).

The shaft's tip elastic compressibility parameter Λ is given as a function of Θ_f, Γ, and Ω as follows:

$$\Gamma = 0.37\left(\frac{L}{D}\right)^{0.5} - 0.15\left[\left(\frac{L}{D}\right)^{0.5} - 1\right]\log_{10}\left(\frac{E_c}{E_m}\right) + 0.13 \tag{3-16}$$

$$\Omega = 1.14\left(\frac{L}{D}\right)^{0.5} - 0.05\left[\left(\frac{L}{D}\right)^{0.5} - 1\right]\log_{10}\left(\frac{E_c}{E_m}\right) - 0.44 \tag{3-17}$$

which gives Λ as

$$\Lambda = 0.0134 E_m \frac{\left(\frac{L}{D}\right)}{\left(\frac{L}{D}+1\right)} \left\{ \frac{200\left[\left(\frac{L}{D}\right)^{0.5} - \Omega\right]\left[\frac{L}{D}+1\right]}{\pi L \Gamma} \right\}^{0.67} \tag{3-18}$$

where E_m = is the mass modulus of the rock;

L = Total length of shaft; and

D = Diameter of the shaft.

In FHWA's (FB-DEEP) tip resistance versus tip displacement approach, the Young's modulus of the rock mass E_m is of significant importance. The latter is different from the Young's modulus of intact rock samples E_i measured in the laboratory (ASTM D3148). The rock mass Young's modulus E_m represents the whole mass including fissures, voids, slip planes, etc. O'Neill et al. (1996) suggests a correlation (Table 3-1) between the E_i and E_m based on rock quality description (RQD). If RQD values are less than 20%, the RQD correlation for 20% is used.

Table 3-1. Estimation of E_m/E_i Based on RQD

Estimation of E_m/E_i based on RQD		
RQD	E_m/E_i	E_m/E_i
%	Closed Joint	Open Joint
100	1	0,6
70	0,7	0,1
50	0,15	0,1
20	0,05	0,05

Source: O'Neill et al. (1996).

Of interest is the relationship between Florida limestone mass modulus E_m and intact Young's modulus E_i. In tests, synthetic limestone specimens with various strengths were cast with different volume percentages of voids (resembled with the inclusion of styrofoam pellets). A comparison of no void Young's modulus (E_i)versus mass modulus (E_m) values with different void volume percentages (i.e., recovery) was completed. Shown in Figure 3-5 are the E_m/E_i ratios as reported by O'Neill et al. (1996) and University of Florida (UF). Evidently, the UF data fall between O'Neill's open and closed joint data. Also, there exists a linear relationship between E_m/E_i for recoveries above 50% and below this is a sharp drop off.

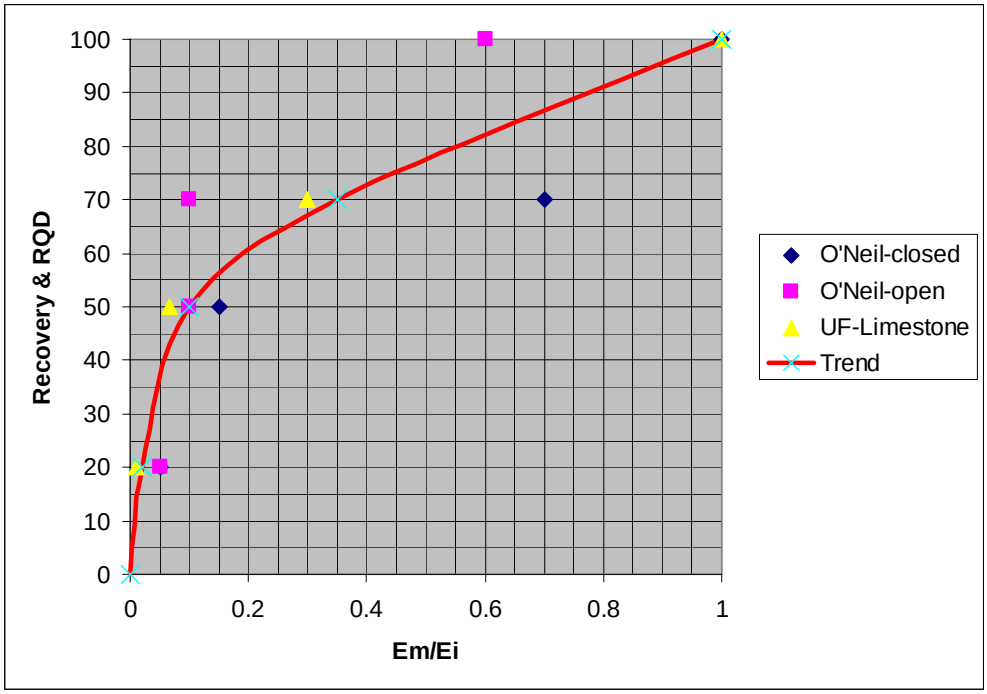

Figure 3-5. O'Neill et al. (1996) E_m/E_i versus RQD and UF E_m/E_i versus recovery.

Shown in Figure 3-6 is a typical stress-strain plot from an unconfined test on Florida limestone recovered from 17th Street Bridge near the load test LTSO4 at Pier 10. A total of 102 unconfined tests were performed by State Materials Office (SMO) personnel on rock cores recovered in six boreholes (see Figure 2-9(a)) at 5-foot spacing near LTSO4. The analysis

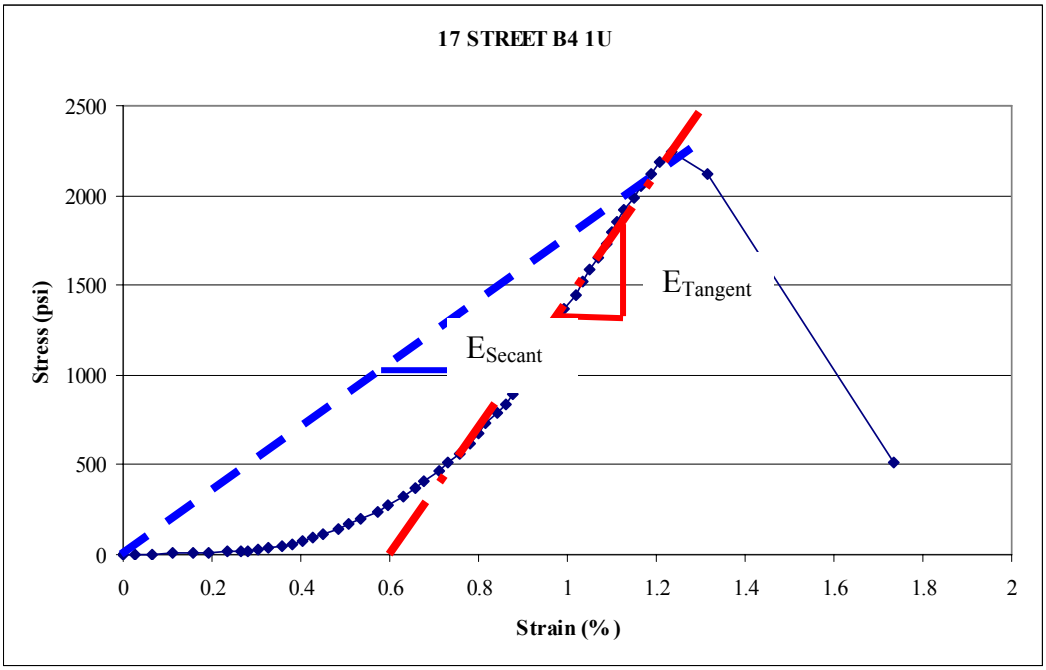

Figure 3-6. Secant versus tangent Young's modulus on 17th Street data from LTSO4.

considered both the secant Young's modulus as well as the tangent Young's modulus in the assessment. From the boring logs, the recoveries varied from 65% to 95% with a mean value of 75%. Based on Figure 3-5, an E_m/E_i ratio of 0.45 was selected, and the mass modulus was computed using both the secant and tangent E_i. Figures 3-7 and 3-8 show the probability density distribution for the tangent and secant mass moduli, using both the recent LTSO4 data (102 tests), as well as the original design data (16 tests). Also shown in each figure are summary statistics (median, mean, standard deviation, and CV) of the data as well as log-normal fits to the data.

Evident from a comparison of Figures 3-7 and 3-8, the mean of the tangent modulus is approximately 1.8 times the secant mean modulus, but the variation CV of each are quite similar. The latter suggests an inherent or systematic bias associated with the testing process. One possible explanation is the sample preparation, i.e., cutting of sample with circulating saw

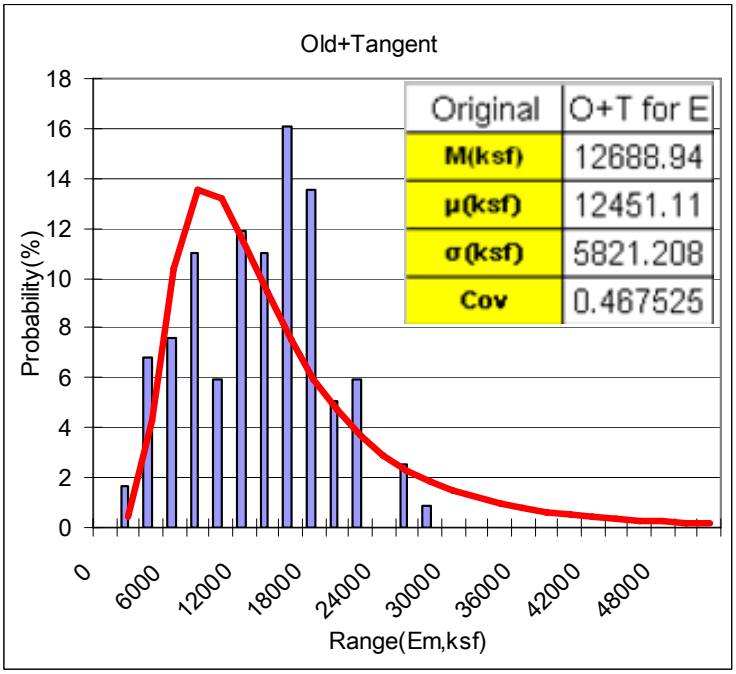

Figure 3-7. Tangent mass modulus of 17th Street Bridge (118 values).

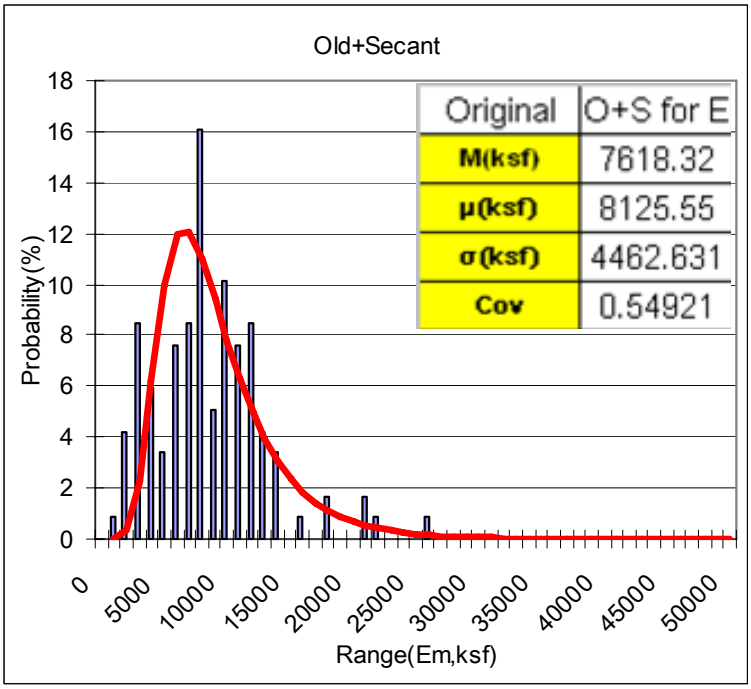

Figure 3-8. Secant mass modulus of 17th Street Bridge (118 values).

may create asperities, wobble, and even vibration-induced micro damage at the ends. Another explanation could be the use of compressible paper or the presence of micro particles at the ends of the specimens. Of interest is the impact the secant versus the tangent mass modulus has on the mobilized tip resistance (Equations 3-16 through 3-18).

Clearly, from Figures 3-7 and 3-8 the mass modulus of the rock varies considerably over the site as well as within 3D below the shaft and must be accounted for in Equations 3-16 through 3-18. The first work on elastic solutions (stress and deformation) for layered material beneath a foundation was reported by Ueshita and Meyerhof (1967) and later by Poulos and Davis (1972). That work featured two layer solutions that considered different stiffness or moduli representations for each layer. The work introduced an equivalent modulus [i.e., E of layer 1 × coefficient (function of E_1/E_2 and layer thickness)] to evaluate footing settlements. Subsequent efforts (Menard et al. 1972) introduced the use of harmonic mean,

$$\frac{n}{E_h} = \left[\frac{1}{E_1} + \frac{1}{E_2} + \ldots + \frac{1}{E_n} \right] \ldots\ldots. \tag{3-19}$$

and in the case of different layer thickness,

$$E_h = \left[\frac{1}{H} \int_0^H \frac{dz}{E(z)} \right]^{-1} \tag{3-20}$$

Recently, Fenton and Griffiths (2005) showed an excellent correlation between finite element modeling (FEM) and a single layer solution using the geometric mean for the material modulus, i.e.,

$$E_g = \left(\prod_{i=1}^{n} E_i \right)^{1/n} = \exp\left(\frac{1}{n} \sum_{m=1}^{n} \ln(E_m) \right) \tag{3-21}$$

It should be recognized that the geometric mean generally lies between the arithmetic and harmonic mean and it was the modulus used to characterize drilled shaft end bearing resistance q_b (Equation 3-14).

Also, of importance is the influence of spatial correlation (e.g., covariance function) on the geometric mean modulus (E_g). Specifically, Equation 3-21 requires the sum or average of ln (E_m) over distance (3D) below the footing. If Y is allowed to equal ln(E_m), i.e., the term inside the parentheses of Equation 3-21, then geometric mean (E_g) becomes the simple arithmetic average, i.e., $1/n \sum Y = F$. Note, because Y [ln(E_m)] is a random variable, so is F and it will have the general summary statistics, i.e., m_F, and σ^2_F. As discussed with side friction, the mean of F(m_F) will be the same as m_Y; however, the variance of F, i.e., σ^2_F will be reduced by the averaging process $(\text{i.e., } 1/n\sum Y = F)$ or $\sigma^2_F = \alpha\, \sigma^2_Y$, where σ^2_Y represents the variance of ln(E_m) over the site. As was found with side friction, Equation 3-5 for α or the nomograph (Figure 3-2) may be used to assess α for the case of D=0 (i.e., thick line), and appropriate vertical correlation length a_v. Once the value of α has been assessed, then the random function F ($m_F = m_Y$, and $\sigma^2_F = \alpha\, \sigma^2_Y$) is known and it may be substituted back into Equation 3-21 to obtain E_g, i.e., E_g = exp (F), which is also a random function.

For the case of 17th Street Bridge, the ln(E_m) was calculated for all the new and old tangent data, i.e., Figure 3-7 with a mean (m_Y of ln (E_m)) of 9.27 ksf, and the standard deviation (σ_Y of ln(E_m)) of 0.41 ksf. Next, the alpha (α) was obtained for D = 0, L=30 ft, and a_v = 5, 10, and 15 from Figure 3-2 from which $\sigma^2_F = \alpha\, \sigma^2_Y$ was found. Subsequently, a Monte Carlo simulation was performed to generate typical F values, which were substituted into Equation 3-21, i.e., E_g = exp (F) to give the distributions shown in Figures 3-9, 3-10, and 3-11.

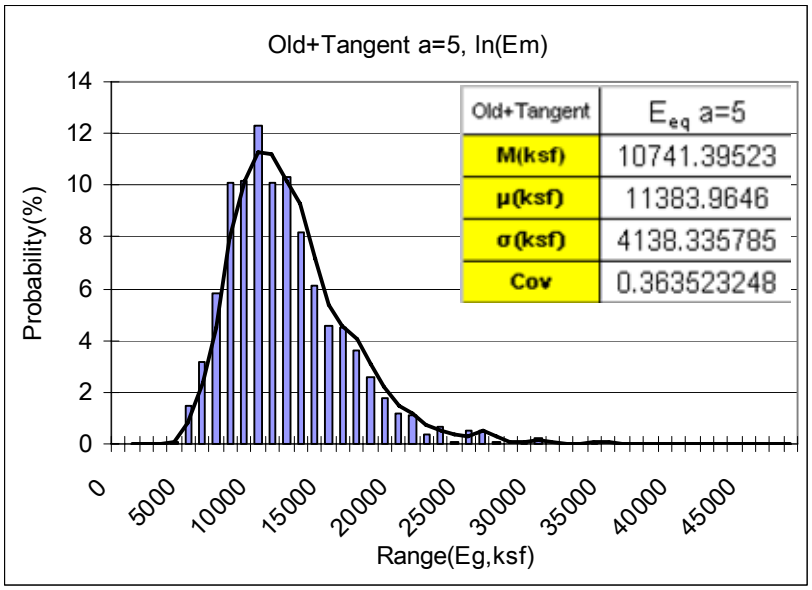

Figure 3-9. Geometric mean modulus E_g assuming correlation length a = 5 ft.

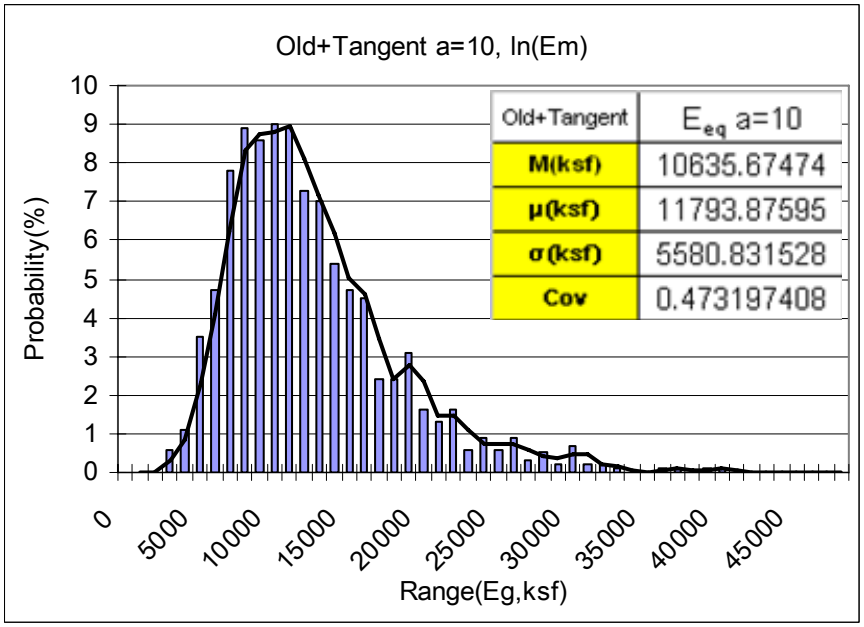

Figure 3-10. Geometric mean modulus E_g assuming correlation length a = 10 ft.

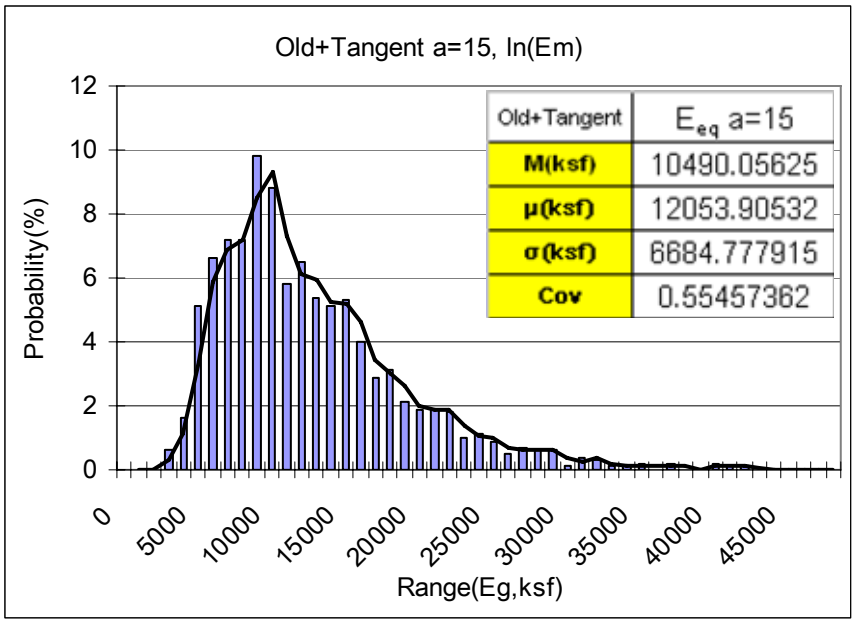

Figure 3-11. Geometric mean modulus E_g assuming correlation length a = 15 ft.

Of interest is a comparison of the geometric mean modulus (E_g) with the original field data (E_m), as well as the inverted log-normal distribution (i.e., exp (Y)), which is shown as the red curve in Figure 3-7 and has summary statistics of mean = 13,140 ksf, standard deviation, σ = 10,326 ksf, and CV = 0.79. The red curve represents what the field samples should look like if enough samples were recovered and the mass modulus (E_m) was log-normally distributed. As expected, the mean of geometric mean (μ) in Figures 3-9 through 3-11, was reduced from both the field sample mean (12,689 ksf) and assumed inverted log-normal mean (13,140 ksf). However, larger changes occurred in the CV of the E_g versus the original field (0.47) and inverted log-normal CV (0.79). Specifically, due to spatial correlation represented in the covariance function as correlation length a (5 ft, 10 ft, and 15 ft), the CV of E_g was reduced to 0.36, 0.47, to 0.55, respectively. The highest reduction in CV of E_g to 0.36 is due to the lack of

correlation between E_m over short distances (i.e., more random), which results in lower variability in E_g when averaged geometrically.

Using the geometric mean function (E_g, Figures 3-9 through 3-11) in Equations 3-16 through 3-18, and subsequently Equation 3-14, the distribution of the contact stress q_b at the bottom of the drilled shaft was obtained for a top shaft movement of 1.6″ (field data), as shown in Figures 3-12, 3-13, and 3-14. Note, the figures represent the expected distribution of end bearing on the east side of the site where all the data were collected (i.e., vicinity of LTSO4). From earlier analysis, i.e., Figure 2-11, the variograms showed typical vertical correlation length of approximately 5 ft, which from Figure 3-12 suggests a mean unit tip resistance of 121 ksf with a range (based on one standard deviation above and below the mean) of 85 ksf to 155 ksf. The actual recorded unit tip resistance was 120 ksf for LTSO4 and the other east side shaft LTSO3 had a resistance of 110 ksf. Both were close to the mean and well within the one standard deviation (84 to 158 ksf).

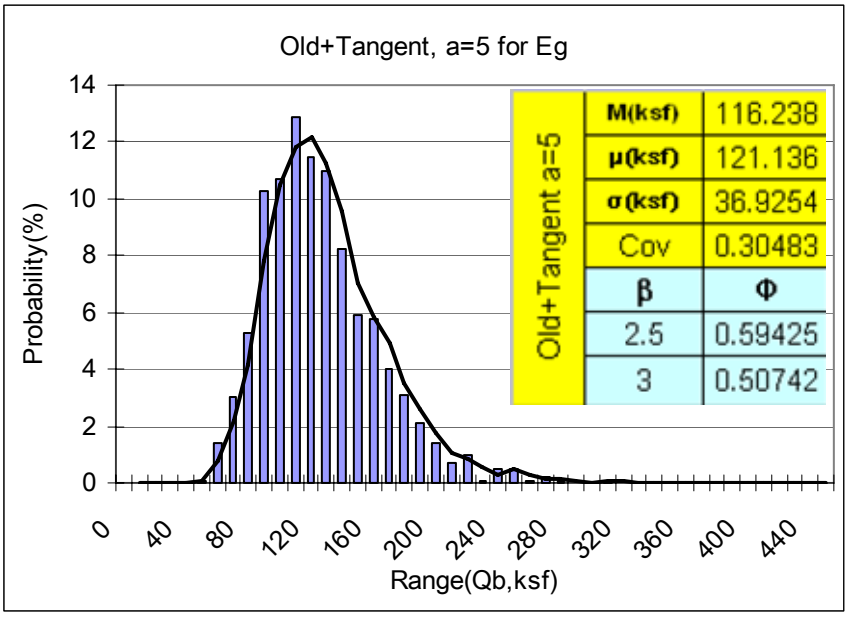

Figure 3-12. Histogram/PDF of contact stress q_b using E_g with correlation length a = 5 ft.

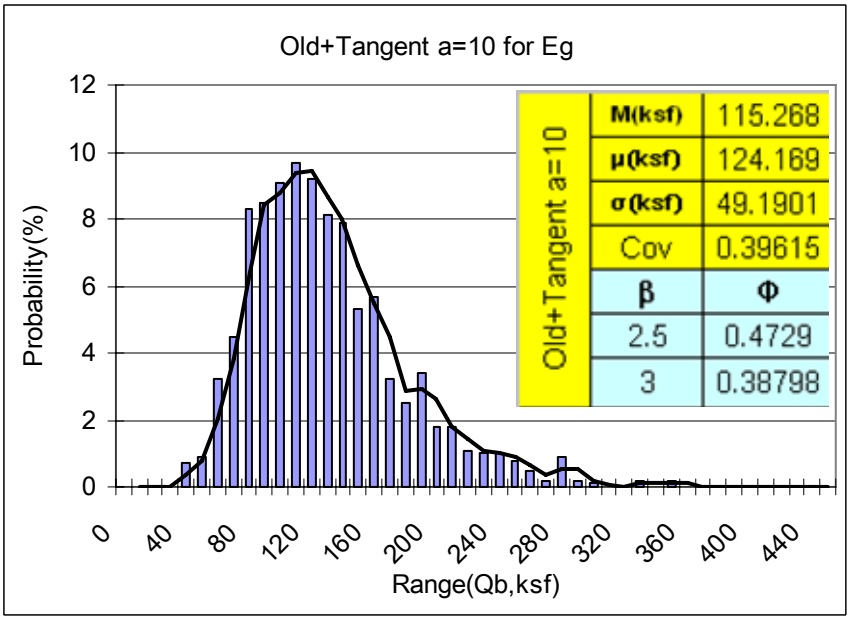

Figure 3-13. Histogram/PDF of contact stress q_b using E_g with correlation length a = 10 ft.

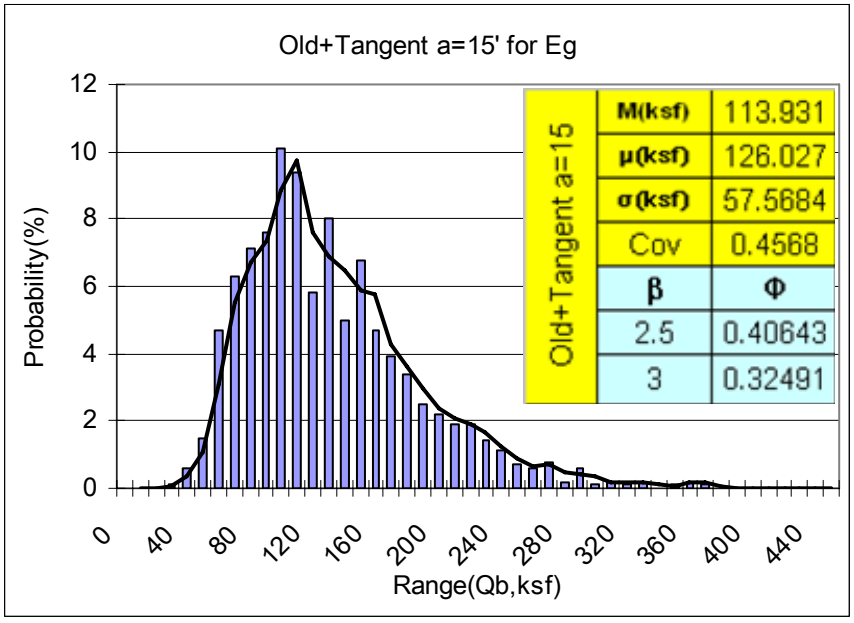

Figure 3-14. Histogram/PDF of contact stress q_b using E_g with correlation length a = 15 ft.

Knowing the mean unit tip resistance, the total nominal tip resistance (after conversion to tsf) is obtained by multiplication with the circular tip area ($A_{tip} = 4^2\pi/4$ for D = 4') resulting in m_{EB} = 760 tons. Its standard deviation or variance $\sigma^2_{EB} = A^2_{tip}(37/2)^2 = 53991$ tons^2 gives a coefficient of variation $CV_{EB} = 0.31$. The variance of the whole shaft (Equation 3-12) may be found, as well as its coefficient of variation CV_R (Equation 3-13) from which the LRFD resistance factors (Φ) may be determined (Section 3.4). Of interest is the scale of variance found for the shaft's side resistance versus its end bearing, which will impact the final LRFD Φ assigned to the whole shaft (see case study in Section 3.6.1).

3.4 Development of LRFD Φ

Knowing CV_R from Equation 3-9 or 3-13, Equation 3-22 as used by the FHWA and Equation 3-23 can be applied to determine LRFD resistance factor Φ

$$\Phi = \frac{\lambda_R\left(\gamma_D \frac{Q_D}{Q_L} + \gamma_L\right)\sqrt{\frac{1+CV_Q^2}{1+CV_R^2}}}{\left(\lambda_{QD}\frac{Q_D}{Q_L} + \lambda_{QL}\right)\exp\left\{\beta\sqrt{\ln\left[\left(1+CV_R^2\right)\left(1+CV_Q^2\right)\right]}\right\}} \tag{3-22}$$

$$CV_Q^2 = \frac{\left(\frac{Q_D}{Q_L}\lambda_{QD}CV_{QD}\right)^2 + \left(\lambda_{QL}CV_{QL}\right)^2}{\left(\frac{Q_D}{Q_L}\lambda_{QD}\right)^2 + 2\frac{Q_D}{Q_L}\lambda_{QD}\lambda_{QL} + \lambda_{QL}^2} \tag{3-23}$$

Here, CV_Q denotes the coefficient of variation of the random loads. Resulting from this, Figure 3-15 shows a chart of Φ as a function of CV_R and user selected reliability index (β). For a given β the probability of failure is known to be G(-β), where G is the standard normal cumulative distribution function. The remaining dimensionless parameters in Equations 3-22 and 3-23 are chosen according to the FHWA/AASHTO recommended values (for load cases I, II, and IV), i.e.,

Dead load factor:	γ_D	= 1.25
Live load factor:	γ_L	= 1.75
Dead to live load ratio:	Q_D/Q_L	= 2
Resistance bias factor:	λ_R	= 1.06
Dead load bias factor:	λ_{QD}	= 1.08
Live load bias factor:	λ_{QL}	= 1.15
Dead load coefficient of variation:	CV_{QD}	= 0.128
Live load coefficient of variation:	CV_{QL}	= 0.18

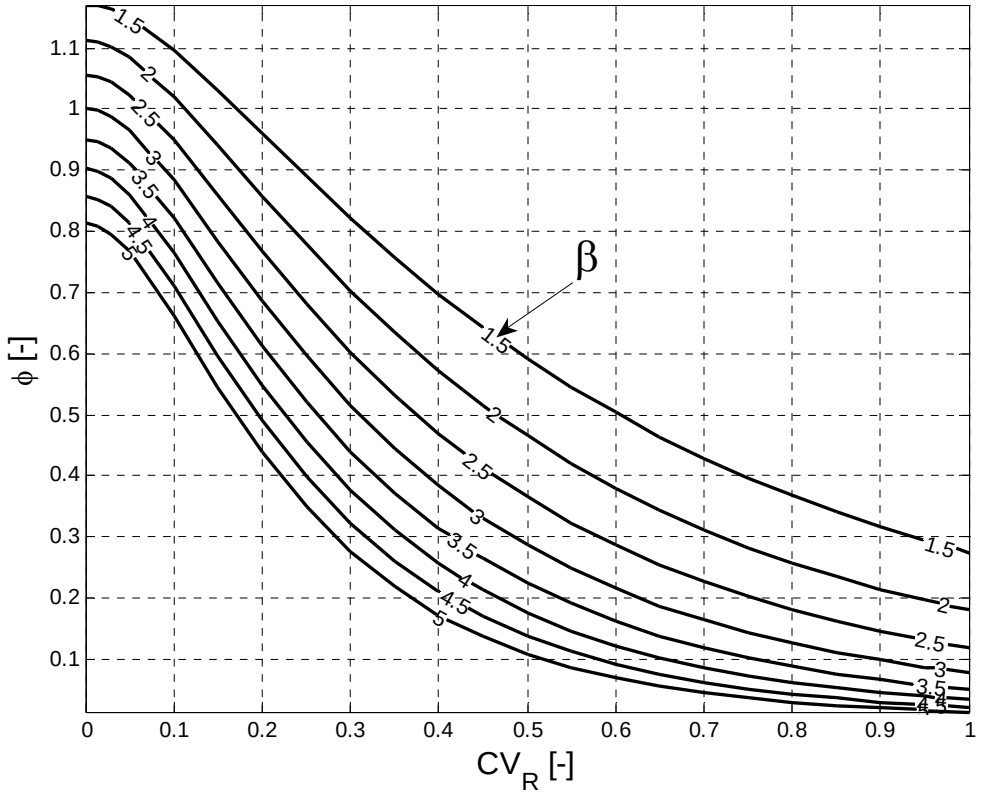

Figure 3-15. LRFD resistance factor Φ as a function of resistance coefficient of variation CV_R and reliability index β (Equation 3-22).

The bias factors λ_R, λ_{QD}, and λ_{QL} are hereby defined as respective means of a large number of observed ratios between measured and predicted values. Furthermore, it is recalled that

Equation 3-22 is based on the assumption of log-normal resistance and load distributions and can be derived by the First Order Second Moment (FOSM) method. While a discussion of the properties of the load distribution exceeds the scope of the present work, the assumption of a log-normal resistance distribution is briefly evaluated. The fact that q is non-negative and typically skewed to the right suggests the fit of a log-normal distribution of q. In the same way as the reduction of variance from q to f_s in Equation 3-2 becomes stronger as data independence over the averaging domain increases, the central limit theorem predicts a reduction in skewness from q to f_s, which increases as more independent data are averaged. It is a property of the log-normal distribution that the skewness decreases with the variance and although means of log-normal variables are not strictly log-normal in theory, it can be a sufficiently accurate approximation for many practical purposes. As a consequence, the assumption of a log-normal resistance distribution in Equation 3-22 is plausible, provided that the distribution of q is reasonably log-normal.

3.5 Practical Implementation

For the past discussions, the nominal resistance R_n and Φ were found for a given site with known pile dimensions. In practice, however, foundation design usually involves knowing the nominal load and selecting the appropriate shaft dimensions L and D for given soil/rock properties and reliability index β. Since Φ is a complex function of L and D, this "inverse problem" deserves special attention. In an effort to find a practitioner-friendly solution to this problem, a graphical iteration method is presented in this section based on the "quadrant chart" depicted in Figure 3-16. Four individual charts are arranged in a way that they share their axes with two neighboring charts such that when one chart is left at one axis, the respective neighboring chart is automatically entered. By prescribing a value for D, each chart possesses a series of curves whose parameters are known. The purpose of this solution is to perform a

graphical iteration process to find L (starting from a guessed initial value) by "looping" through the quadrant chart in counter-clockwise direction as described below and demonstrated in the next section.

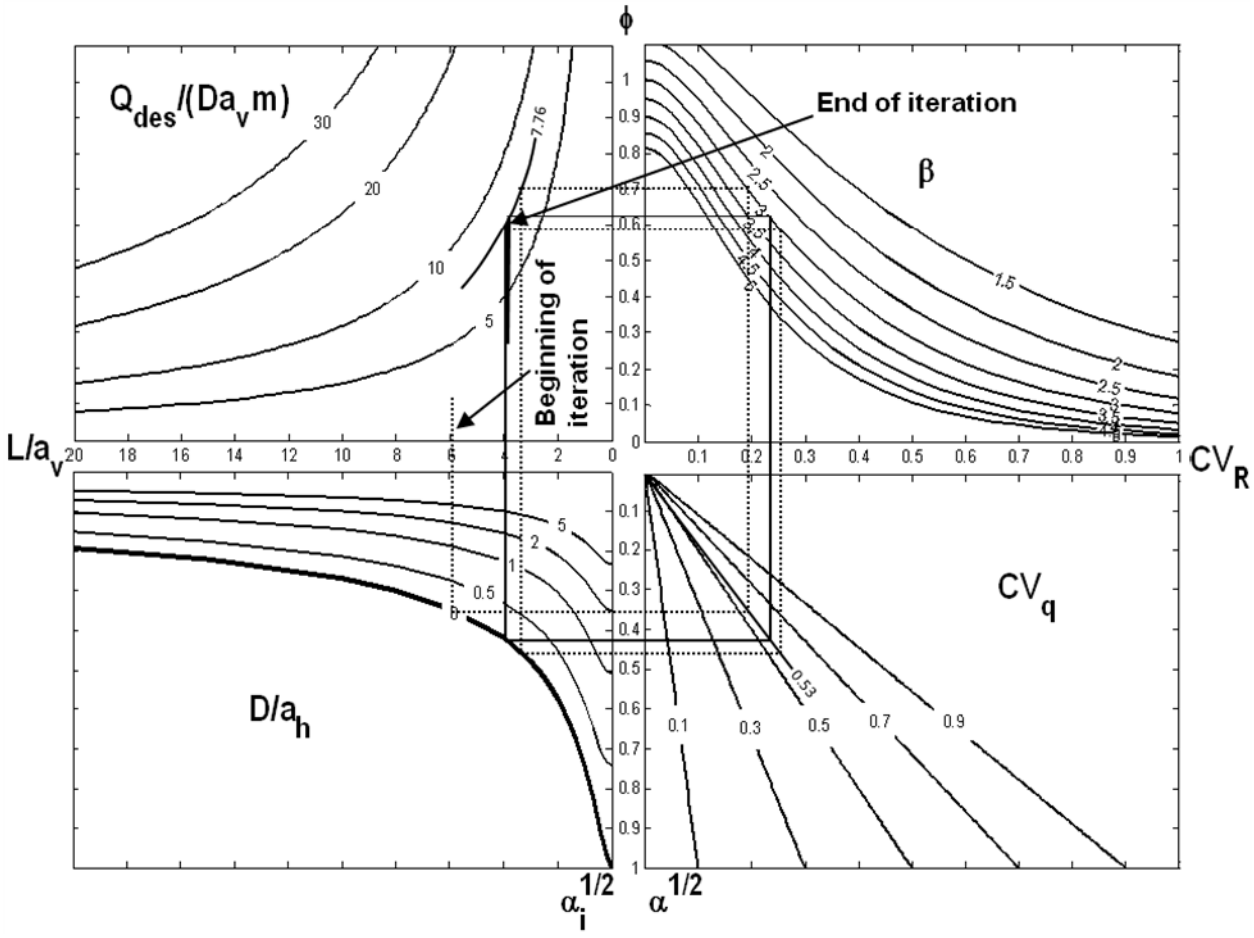

Figure 3-16. Dimensionless quadrant chart for single shaft design by graphical iteration.

Each individual quadrant of the chart represents a fundamental relationship of the design process. Starting in the top-right corner and going counter-clockwise, these relationships are:

- **<u>1st quadrant</u>**: $\Phi = f(CV_R)$ as shown in Figure 3-15 from Equation 3-22 where β is a known parameter;
- **<u>2nd quadrant</u>**: $L/a_v = f(\Phi)$ using the LRFD design equation, $Q_{des} = R_n\Phi = DL\pi m\Phi$ (from Equation 3-3) gives $L/a_v = Q_{des}/(Da_v m\pi\Phi)$, which are hyperbolas where $Q_{des}/(Da_v m)$ is a known parameter;

- **3rd quadrant**: $\alpha^{1/2} = f(L/a_v)$ using Equation 3-4 where D/a_h is a known parameter; and
- **4th quadrant**: $CV_R = f(\alpha^{1/2})$ using Equation 3-9 are straight lines where CV_q is a known parameter.

Figure 3-16 contains Figure 3-2(a) (variance reduction chart for single shafts) in the 3rd quadrant and, as a consequence, is limited to the design of single shaft foundations. With the substitution of either Figure 3-3 or 3-4 (or similar figure for other multiple shaft configuration) into the 3rd quadrant of Figure 3-16 results in respective quadrant design charts for triple or quadruple shafts. This type of quadrant chart is, thus, directly applicable to single and multiple shaft foundations within a single geological layer and neglecting end bearing, however, Equation 3-8 must be applied in the transition from the 3rd to the 4th quadrant in the presence of nested variogram structures ($n_v > 1$). It is hereby noted that LRFD Φ values obtained for multiple shaft foundations correspond to prescribed probabilities of failure for the whole pier (as opposed to individual piles separately).

Figure 3-16 nicely illustrates the influence of each parameter involved on final Φ values. An increase in CV_q (larger variability in local strength) or β (lower probability of failure) leads to a reduction in Φ. An increase in Q_{des}/m requires larger shaft dimensions causing a higher degree of spatial averaging and, thus, variance reduction, which increases Φ. The same is true for a decrease in a_v, as well as for a reduced D, which implies larger L to achieve the required resistance and, again, a larger degree of variance reduction (less uncertainty in resistance, especially when spatial averaging in the horizontal direction is neglected). The third quadrant shows how $D/a_h = 0$, in fact, is the most conservative assumption for unknown a_h, since it leads to a minimum value of Φ for all L/a_v.

If a foundation is known to penetrate more than one geological layer and, if end bearing resistance is to be accounted for, then the problem of finding the entire shaft length L from above

turns into the problem of finding the required embedment length L_{bot} of the shaft in the bottom-most layer (i.e., usually the bearing layer) penetrated by the foundation. Assuming end bearing resistance and variance are known (Section 3.3), and also knowing the thickness, mean strength, and variance (after upscaling over respective portion of foundation depth) of each layer that is penetrated through by the shaft, Equation 3-11 and 3-13 can be used to determine a nominal value R_{n0} and coefficient of variation CV_{R0} of the total foundation (single or multiple shaft) resistance minus the contribution of side friction in the bottom-most layer (= $DL_{bot}\pi m_{bot}$). The LRFD design equation for the 2nd quadrant of Figure 3-16 then becomes $Q_{des} = R_n\Phi = (R_{n0} + R_{bot})\Phi$, where m_{bot} and $R_{bot} = DL_{bot}\pi m_{bot}$ are the mean local strength and side friction resistance, respectively, in the bottom-most layer. By substituting the expression for R_{bot} into the LRFD equation and dividing by the vertical correlation length of the bottom-most layer $a_{v,bot}$ one finds

$$\frac{L_{bot}}{a_{v.bot}} = \frac{Q_n}{\Phi D\pi m_{bot} a_{v,bot}} - \frac{R_{n0}}{D\pi m_{bot} a_{v,bot}} = \frac{L}{a_{v,bot}} - \frac{R_{n0}}{D\pi m_{bot} a_{v,bot}} \tag{3-24}$$

where $L/a_{v,bot} = Q_{des}/(Da_{v,bot}m_{bot}\Phi\pi)$ is known from above as the relationship obtained for the 2nd quadrant if a single layer of properties m_{bot} and $a_{v,bot}$ was present without end bearing. In this sense, L represents an equivalent foundation depth due to side friction only in a single layer without end bearing, which possesses the same nominal resistance as the actual foundation. As variance reduction is only to be applied to the foundation portion corresponding to L_{bot}, the variance reduction chart in the 3rd quadrant is entered with the reduced value of $L_{bot}/a_{v,bot}$. Note that the other variances of side friction in the overlaying layers and of end bearing are already known and combined in CV_{R0}. In fact through the present approach, the problem of accounting for several layers plus end bearing is effectively reduced to an equivalent problem of a foundation without end bearing, which fully passes a top layer of known thickness (R_{n0}, CV_{R0}) and partially penetrates a bottom layer of embedment L_{bot}.

Leaving the 3rd quadrant, one obtains a value of $\alpha^{1/2}$ resulting in a variance $\sigma^2_{bot} = \alpha(CV_{q,bot}DL_{bot}\pi m_{bot})^2$ of side friction resistance in the bottom-most layer, where $CV_{q,bot}$ is the local strength coefficient of variation in the said layer. In analogy to Equation 3-13, CV_R of the whole foundation (i.e., all layers plus end bearing) is found as

$$CV_R = \frac{\sqrt{CV_{R0}^2 + \alpha\left(\frac{R_{bot}}{R_{n0}} CV_{q,bot}\right)^2}}{1 + \frac{R_{bot}}{R_{n0}}} \tag{3-25}$$

which is used instead of the 4th quadrant in Figure 3-16, then to enter the 1st quadrant from below and continue the iteration. This procedure assures that the final LRFD Φ values and foundation (single or multiple shafts) design lengths correspond to a prescribed probability of failure for the entire foundation (as opposed to each layer and end bearing, separately). It may be easily seen from Equations 3-24 and 3-25 that the approach collapses to the direct application of Figure 3-16 for $R_{n0} = 0$, i.e., single layer without end bearing.

3.6 Case Studies

This section represents a continuation of the case studies in Section 2.5 where respective outcomes are used to demonstrate the results of the present chapter for different site conditions. Section 3.6.1 works with a well defined variogram and illustrated effects of a nugget component in the variogram, unknown horizontal range (line shaft approximation), random areal trend, and, finally, demonstrates an application of the quadrant chart in Figure 3-16. In Section 3.6.2, the site possesses two distinct layers with deterministic trends, and variograms do not indicate a horizontal or a vertical range to work with such that conservative ways of handling this are discussed.

3.6.1 17th Street Bridge

Figure 2-11 indicates the horizontal and vertical correlation ranges are well estimated by a_h = 12 ft and a_v = 5 ft, respectively, while the presence or not of a 40% nugget component in the total variance may not be reliably determined (Figures 2-11(a) and 2-11(c) versus Figures 2-11(b) and 2-11(d)). The mean local strength from core sample data is further known to be m = 16.1 tsf with a respective coefficient of variation of CV_q = 0.53 (Figure 2-10(a)). Assuming no nugget effect, L = 25 ft and D = 4 ft, such that $L/a_v = 5$ and $D/a_h = 0.33$ gives $\alpha^{1/2} = 0.33$ from Figure 3-2(a), CV_R = 0.17 from Equation 3-9 and, finally, **Φ = 0.74** from Equation 3-22 or Figure 3-15 (for $\beta = 3$). Maintaining everything the same, but adding a 40% nugget variance to the variogram, Equation 3-8 dictates that $\alpha = 0.33^2$ only applies to 60% of the total variance, while $\alpha = 0$ applies to the remaining 40% nugget variance (D/a_h and L/a_v very large in Figure 3-2). With this, an overall $\alpha = 0.6 \cdot 0.33^2 + 0.4 \cdot 0 = 0.07$ is obtained leading to CV_R = 0.14 and **Φ = 0.80**. **This illustrates the fact that it is conservative to not assume nugget components in the variogram if they are not clearly indicated by the data, since the theoretically perfect averaging of the nugget component may lead to underestimation of the actual shaft resistance uncertainty**. By following the same procedure, but using Figures 3-3 or 3-4 instead of Figure 3-2, respective Φ values can be obtained for triple and quadruple shaft foundations.

If it is assumed that a_h is unknown, which is typical for many practical situations, and then the line shaft approximation (thick continuous line) may be adopted, which is the same for single and multiple shaft foundations. For example, without the nugget effect, $\alpha^{1/2} = 0.38$ is obtained from Figures 3-2, 3-3, or 3-4 leading to CV_R = 0.20 and **Φ = 0.69**. This is smaller than the respective value of 0.74 for a_h = 12 ft from above. An important factor adding uncertainty to shaft resistance is random areal trends, which are a type of zonal anisotropy where the vertical variogram reaches its sill below the local strength variance. The portion of variability only

contained in the horizontal direction does not experience any effective averaging and, hence, variance reduction. To illustrate this effect, it is assumed that in addition to unknown a_h the vertical variogram in Figure 2-11 reaches its sill at 0.8 instead of 1. $L/a_v = 5$ is not affected, however, its corresponding $\alpha^{1/2} = 0.38$ now only applies to 80% of the total variance. For the remaining 20% of the random areal trend component, $L/a_v = 0$ leading $\alpha^{1/2} = 1$ for the line shaft approximation. The combined variance reduction factor is then obtained as $\alpha = 0.8 \cdot 0.38^2 + 0.2 \cdot 1 = 0.32$ giving further $CV_R = 0.30$ and **$\Phi = 0.51$**, which illustrates the significant impact of a random areal trend component when compared to 0.69 for without random areal trend component.

Assuming now that a nominal load $Q_{des} = 2500$ tons is given, for example, rather than the shaft dimensions, Figure 3-16 may be applied to find a respective Φ for a given shaft diameter (e.g., 4 ft). For the case of unknown a_h (without random areal trend) and using $a_v = 5$ ft, an initial (guessed) value of L = 30 ft gives $L/a_v = 6$, which is used as the starting point for the graphical iteration (looping) indicated in Figure 3-16. Theoretically, the iteration could be started anywhere in the chart as long as the direction of the iteration is counter-clockwise. Following the dotted line downwards to the continuous line of $D/a_h = 0$ in the third quadrant, $\alpha^{1/2} = 0.35$ is obtained. Following the dotted line further to the right into the fourth quadrant, until the line of $CV_q = 0.53$ (the coefficient of variation for core sample mean local strength), gives $CV_R = 0.19$ and, further, $\Phi = 0.70$ for $\beta = 3$ in the first quadrant. Entering the second quadrant with this value of Φ shows that the nominal load for the chosen L is almost twice as large as needed ($Q_{des}/(Da_vm) \approx 13$) for the required $Q_{des}/(Da_vm) = 7.76$ (D = 4 ft, $a_v = 5$ ft and m = 16.1 tsf). Following the dotted line to the left, until the curve for the required $Q_{des}/(Da_vm) = 7.76$ is met, initiates a second iteration loop and, by following the sequence of thin dotted lines to thick

continuous lines, convergence to design values of L = 20 ft ($L/a_v = 4$) and **$\Phi = 0.62$**, is reached rapidly. This may be compared to an $\Phi = 0.69$ for equal site conditions, but for L = 25 ft. Value Φ, in this case, is larger as a result of the stronger effect of spatial averaging over the longer shaft. Nominal resistances R_n are simply obtained by $Q_{des}/\Phi = LD\pi m$ and are equal to 4044 and 5044 tons for L = 20 and 25 ft, respectively.

In order to include the contribution of end bearing to total shaft resistance, Equations 3-24 and 3-25 may be used with $R_{n0} = m_{EB} = 760$ tons and $CV_{R0} = CV_{EB} = 0.31$, which are the outcomes in Section 3.3. Knowing that for a single layer $m_{bot} = m$ and $a_{v,bot} = a_v$, the last term in Equation 3-24 is evaluated as $R_{n0}/(D\pi m a_v) = 0.75$, which means that every time the 2nd quadrant is left during an iteration cycle, the third quadrant is entered with 0.75 (L/a_v)-units to the right of the value found for L/a_v. This is illustrated in Figure 3-17, which contains a replicate of the quadrant chart of Figure 3-16 (except for the 4th quadrant) with the present iteration process. The chart is entered at $\Phi = 0.62$ (value obtained above without end bearing, but could be any other value) and the line is followed to the left until it meets $Q_{des}/(Da_v m) = 7.76$ giving $L/a_v = 4$ as previously obtained. However, the 3rd quadrant is now entered at $L_{bot}/a_v = 4 - 0.75 = 3.25$ as indicated by the arrow pointing to the right. Value $\alpha^{1/2} = 0.47$ is obtained from the line shaft approximation curve and Equation 3-25 with known values of $CV_{R0} = 0.31$, $R_{bot} = D(L_{bot}/a_v)a_v\pi m = 4 \cdot 3.25 \cdot 5\pi \cdot 16.1 = 3286$ tons, $R_{n0} = 760$ tons, and $CV_{q,bot} = CV_q = 0.53$ (Figure 2-19(a)) renders $CV_R = 0.21$, which is used to enter the first quadrant. Value $\Phi = 0.66$ is now found and $L_{bot}/a_v = 3.0$ leading to $R_{bot} = 3033$ tons and $\alpha^{1/2} = 0.48$. With all other parameters as before, Equation 3-25 now gives $CV_R = 0.21$, which is the same as in the previous iteration, thus indicating that the result has converged to a shaft length of $L = L_{bot} = 3 \cdot 5 = 15$ ft and **$\Phi = 0.66$**. This may be compared to L = 20 ft and $\Phi =$

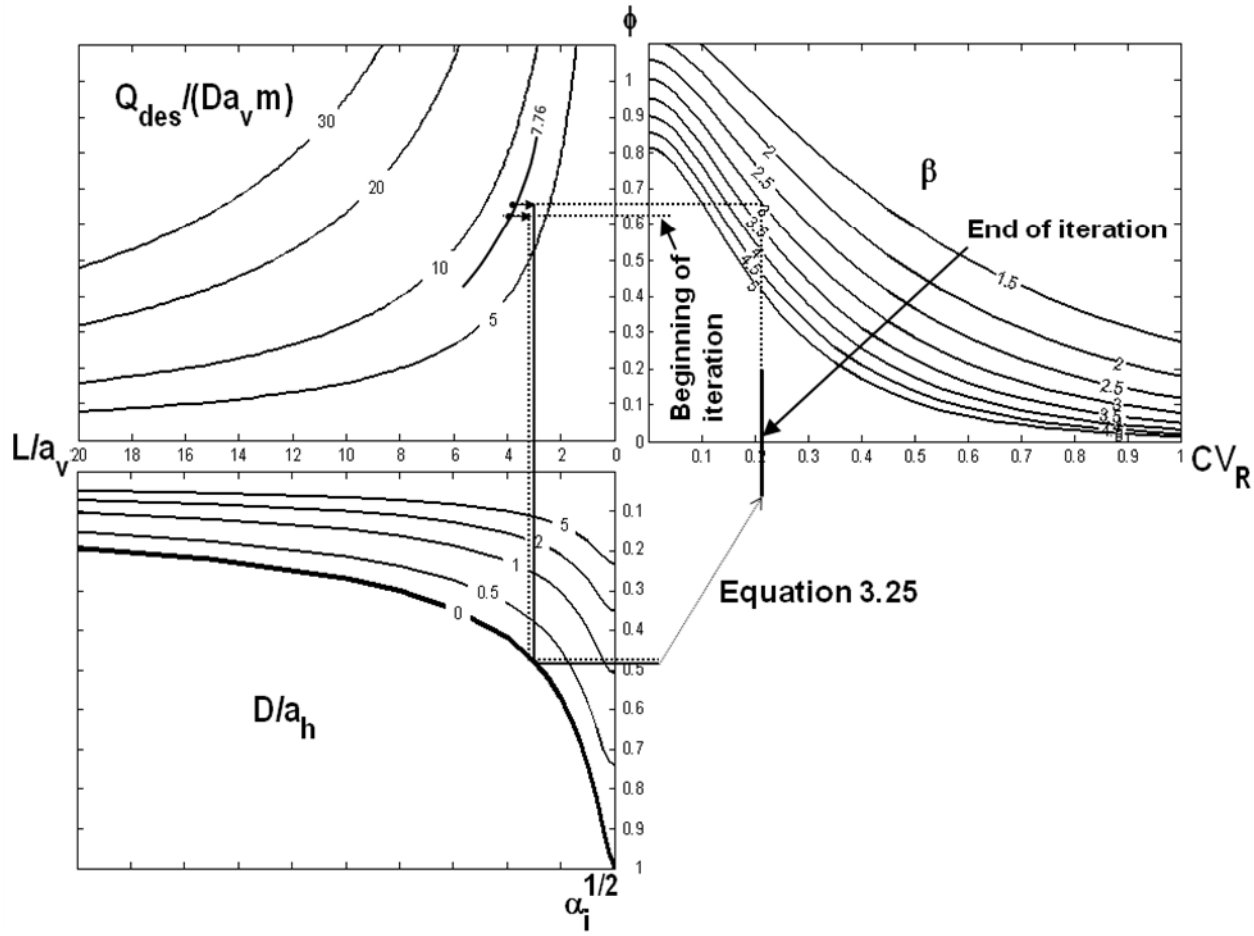

Figure 3-17. Quadrant chart of Figure 3-16 (except 4th quadrant) with graphical iteration taking into account end bearing at 17th Street.

0.62 from above, if end bearing is neglected. However, no general conclusion should be drawn from this in terms of increase or decrease in Φ when including end bearing as this depends on many factors, such as the magnitudes of side friction versus end bearing resistance and side friction versus end bearing CV. Moreover, it is not only Φ that is affected but obviously nominal resistance as well. For example, Φ with end bearing could be lower than that without end bearing, but the shaft dimensions must be generally smaller due to the increase in R_n when including end bearing. In other words, R_{n0} from end bearing may have a very small expected value m_{EB} with a large CV, but due to the fact that R_{n0} is a strictly positive random variable (end bearing cannot decrease side friction resistance), it must have some beneficial effect on design in

terms of shaft size reduction, but not necessarily in terms of increasing Φ. It is surmised that in cases of extremely low R_{n0}/R_{bot} and extremely large $CV_{R0}/(\alpha^{1/2}CV_{q,bot})$, which should be irrelevant for practice, shaft dimension results could be larger when including end bearing. This would be a result of a large error in the assumption of log-normality in R_n being the sum of the two log-normals R_{n0} and R_{bot}.

Note that data used in this example are limited to a specific portion of the site and as such R_n and Φ obtained are pertinent to that zone only. Moreover, it is emphasized that the resistance bias factor λ_R used in Equation 2-22 for computing Φ is equal to 1.06 as prescribed by FHWA/ AASHTO. Value Φ is directly proportional to λ_R, and particular treatment of resistance bias is contained in Chapter 6.

3.6.2 Fuller Warren Bridge

As illustrated by Figures 2-12 and 2-14, this site consists of two distinct geological layers, which must be treated as separate sub-domains. Moreover, each layer possesses a deterministic trend component (Figure 2-14(a)), which needs to be removed before geostatistical analysis. The top layer was found to be 10-ft thick with a trend in local strength q as a function of elevation z of $q_{top} = -0.97z + 29.56$ ($16 < z < 26$ ft), while core sample data of the bottom layer are available down to 17 ft below the bottom of the top layer. The respective deterministic trend function is $q_{bot} = 0.14z + 0.72$ ($0 < z < 16$ ft). The local strength variances of the residuals in each layer are known as $\sigma^2_{top} = 18.49$ tsf^2 and $\sigma^2_{top} = 0.45$ tsf^2 with variograms shown in Figures 2-15(a) and 2-15(b). As noted in combination with these figures, it may not be expected to obtain a reasonable horizontal variogram from the available data (only 3 borings spaced by approximately 40 ft; Figure 2-12(a)). Furthermore, the number of data for a vertical variogram is very limited as well and impairs a reliable interpretation of the vertical variogram of the top layer in Figure

2-15(b) (i.e., number of data points in each variogram point < 30). The vertical variogram for the bottom layer in Figure 2-15(a) is better defined (based on more data) and indicates absence of a random areal trend component (vertical variogram fluctuates about the total normalized variance of one); however, no spatial correlation structure (i.e., a_v) may be inferred. As it is highly non-conservative to adopt nugget variograms for spatial averaging (α would be zero), this situation deserves special attention.

One possibility is to adopt a_v as the distance of minimum data spacing in the vertical direction which would approximately correspond to the lag distance of the first point in the experimental variogram (e.g., 2 ft in the current example). However, larger a_v may be obscured by sub-optimal data acquisition and the majority of the data may have larger separations. As a conservative method it is, thus, recommended to use the minimum number n_{min} of data in a boring and over the depth interval of shaft implementation to determine α_0 as $1/n_{min}$. This is even conservative for equally spaced data, e.g., for $L/a_v = 10$, where a variogram slope would only be observed if more than 10 (regularly spaced) samples are taken over L. If exactly 10 samples are taken, the variogram would still appear as a pure nugget effect and a conservative adoption of a_v would give $a_v = L/10$, i.e., $L/a_v = 10$ and $\alpha_0 = 0.27^2 = 0.07$ from Figure 3-2. In contrast, $\alpha_0 = 1/n_{min} = 1/10 = 0.10$, which is more conservative. In the same way, if only 5 samples were taken, a conservative a_v would be L/5, i.e., $L/a_v = 5$ and $\alpha_0 = 0.38^2 = 0.14$ from Figure 3-2, as opposed to $\alpha_0 = 1/n_{min} = 1/5 = 0.20$. However, if many data are collected and the experimental variogram still does not indicate any spatial correlation structure, then $\alpha_0 = 1/n_{min}$ leads to smaller, yet conservative, values. Thus, it is assured that small values of a_v may only be adopted if it is clearly indicated by the experimental variogram or, if no spatial correlation is indicated, but a sufficiently large amount of data are collected.

For the present case, assuming L = 25 ft (i.e., 10 ft in top layer and 15 ft in bottom layer such that z > 1 ft), Appendix A indicates $n_{min,top} = 7$ and $n_{min,bot} = 8$ leading to $\sigma^2_{R,top} = \sigma^2_{top}/7 = 2.64$ and $\sigma^2_{R,top} = \sigma^2_{top}/8 = 0.06$ tsf^2. These variances apply to the nominal resistances $R_{n,top}$ and $R_{n,bot}$, which are obtained by integrating the deterministic trend functions of q over the respective portions of the foundation (single or multiply shaft) surface. As the trend functions are linear, this is equivalent to finding the mean of the trend function for the shaft embedment in each layer and multiplying by the respective shaft surfaces. With this, $R_{n,top} = A_{top}(14.04 + 4.34)/2 = 1154$ tons and $R_{n,bot} = A_{bot}(0.86 + 2.96)/2 = 360$ tons (assuming single shaft: $A_{top} = 4 \cdot 10 \cdot \pi = 125.6$ ft^2; $A_{bot} = 4 \cdot 15 \cdot \pi = 188.4$ ft^2). As indicated by Equation 3-13 (without end bearing), the total shaft resistance $R_n = R_{n,top} + R_{n,bot} = 1514$ tons with a variance of $\sigma^2_R = A^2_{top}\sigma^2_{R,top} + A^2_{bot}\sigma^2_{R,bot} = 43777$ tons^2 giving $CV_R = 0.14$. For a chosen value of $\beta = 3$, this results in **$\Phi = 0.80$** from Figure 3-5. Note that data used are limited to a specific portion of the site and as such R_n and Φ obtained are pertinent to that zone only. Moreover, it is emphasized that the resistance bias factor λ_R used in Equation 2-22 for computing Φ is equal to 1.06 as prescribed by FHWA/ AASHTO. Value Φ is directly proportional to λ_R, and particular treatment of resistance bias is contained in Chapter 6.

Without previous treatment of the data (separation into layers and trend removal), Figure 2-13 shows $CV_q = 1.07$. Allowing for a (generous) variance reduction factor of $\alpha = 1/(7 + 8)$, i.e., considering 15 samples per boring, $CV_R = 0.28$ and **$\Phi = 0.55$**. In addition, not considering two separate layers could lead to significant misinterpretations of the variogram, e.g., inference of a large variogram range, which would only be due to the discontinuity between the layers. By taking the average of all data in Figure 2-13(a) a respective nominal resistance would be $R_n = 1444$ tons.

CHAPTER 4
USE OF PRE-DESIGN BOREHOLE STRENGTH DATA

4.1 Uncertainty due to Limited Data

While results of the previous chapter are based on the assumption of perfectly known geostatistical site parameters of local strength q (i.e., mean, variance and variogram), this section considers the more practical situation of a limited number of n_c core sample data available from n_b borings of approximately equal depth (e.g., 30 ft) and approximately equally spaced (e.g., every 150 ft) along a bridge site. This may correspond to a first set of borehole data obtained from a site before initiating the design process indicating (1) whether the site is geostatistically homogeneous and can be treated as a whole or needs to be split up into a number of sub-domains of different but internally stationary geostatistical parameters to be studied separately (see Chapter 2); (2) mean m and variance σ^2 of q; and (3) the variogram γ_v in the vertical direction (along boreholes). Since data at equal depth (i.e., horizontally aligned) are typically scarce and excessively far spaced at this stage of site characterization, the horizontal variogram γ_h remains unknown. Obviously, depending on where exactly and how many borings and core samples are taken, estimates of m may vary reflecting an additional uncertainty which is not considered in Equation 3-4. As the locations of individual foundations to be constructed are not yet determined at this stage (i.e., random in some sense), the variance of this uncertainty simply adds to the variance in resistance R due to the unknown distribution of q over the (single or multiple) shaft surface leading to $\sigma_R^2 = \alpha\sigma^2 + \sigma^2/n_e$, where n_e is an effective number of independent core sample data collected (σ^2/n_e can be shown to correspond to the kriging estimation variance of m (Kitanidis 1997)). Since core sample data are correlated in the vertical direction according to γ_v and may be considered uncorrelated horizontally due to the large separation distances $n_e = n_b/\alpha_0$ ($n_b \le n_e \le n_c$), where α_0 is the variance reduction factor for a fictitious shaft replicating a boring

of length L_b and very small diameter D = 0. Knowing $L \approx L_b$ and conservatively approximating α by α_0 (using line shaft approximation as horizontal range a_h is unknown; thick continuous line in Figure 3-2), $\sigma_R^2 = \alpha_0\sigma^2 + \alpha_0\sigma^2/n_b$ may be written leading to

$$\alpha_b = \frac{\sigma_R^2}{\sigma^2} = \alpha_0\left(1+\frac{1}{n_b}\right) = \left[\frac{0.75}{\left(L/a_v\right)} - \frac{0.2}{\left(L/a_v\right)^2}\right]\left(1+\frac{1}{n_b}\right) \tag{4-1}$$

where the last expression results from Equation B-5 (see Appendix B) and is valid for $L/a_v \geq 1$, which is typically the case in practice. Equation 4-1 is used instead of α in Equation 3-9 to account for limited sampling in the presence of unknown horizontal variogram. In the presence of more than one layer α from Equation 4-1 with respective layer thicknesses L is used instead of α_{Lj} for each layer in Equation 3-13. If γ_v is nested, Equation 3-8 may be used to find a respective value of α_0 to be used in Equation 4-1 or, alternatively, α_b from Equation 4-1 is used in Equation 3-8 to obtain a final variance reduction factor. Evidently $\alpha_b > \alpha$, since $\alpha_0 > \alpha$ (neglecting horizontal averaging) and $1/n_b > 0$ (limited/incomplete sampling of the site). For large n_b, sampling is exhaustive and $\alpha_b = \alpha_0$. This is illustrated in the graphs in Figure 4-1, which is equivalent to Figure 3-2(a) with additional dashed curves from Equation 4-1 for n_b = 3 and 6. In the same way as the line shaft approximation (thick continuous line) is the same for single and multiple shaft foundations, Equation 4-1 is also equally valid for single and multiple shaft foundation, i.e., the dashed lines in Figure 4-1 may be directly transferred to Figures 3-3 and 3-4 for triple and quadruple shafts, for example. Resulting charts are, hence, extensions of Figures 3-2, 3-3, and 3-4 and may directly be used in the 3rd quadrant of Figure 3-6. Furthermore, all aspects of deterministic layering and inclusion of end bearing discussed in connection with Figure 3-6 remain valid.

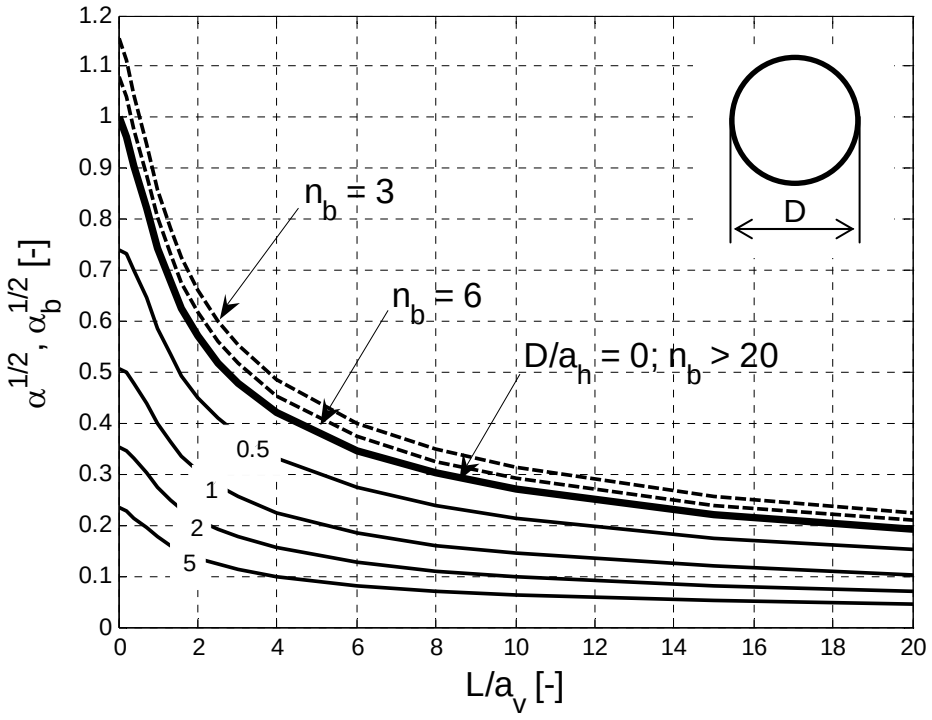

Figure 4-1. Term $\alpha^{1/2}$ (continuous) from Figure 3-2(a) as a function of L/a_v and D/a_h. Term $\alpha_b^{1/2}$ (dashed) from Equation 4-1 as a function of L/a_v and n_b ($D/a_h = 0$).

Besides LRFD Φ, a nominal strength for foundation design is required. Once the pier locations are known, it would be conservative to select the nominal strength as the lower value between the mean strength measured at the nearest boring and the mean strength over all borings in the defined sub-domain. The former corresponds to the worst case scenario if correlation between shaft and boring is strong, while the latter corresponds to the opposite case of no correlation.

4.2 Minimum Data Requirements

Equation 4-1 immediately shows how α_b decreases (and, hence, Φ increases) as n_b increases, i.e., as more borings are deployed, thus improving site characterization. Preliminary experience indicates that $n_b \geq 3$ per site (or homogeneous sub-domain; see Chapter 2) may be an

acceptable guideline based on the criterion of reliable inference of m, σ^2, and γ_v. The total number of core samples n_c does not directly affect α_b, which is due to the assumption that they are taken at intervals below the vertical correlation range and down to a depth of approximately L. The former is required in the first place to be able to infer a reliable vertical variogram for determination of α_0 and additional core samples between n_c existing core samples would only deliver redundant (highly correlated) data, which do not significantly contribute to improve site characterization (i.e., increase n_e). From this perspective, vertical correlation ranges at the order of 4 to 8 ft, as observed at a limited number of sites in Florida, would ask for core sampling at approximately 2- to 3-ft intervals. Knowing the vertical variogram from the first three borings, the vertical sampling resolution of additional borings may be decreased to intervals not larger than the vertical correlation range observed from the first three borings (in order to not significantly invalidate Equation 4-1). From this, it is expected that typical values of approximately $50 < n_c < 100$ are required in practice, which is considered sufficient for histogram construction and estimation of m and σ^2. Separate inference of σ^2 from the variogram is of great importance, since only the sill of the (unknown) horizontal variogram s_h may reach σ^2, while the sill of the (known) vertical variogram s_v may be smaller than σ^2, thus underestimating the spatial variability of a site. The difference of $\sigma^2 - s_v$ is due to variability only present in the horizontal direction and referred to as random areal trend (see Chapters 2 and 3). It is a form of zonal anisotropy, which reflects the intuitive and non-conservative fact that a whole shaft might be located in a horizontal area of either weak or strong ground, such that variance reduction due to spatial averaging does not fully occur. The condition $n_b \geq 3$ also serves to guarantee detection of possible random areal trends at a site.

4.3 Case Study – 17th Street Bridge

In the example of Section 3.6.1, m = 16.1 tsf was assumed to be reliably known. From Figure 2-9(a), however, it is seen that this information is based on 6 borings only. By ignoring the horizontal correlation between these borings (in practice they would be spaced much further than 10 ft on average), and regarding the horizontal correlation length a_h as unknown, this translates into using Equation 4-1 with $n_b = 6$. Maintaining the vertical correlation length $a_v = 5$ ft, coefficient of variation in local strength $CV_q = 0.53$, nominal load $Q_{des} = 2500$ tons, shaft diameter D = 4 ft, and reliability index $\beta = 3$, Figure 4-2 may be used to graphically find a design shaft length L by the same procedure described in Section 3.6.1, but by using Figure 4-1 and

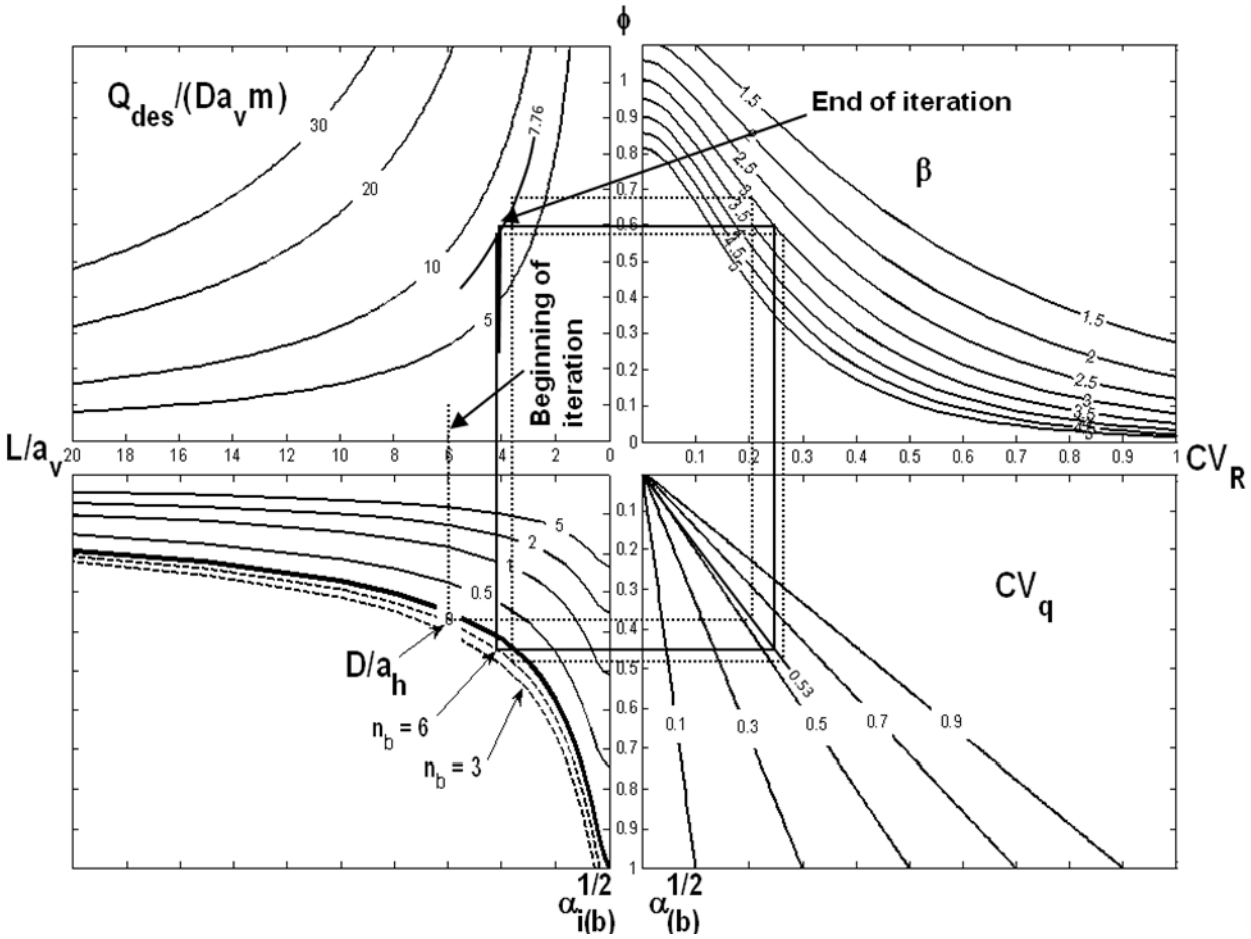

Figure 4-2. Design quadrant chart of Figure 3-6 with Figure 4-1 in 3rd quadrant.

the graph for $n_b = 6$ instead of Figure 3-2(a) in the 3rd quadrant. As shown by the iteration loops in Figure 4-2, this results in a shaft design length L = 21 ft ($L/a_v = 4.2$) and **$\Phi = 0.60$**, as opposed to L = 20 ft and $\Phi = 0.62$, if m is assumed to be reliably known. Clearly, for $n_b < 6$ the difference would be greater.

CHAPTER 5
USE OF BOREHOLE STRENGTH DATA INSIDE THE FOOTPRINT OF A SHAFT

5.1 Uncertainty Reduction due to Data in Shaft Footprint

Knowing the exact locations of each foundation in the design process, allows for collection of additional boring data at intervals smaller than the vertical correlation length observed from previous borings (Chapter 4) at the center of some or all of the designed foundations. This additional center boring data in the footprint of the foundation allows for improved assessment of α and, generally, a higher value of Φ.

In order to incorporate the influence of boring data in the footprint of a shaft/pier, kriging (Section 2.4) is used, which transforms the spatial correlation between the data and the shaft into a reduction in final shaft resistance uncertainty σ^2_f. Mathematically, this is expressed by Equation 2-13 through the negative covariance term. If Equation 2-13 is divided by the local point-to-point strength variance σ^2, an equation is obtained for a variance reduction factor α_c in the presence of a center boring between σ^2 and shaft mean side friction uncertainty σ^2_f.

$$\alpha_c = \frac{\sigma_f^2}{\sigma^2} = \frac{\sigma_q^2}{\sigma^2} + \frac{\sigma_m^2 - 2C(m,q)}{\sigma^2} = \alpha_0 \pm A \qquad (5\text{-}1)$$

Assuming for now that data are limited to a single boring at the center of a foundation (data from other borings outside the pier will be included later), the first term in Equation 5-1, i.e., σ^2_q/σ^2, is equal to α_0, since σ^2_q is the variance of Equation 2-12 and $\lambda_i = 1/n$ (estimate of mean unit side friction on shaft surface is equal to arithmetic mean of core sample strength in center boring). The term σ^2_q/σ^2 only depends on L/a_v which is identical to the variance reduction from the line shaft approximation. The last term in Equation 5-1, i.e., A may be zero, positive, or negative, and is a function of both L/a_v and D/a_h. Using Equations 2-10, 2-14, and 2-15 with $\lambda_i = 1/n$,

Equation 5-1 may be evaluated for different combinations of L/a_v and D/a_h with respective results shown in Figures 5-1, 5-2, and 5-3 for single, triple, and quadruple shafts, respectively. By requiring large enough n such that sample separation is smaller than the vertical correlation length (see above), the actual number of n becomes irrelevant as additional samples would be highly correlated (i.e., deliver redundant information mostly already contained in previous samples) and would not affect the outcome of Equation 5-1. This is equivalent, in other words, to assuming that the boring is continuously sampled over the shaft depth.

Independent of D/a_h, it may be observed that α_c decreases with increasing L/a_v, which is an expected outcome due to the increasing degree of spatial averaging in the vertical direction. Variable A in Equation 5-1 approaches zero when D/a_h becomes very large (i.e., very small horizontal ranges a_h), such that spatial averaging over the shaft surface reduces σ^2_m towards zero

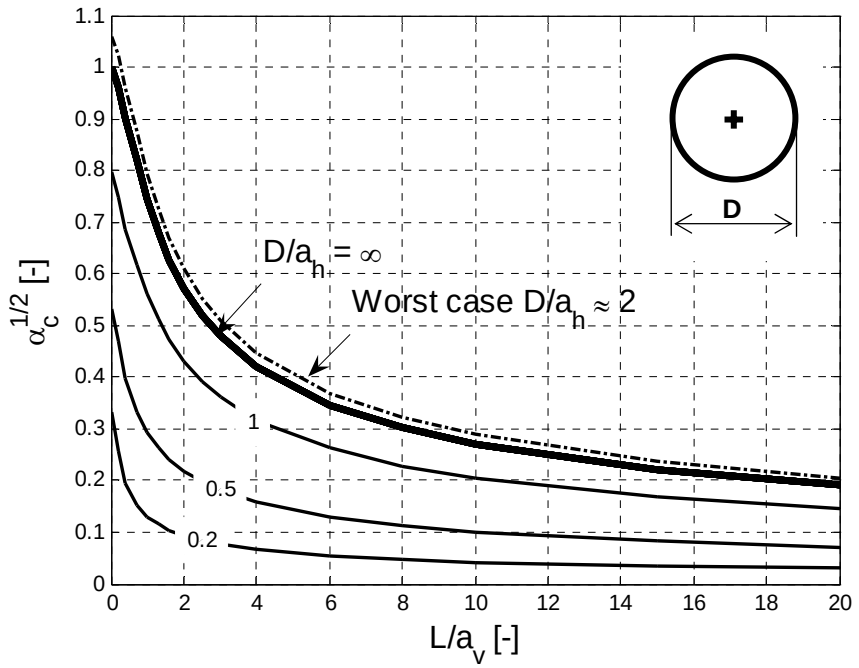

The thick continuous line for $D/a_h = \infty$ is identical to α_0 (line shaft approximation). The dash dotted line for $D/a_h \approx 2$ represents maximum values of $\alpha_c^{1/2}$ for a given L/a_v, while thin continuous lines indicate $\alpha_c^{1/2}$ for $D/a_h < 2$.

Figure 5-1. Term $\alpha_c^{1/2}$ for a single shaft with one single boring (cross) at the center as a function of L/a_v and D/a_h.

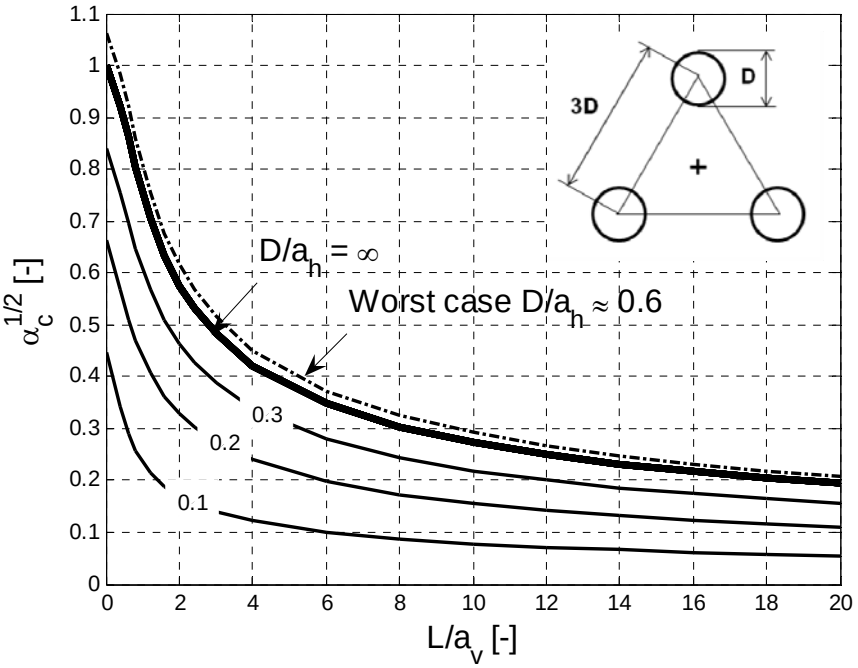

The thick continuous line for $D/a_h = \infty$ is identical to α_0 (line shaft approximation). The dash dotted line for $D/a_h \approx 2$ represents maximum values of $\alpha_c^{1/2}$ for a given L/a_v, while thin continuous lines indicate $\alpha_c^{1/2}$ for $D/a_h < 2$.

Figure 5-2. Same as Figure 5-1, except for triple (triangle) shaft foundations.

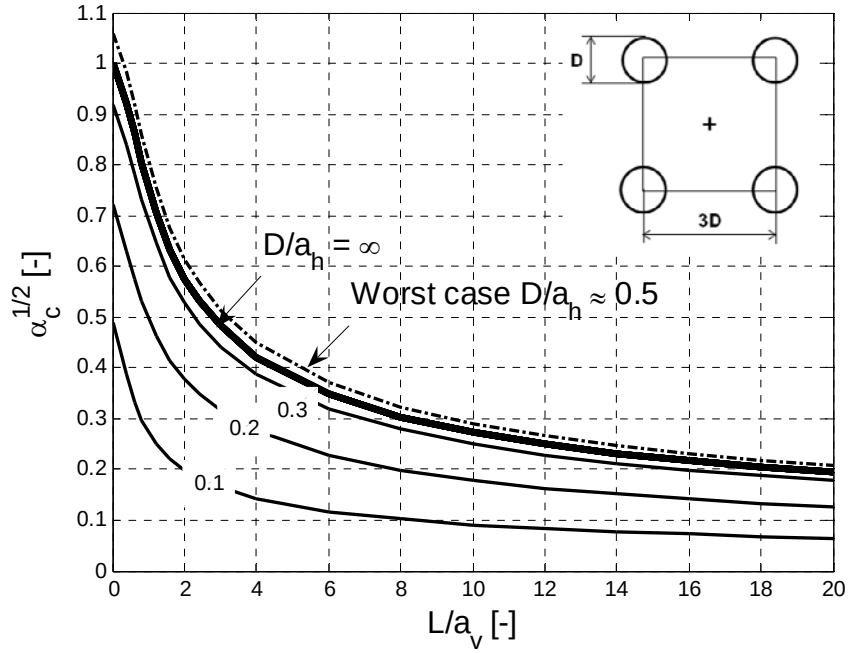

The thick continuous line for $D/a_h = \infty$ is identical to α_0 (line shaft approximation). The dash dotted line for $D/a_h \approx 2$ represents maximum values of $\alpha_c^{1/2}$ for a given L/a_v, while thin continuous lines indicate $\alpha_c^{1/2}$ for $D/a_h < 2$.

Figure 5-3. Same as Figure 5-1, except for quadruple (square) shaft foundations.

and the distance between data and shaft surface is larger than a_h such that Cov(m,q) = 0. This is shown by the thick continuous lines in Figures 5-1, 5-2, and 5-3, which are all the same and identical to the variance reduction α_0 of the line shaft approximation as stated above. As a_h is increased from zero, σ^2_m increases as well while Cov(m,q) remains zero until a_h spans the minimum distance between the center boring and the shaft surface. This causes α_c to increase up to a maximum (worst case; dash dotted line) above which an increase in a_h still increases σ^2_m, however, to a smaller degree. On the other hand, Cov(m,q) now also increases such that the overall effect is a decrease in α_c (thin continuous lines). For very large values of a_h, the correlation between the center boring and the shaft surface is very large and α_c approaches zero.

Interesting to observe from Figures 5-1, 5-2, and 5-3 is that the worst case of α_c very consistently exceeds α_0 by approximately 15%, i.e., $\alpha_{c,max} = 1.15\alpha_0$ for all L/a_v and foundation types shown (note that this is not generally true for multiple shaft foundations, if pile separation is different from 3D; however, respective values can be computed). If the center boring (hypothetically) were the only data available, $\alpha_{c,max}$ would be the most conservative value of variance reduction to adopt for known a_v but unknown a_h. Since $\sigma^2_q/\sigma^2 = \alpha_0$ and the worst case scenarios occur when Cov(m,q) is still approximately zero, $A = \sigma^2_m/\sigma^2 = 0.15\alpha_0$ may be inferred from Equation 5-1.

The additional borings at the center of foundations add to the n_b borings throughout the zone or region considered in the previous chapter. However, it is conservative to assume that borings near the same pier location may not necessarily contain independent information (data may be correlated), such that the number of independent borings available in a sub-domain is defined as $n_f = n_b + n'_f$, where n'_f is the number of borings taken inside the footprint of a pier (one boring per pier), where previously none of the n_b borings (from Chapter 4) were located. If

preliminary borehole testing was performed in the vicinity of every pier location, then $n_f = n_b$. Without affecting $\sigma^2_m/\sigma^2 = 0.15\alpha_0$ the total amount of (uncorrelated) borings available in a sub-domain is accounted for by writing $\sigma^2_q/\sigma^2 = \alpha_0/n_f$ and Equation 5-1 gives

$$\alpha_c = \alpha_0\left(0.15+\frac{1}{n_f}\right) = \left[\frac{0.75}{\left(L/a_v\right)} - \frac{0.2}{\left(L/a_v\right)^2}\right]\left(0.15+\frac{1}{n_f}\right) \tag{5-2}$$

Direct comparison to Equation 4-1 is depicted in Figure 5-4 and shows a reduction from α_b to α_c, which is due to a possible increase from n_b to n_f, but mostly to the substitution of the line shaft approximation by the worst case D/a_h, provided there is a boring at the center of the pier. Equation 5-1 is used instead of α in Equation 3-9 to find CV_R and, subsequently, Φ for the presence of a boring in the footprint of a (single or multiple shaft) foundation when the

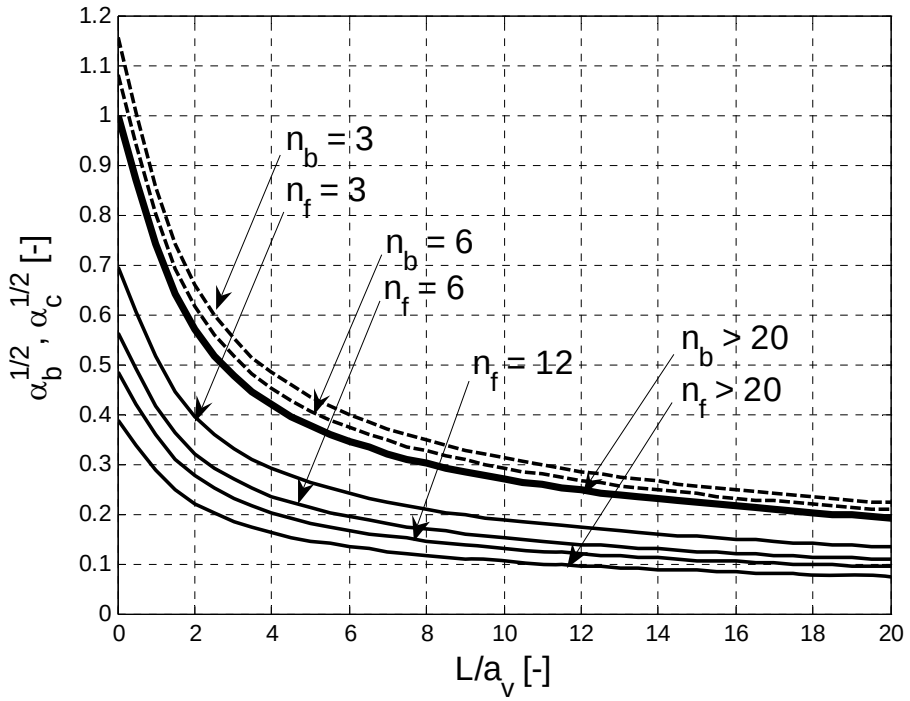

Figure 5-4. Functions $\alpha_b^{1/2}$ (dashed) and $\alpha_c^{1/2}$ (thin continuous) from Equations 4-1 and 5-2, respectively. Thick continuous line is α_0.

horizontal range is unknown. In the presence of more than one layer α_c from Equation 5-1 with respective layer thicknesses as L is used instead of α_{Lj} for each layer in Equation 3-13. If the vertical variogram is nested, Equation 3-8 may be used to find a respective value of α_0 to be used in Equation 5-1 or, alternatively, α_c from Equation 5-1 is used in Equation 3-8 to obtain a final variance reduction factor.

Since the worst case scenario occurs when Cov(m,q) is still zero or very small, the best estimate of nominal strength for pier design for this scenario is given by the mean strength over all borings in the sub-domain. However, although α_c would be more favorable, the true (but unknown) a_h may be large enough to lead to a best estimate of nominal strength at a pier, which is equal to the mean strength measured at the respective center boring. Hence, in analogy to Chapter 4 (when pier location are already known), it is conservative to use α_c from Equation 5-2 with a nominal strength equal to the lower value between the mean strength at the center boring and the mean strength over all borings in the sub-domain.

5.2 Knowing the Horizontal Correlation Length

For completeness, this section briefly discusses the rather theoretical situation of a known horizontal correlation length a_h at a pier location or over a whole sub-domain. In order to infer a reliable value of a_h, a sufficient amount of borings (say > 4) need to be located at sufficiently small separation distances (say between 3 to 20 ft), which is not expected to occur in general design practice (17^{th} Street data are rather an exception for investigation purposes). However, assuming that a_h is known, then Figures 5-1, 5-2, and 5-3 are directly applicable to obtain α_c and to continue design as discussed in the previous section (above figures are even emendable to being plugged into the 3^{rd} quadrant of Figure 3-16, for example). Direct use of Figures 5-1, 5-2, and 5-3, however, does not account for the presence of additional data from other borings than

the center boring at a pier location in question. That is, not all the information available is used, such that α_c may be larger than from Equation 5.1, where n_f is considered. In order to obtain a consistent estimate of variance reduction and nominal load for known a_h, while accounting for all borings available (and particularly borings close to the pier location in question), a full kriging approach must be taken (see Section 2.4). That is, data in each boring will receive different weights for estimating nominal resistance as a function of their distances to the shaft and among each other, and α_c will be a function of these weights.

5.3 Case Study – 17th Street Bridge

In the example of Section 4.3.1, the pier location was not yet defined and m = 16.1 tsf was assumed to be the nominal unit side friction based on a limited amount of data from 6 borings. The present section continues this case study by assuming that a (single or multiple shaft) foundation is located at a particular boring location (where horizontal correlation between borings is again ignored, as in practice borings will be further apart, anyway). Figure 5-4 may be directly plugged into the quadrant chart of Figure 3-16 (3rd quadrant), which is depicted in Figure 5-5. Assuming that the foundation is located at a boring with a mean strength larger than m = 16.1 tsf for the whole site (see Figure 2-9(a)) and as discussed above; the nominal unit side friction is conservatively adopted as m. An example for locating the foundation at a boring of mean strength below m is given below for comparison. Maintaining the vertical correlation length a_v = 5 ft, coefficient of variation in local strength CV_q = 0.53, design load Q_{des} = 2500 tons, shaft diameter D = 4 ft, and reliability index β = 3, Figure 5-5 shows the respective graphical iteration process (i.e., starting from L/a_v = 6, or L = 30 ft as discussed in more detail in Chapters 3 and 4) using n_f = 6. Design values obtained are a shaft length L = 15 ft (L/a_v = 3.0) and **Φ = 0.78**, which compares to L = 21 ft and Φ = 0.60 from Section 4.3.1 without a boring in the footprint.

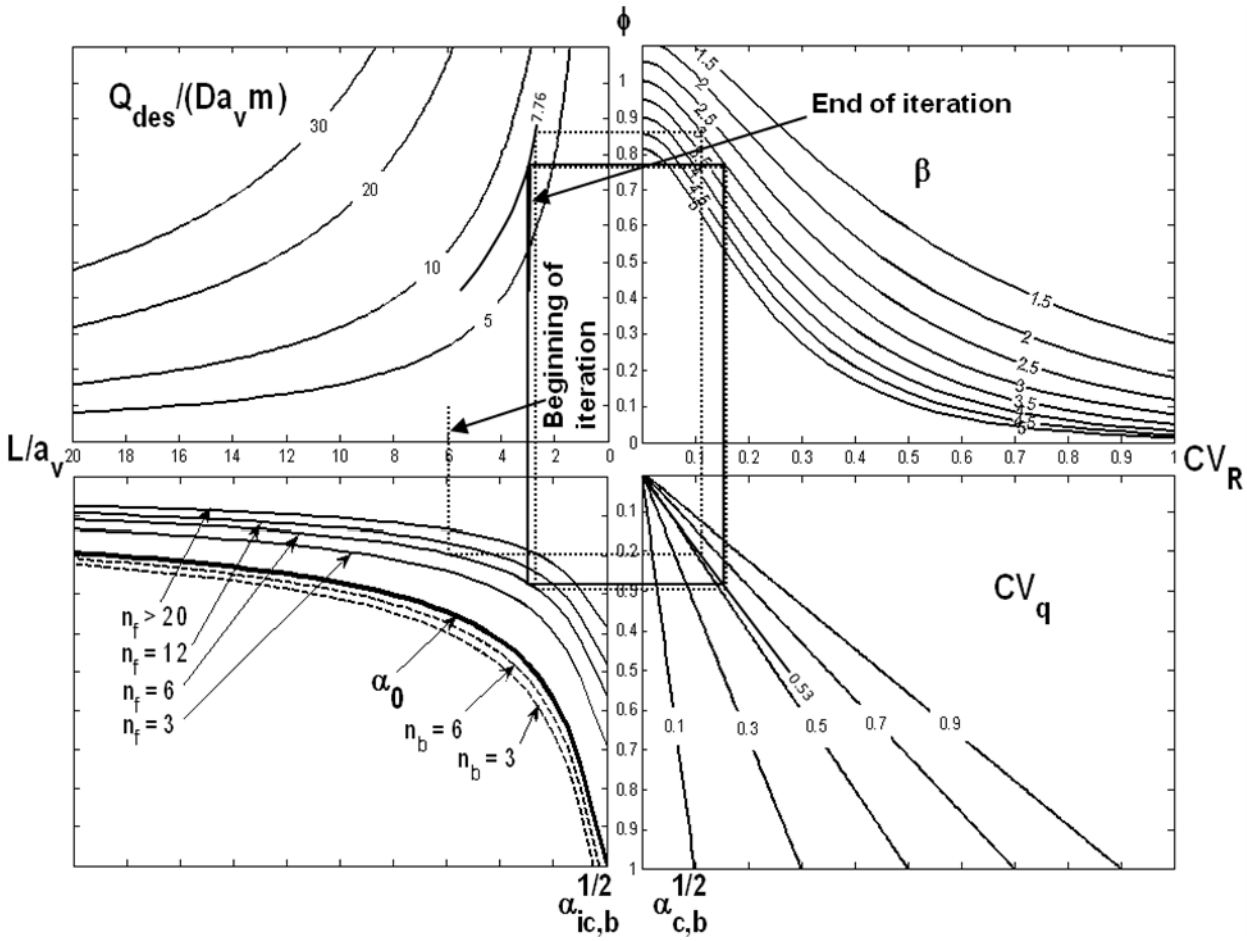

Figure 5-5. Quadrant chart with Figure 5-4 in 3rd quadrant and graphical design iteration for nominal unit side friction of m = 16.1 tsf.

If a pier is located at a boring location where the mean strength at the borehole is less than the site average m = 16.1 tsf, then it is conservative to use the mean strength value of that particular boring for design. If the same nominal value m = 16.1 tsf was used for the whole site, then the target probability of failure would be met on average over the whole site. However, given the information from the center borings at production shaft locations, individual probabilities of failure would be larger and smaller than the target value. A shaft at a borehole indicating low strength would have a probability of failure above the target value, which also leads to a higher probability of failure for the whole bridge, especially when failure of the whole bridge

may be caused by failure of a single pier. Assuming, for example, that a foundation is located at the top boring in Figure 2-9(a), the nominal design unit side friction would be 11.8 tsf leading to $Q_{des}/(Da_vm) = 10.59$, with all other parameters from above. Figure 5-6 shows the respective iteration process resulting in L = 20 ft ($L/a_v = 4$) and **$\Phi = 0.82$**. As expected, it is seen that the smaller unit skin friction used leads to larger shaft dimensions. However Φ also increases, which may be somehow counterintuitive at first, but may be explained by the larger degree of spatial averaging over the necessarily larger shaft (compare discussion immediately after Figure 3-16).

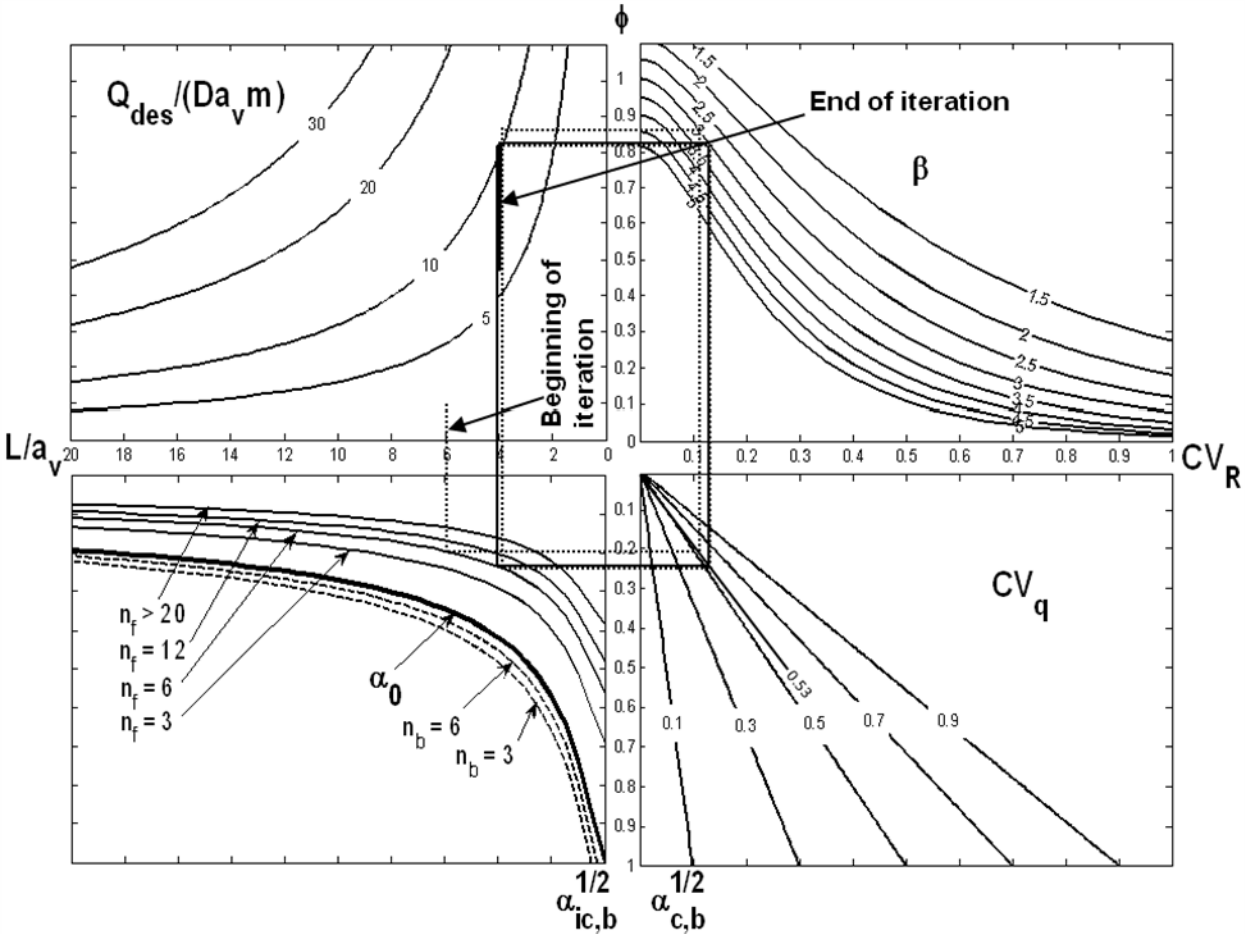

Figure 5-6. Quadrant chart with Figure 5-4 in 3rd quadrant and graphical design iteration for nominal unit side friction of 11.8 tsf.

This indicates that Φ, being a function of shaft dimensions in the present approach, loses its direct relationship with probability of failure/reliability and, as a consequence, appears to be reduced to an auxiliary variable equal to Q_{des}/R_n, whose increase or decrease is no longer strictly related to an increase or decrease in probability of failure when comparing shafts of different dimensions. The meaning of Φ as a direct link to probability of failure remains valid only when comparing shafts of equal dimensions.

CHAPTER 6
DEVELOPMENT OF LRFD Φ AS A FUNCTION OF SPATIAL VARIABILITY AND LOAD TESTING

6.1 AASHTO's LRFD Bias Factor λ_R

In the previous chapters, uncertainty in shaft (foundation) resistance was considered due to spatial variability in local strength q over the shaft surface, as well as between typically limited available data and the shaft surface. LRFD Φ values were obtained by assuming log-normal load and resistance distributions with Equation 3-22 containing the resistance bias factor λ_R as proportionality constant. Factor λ_R is defined as the average ratio of (load test) measured over (borehole) predicted resistances and its value is determined from a large amount of historic data from many sites. The use of λ_R in Equation 3-22, hence implies the assumption that borehole data consistently under- or over-estimate hypothetical production shaft (i.e., load test) resistances by a factor λ_R. If such a unique proportionality constant between borehole and load test resistances exists, and if it may be reliably determined, then the approach of the previous chapters is fully valid (see remarks in Section 6.7.4).

However, these conditions may not be met in general practice due to spatial variability within sites and variable conditions between sites. To overcome this, the present chapter lays out a concept for site specific bias correction based on site specific borehole and load test data. Instead of a simple proportionality constant, the approach uses linear regression (i.e., straight line fit through cloud of data points) to describe the relationship between load test resistances and borehole predicted resistances in the respective footprints of the load tests. This site specific relationship is then used to estimate production shaft resistances and uncertainties from borehole data at production shaft locations. Thus, for each particular site, the method accounts for spatial uncertainty between borehole data and shaft surface; systematic and random errors in the

borehole prediction method; and the amount of spatial averaging in the horizontal and vertical directions on the shaft surface. While the following sections give a detailed description of the theoretical approach, a practical case study from a site where borehole data are available in the footprints of load tests (Jewfish Creek) concludes the chapter.

6.2 Linear Regression between Borehole and Load Test Data

In order to establish a reliable relationship between borehole predicted and load test measured resistances for a given site, core samples must be taken at the center of every load test location prior to actual load testing (Figure 6-1). Core samples are analyzed in the laboratory (e.g., q_u, q_t) to estimate local skin friction values q_{Bi} by the selected method, while load test shafts are equipped with strain gages allowing for measuring contributions to total shaft resistance from a number of vertical shaft intervals. By knowing the surface area of each shaft interval, these resistance components may then be transformed into load test measured local (i.e., averaged over respective shaft interval) strengths q_{Li}.

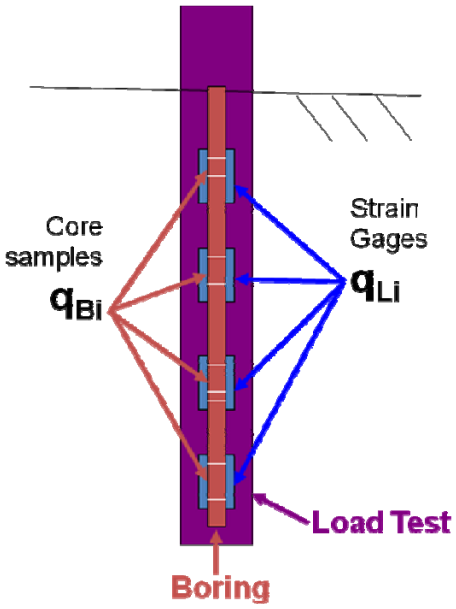

Figure 6-1. Example of core samples taken from borehole in center of subsequent load test. Core samples are analyzed in laboratory to predict local strengths and load test possesses strain gages to measure local strengths (unit side friction) over vertical shaft intervals.

Figure 6-2 depicts a scatterplot of q_{Li} against q_{Bi} where the red line represents the linear regression fit to the data, i.e., the red line is a best fit to the data points in the sense that the sum of the vertical squared differences between the data points and the regression line is a minimum. The regression line is defined by the equation

$$q_{Li} = a + bq_{Bi} + \varepsilon \tag{6-1}$$

where a and b are deterministic coefficients representing intercept and slope of the regression line, respectively, and ε is a random residual of mean zero and minimized variance σ^2_{ε}.

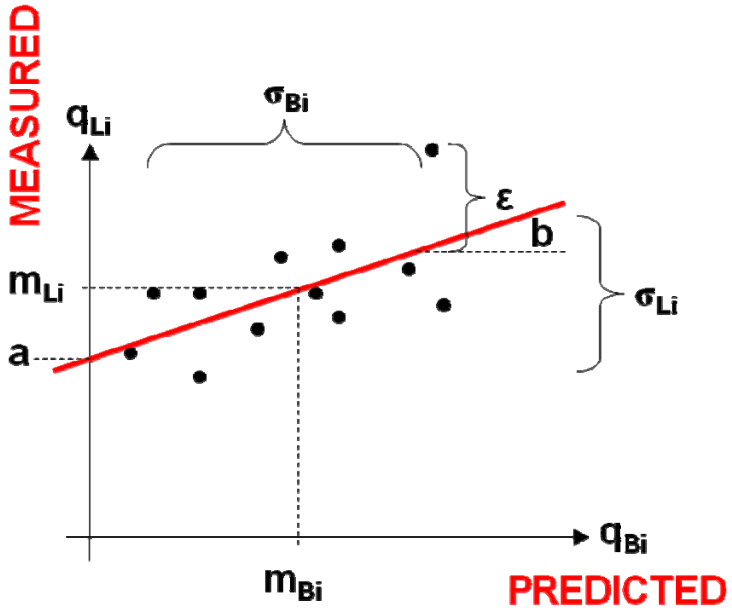

Figure 6-2. Data points of measured versus predicted strengths with linear regression line (red) and linear regression parameters.

Coefficients a and b may be interpreted as parameters accounting for systematic prediction bias (e.g., consistent over- or under-estimation) and a larger degree of spatial averaging over the shaft intervals than over core samples. Residual ε, in turn, is a random prediction error which includes spatial variability between borehole and shaft surface as well as random measurement errors, irregularities in test shaft surface, etc. From linear regression theory, it is known that

$$a = m_{Li} - b m_{Bi} \tag{6-2}$$

$$b = r_i \frac{\sigma_{Li}}{\sigma_{Bi}} \tag{6-3}$$

where m_{Li}, σ_{Li}, and m_{Bi}, σ_{Bi} are the respective means and standard deviations of load test and borehole data, and r_i is the correlation coefficient between them. The term r^2_i is often written as R^2 and called coefficient of determination. It expresses the portion of variability in q_{Li} (i.e., the portion of σ^2_{Li}), which is explained by the regression model. The portion of σ^2_{Li} not explained by the regression model is equal to the variance σ^2_ε of the random residual and given by

$$\sigma^2_\varepsilon = \sigma^2_{Li}\left(1 - R^2\right) \tag{6-4}$$

For example, $R^2 = 1$ would mean perfect correlation between q_{Li} and q_{Bi} such that all data points fall exactly onto the regression line and $\sigma^2_\varepsilon = 0$, indicating the q_{Bi} is a good estimator of q_{Li}. On the other hand, $R^2 = 0$ corresponds to zero correlation and zero predictive power of q_{Bi} on q_{Li}, such that $\sigma^2_\varepsilon = \sigma^2_{Li}$, i.e., information in terms of q_{Bi} does not improve estimation of q_{Li}. Regression model fits, as shown in Figure 6-2, are available as a standard function in Microsoft Excel, for example, which directly inform resulting values of a, b, and R^2 for a given data set.

6.3 Upscaling from Shaft Intervals to Whole Shafts

Since it is the resistance of entire shafts that is of interest rather than vertical intervals thereof, the obtained regression relationship needs to be upscaled. Borehole and load test data indexed by the letter "i" emphasize that respective values are defined on a support equal to the size of the shaft intervals. Assuming that borehole strength is a good predictor of shaft resistance (i.e., r_i close to one or $\sigma^2_\varepsilon/\sigma^2_{Li} << 1$), and based on the fact that core samples and load tests measure the same physical parameter, the vertical range a_v from borehole data (inferred from all borings in a sub-domain, not just at load test locations) can be applied to load test data (which

typically is too sparse for variogram analysis). Possible nugget components in the vertical variogram may be due to portions of σ^2_ε, which are not due to spatial variability such as instrumentation errors or similar. However, it is again conservative to fit a variogram through the origin, which is equivalent to attributing spatial correlation range a_v to these errors for conservative variance reduction. Assuming that load test intervals are of approximately the same length as borehole sample spacing, spatial averaging in the vertical direction is then the same for borehole and load test data resulting in the upscaled load test and borehole variances, i.e., $\sigma^2_L = \alpha_0\sigma^2_{Li}$ and $\sigma^2_B = \alpha_0\sigma^2_{Bi}$, respectively. The term α_0 is the variance reduction factor for a vertical line of test shaft length L (line shaft approximation) and may be found from Figure 3-2 (thick continuous line) or Appendix B, for example. For the common case of $L/a_v \geq 1$ and a spherical variogram

$$\alpha_0 = \frac{0.75}{\left(L/a_v\right)} - \frac{0.2}{\left(L/a_v\right)^2} \tag{6-5}$$

is a simple way of finding α_0. Note, however, that α_0 is only applicable to the variance contained in the vertical direction and needs to be used in Equation 3-8 in the presence of a random areal trend (i.e., variability contained in horizontal direction only). In this case, $s_v < 1$, and instead of α_0 from above, a variance reduction factor of $\alpha_0 s_v + (1 - s_v)$ is to be applied (see Section 3.6.1 17th Street Bridge example), where s_v is the sill of the variogram normalized to unit total variance (i.e., the portion of variance in σ^2 contained in the vertical direction). If the distance between center boring and shaft surface is not too large, however, (typically < 5 ft) such that the range of a random areal trend component may be assumed much larger, then it is still safe to use Equation 6-5 directly. In this case, the random areal trend component does not become effective over the short distance between boring and shaft.

After all, load test and borehole variances are both scaled by a factor (say α_0 in the sequel) being equivalent to a horizontal and vertical scaling of each data point by a factor $\alpha_0^{1/2}$ towards the respective mean values $m_L = m_{Li}$ and $m_B = m_{Bi}$, which remain the same after upscaling (Figure 6-3). As a consequence, the correlation coefficient is not affected by upscaling either, i.e., $r = r_i$, such that a, b, and R^2 in Equations 6-2, 6-3, and 6-4 are directly applicable to the upscaled regression model. Equation 6-4 further shows that σ^2_ε becomes $\alpha_0\sigma^2_\varepsilon$ after upscaling as $\sigma^2_L = \alpha_0\sigma^2_{Li}$ was found above. Consequently, Equation 6-1 after upscaling to shaft size may be written as

$$q_L = a + bq_B + \sqrt{\alpha_0}\varepsilon \tag{6-6}$$

where q_L is the mean unit side friction over the shaft surface of length L and q_B is the estimate of mean strength from a boring inside a shaft's footprint.

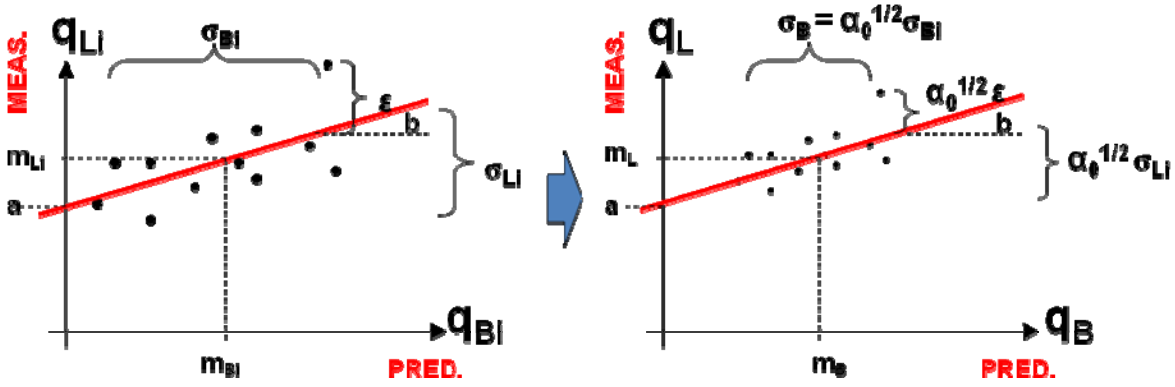

Figure 6-3. Shaft interval related data of Figure 6-2 (left) upscaled to whole shaft size (right) with respective regression parameters.

Equation 6-6 is a random equation with deterministic constants a, b, and α_0 and random variables q_L, q_B, and ε. Taking the expectation (mean) of both sides of the equation leads to the equation of the regression line

$$m^*_L = a + bm^*_B \tag{6-7}$$

since ε is an error component of zero mean (i.e., after bias correction, the average error is zero). The term m^*_B represents the predicted mean borehole strength over a depth L, which is converted by Equation 6-7 into an expected (nominal) unit side friction m^*_L over a (production) shaft surface corrected for prediction bias and horizontal variance reduction. By subtracting Equation 6-7 from Equation 6-6, one obtains the residuals, which after squaring and taking the expectation (as shown in the bottom of Appendix B), the equation for the variances results.

$$\sigma^{*2}_L = b^2\sigma^{*2}_B + \alpha_0\sigma^2_\varepsilon \tag{6-8}$$

Here, σ^{*2}_L is the expected (bias corrected) variance of m^*_L, while σ^{*2}_B is the prediction uncertainty about m^*_B. The square root of Equation 6-8 divided by Equation 6-7, results in the bias corrected coefficient of variation CV_R of shaft resistance

$$CV_R = \frac{\sigma^*_L}{m^*_L} = \frac{\sqrt{b^2\sigma^{*2}_B + \alpha_0\sigma^2_\varepsilon}}{a + bm^*_B} \tag{6-9}$$

With this and a given reliability index β, a value of LRFD Φ_u may be found from Figure 6-4, which is based on Equation 3-22 with unit resistance bias factor, i.e., $\lambda_R = 1$.

In other words, the classic LRFD design equation $Q_{des} = \Phi R_n$ is reformulated as $Q_{des} = \Phi_u m^*_L A_s$ (A_s being the lateral shaft surface area) as bias correction is now contained in m^*_L and no longer in Φ. A design unit side friction can thus be defined as $f_{des} = \Phi_u m^*_L$. A graphical comparison between the classic and present bias correction approach is presented in Figure 6-5 showing that λ_R is simply a proportionality constant (slopes of blue lines) between load test measured and borehole predicted strengths, while the regression line (red) parameters a and b provide more flexibility to fit the general tendency of the data points. Horizontal averaging over test shafts, for example, tends to decrease the variance in σ^2_L with respect to σ^2_B, leading to a > 0 (larger stretching of the data cloud along x-axis than along y-axis). This would result in generally

larger values of λ_R for small values of q_B and smaller values of λ_R for large values of q_B, which cannot be captured by a single (average) value of λ_R as currently used.

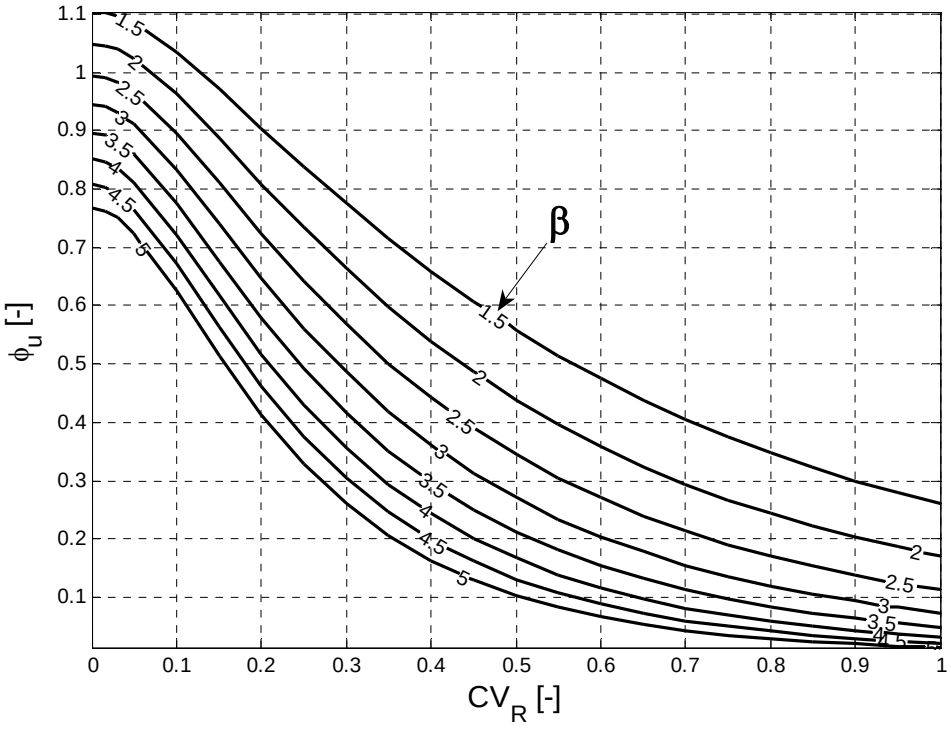

Figure 6-4. LRFD resistance factor Φ_u as a function of resistance coefficient of variation CV_R and reliability index β for unit resistance bias factor $\lambda_R = 1$ (Equation 3-22). Variable Φ from Figure 3-15 is equal to $1.06\Phi_u$ from this figure.

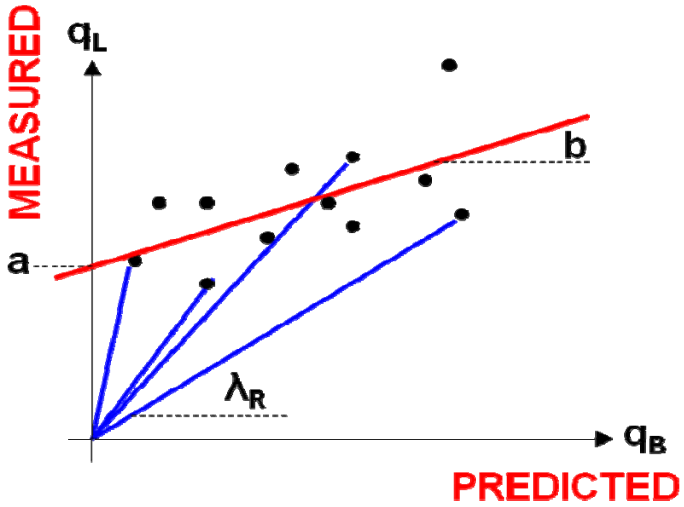

Figure 6-5. Comparison of classic (blue lines) and present (red line) approach for bias correction.

6.4 Design without Center Boring

In the same way as in Chapter 4, it is assumed here that n_b borings with core sample data are available from a site (or sub-domain if previously divided). The data resolution of the first 3 to 4 borings must be sufficient to construct a vertical variogram (i.e., sample spacing smaller than vertical range a_v), while the remaining borings may be sampled at a separation not larger than a_v. Next, load testing with a shaft of dimensions similar to a future production shaft is performed at locations within the zone or region for which the borings were sampled and a variogram was established. Note, a sample boring is also performed in the footprint of the load test or tests from which the resulting parameters a, b, and σ^2_ε from Equations 6-2, 6-3, and 6-4 may be determined.

For a yet unknown production shaft location (or a known location without center boring), the best predictor of design unit skin friction m^*_B is the mean borehole strength m of all n_b borings with a variance $\sigma^{*2}_B = \sigma^2_m$ given by Equation 3-9 using a variance reduction factor α from Equation 4-1. Note that Equation 3-8 needs to be considered as well in the presence of a nested variogram, e.g., random areal trend such that

$$\sigma^{*2}_B = \alpha_0 \left(1 + \frac{1}{n_b} \right) \sigma^2 \qquad (6\text{-}10)$$

where α_0 corresponds to averaging along a vertical line of shaft length L (including possible random areal trend), and σ^2 is the total variance in local strength data from all borings. With this and Equation 6-7, all the parameters in Equation 6-9 are defined to determine CV_R and, subsequently, Φ_u (Figure 6-4) and $f_{des} = \Phi_u m^*_L$.

6.5 Design with Boring in Footprint of Production Shaft

As opposed to the previous section, where production shaft location is unknown, the present section considers the scenario of Chapter 5, where borehole data are available inside the footprint of a production shaft. In this case, the best predictor m^*_B of shaft unit side friction is the mean m_B of the strength data from the boring in the footprint. As m_B is actually an observed value in the design foundation footprint, its variance is zero leading to $\sigma^{*2}_B = 0$. With this, Equation 6-9 reduces to

$$CV_R = \frac{\sqrt{\alpha_0 \sigma_\varepsilon^2}}{a + bm^*_B} \tag{6-11}$$

which is independent of n_b and always smaller than CV_R from Equation 6-9 with $\sigma^{*2}_B > 0$. The expected (nominal) unit side friction m^*_L over a (production) is again found from Equation 6-7. Important to notice is that in order for the regression model from load tests to be applicable to production shafts, the borehole sampling and test shaft configurations (i.e., borehole sample density and shaft diameter) need to be similar to the conditions at the production shaft. In general, it may be stated that the larger the correlation is between borehole and respective load test data, the smaller will be CV_R and the larger Φ (for constant shaft dimensions).

6.6 Design without Load Testing

As identified earlier, in order to construct the linear regression model instead of AASHTO bias λ_R, a minimum number of load test and borehole data is required. Due to costs, generally the limiting factor in practice is the number of load tests performed. However, linear regression theory provides relationships for the uncertainty of the parameters obtained as a function of the number n_i of data pairs available (i.e., the number of load test intervals with corresponding

borehole data). For example, the variances of the parameters a and b (e.g., Equation 6-6) are known to be

$$\sigma^2{}_a = \sigma^2{}_b\left(\sigma^2{}_{Bi} + m_{Bi}{}^2\right) \tag{6-12}$$

$$\sigma^2{}_b = \frac{\sigma^2{}_\varepsilon}{n_i \sigma^2{}_{Bi}} \tag{6-13}$$

such that a possible criterion for a minimum number of load test intervals may be that the coefficient of variation $CV_b = \sigma_b/b$ be smaller than a certain threshold (e.g., 10%). It is expected from Equation 6-13 that 10 to 15 pairs of estimated and measured unit skin friction be sufficient to establish reliable regression coefficients (i.e., a and b). In addition, borehole data should be available prior to any load testing in order to assist in defining load test locations, such that load tests are performed over a wide range of strength conditions (e.g., one load test at a boring indicating weak rock and another load test at a boring indication strong rock). This should help in constructing a regression model, which is representative of all possible conditions at a site.

It may be of interest not to perform any load testing at a site (e.g., small bridge), but still use the linear regression bias approach of Equation 6-6. For such situations, conservative values of a, b, and σ^2_ε need to be defined, which can only be improved upon by actual load testing and regression analysis. Figure 6-6 illustrates this conceptual idea by showing a series of possible outcomes of bias regression relationships (black lines) inferred from load testing at many sites and a most conservative regression line (red dashed), which should be adopted if no load testing is done. From Equation 6-7, it is seen that a = 0 and some value of b < 1 would be conservative (e.g., b = 0.75), such that a conservative version of Equation 6-7 could be

$$m^*{}_L = 0.75 m^*{}_B \tag{6-14}$$

where m^*_B = m for no center boring (or unknown shaft location) and which would be equivalent to adopting $\lambda_R = 0.75$ in the classic bias approach.

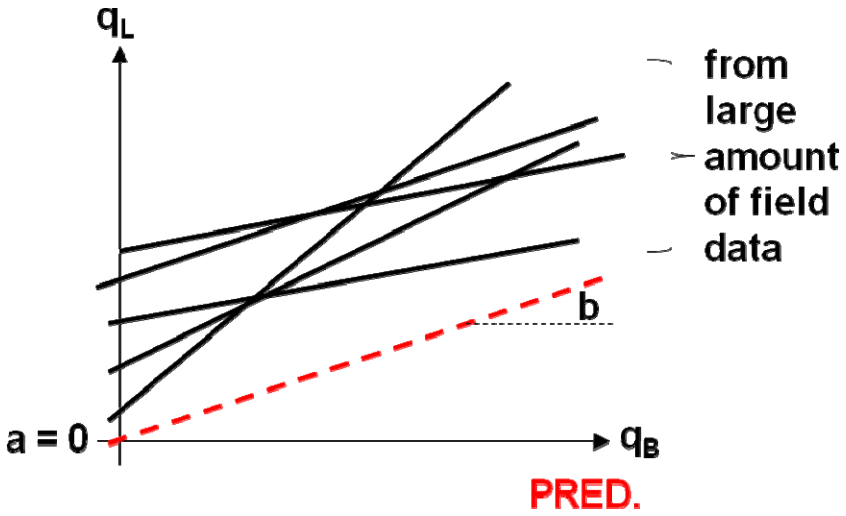

Figure 6-6. Possible outcomes of regression lines for load testing at many sites (black lines) and conceptual example of conservative regression line (red dashed), if no load testing is performed.

In Equation 6-8, however, it is conservative to not use a small value of b, i.e., b = 1, and some conservative value of σ^2_ε needs to be found as well. Similar with the selection of a and b, a value of $\sigma^2_\varepsilon = 0.2\sigma^2$ (i.e., 20% of local strength variance) may be used for illustration, noting that the numerical values are subject to future modification and validation as load tests with collo-cated boring results become available. It should be noted that while σ^2_ε consists of a component due to spatial variability between boring and shaft (see Chapter 5), it also includes some random measurement error component, as well as precision issues related to core sample strength testing which must be considered in giving a sound theoretical basis to a most conservative value of σ^2_ε. With the example numbers, a conservative version of Equation 6-8 would be

$$\sigma^{*2}_L = \alpha_0\left(1.2 + \frac{1}{n_b}\right)\sigma^2 \qquad (6\text{-}15)$$

where Equation 6-10 was used. Equation 6-14 and 6-15 may be combined to express CV_R in analogy to Equation 6-9, which simplifies to

$$CV_R \approx 1.46\sqrt{\alpha_0}CV_q \approx \sqrt{2\alpha_0}CV_q \tag{6-16}$$

for large n_b (say > 20). For the conservative example values chosen, Equation 6-16 indicates that the penalty for no load tests results in a CV_R of 46% larger than the line shaft approximation (Chapter 3) which corresponds approximately to doubling the respective variance reduction factor (right hand side of Equation 6-16).

In case borehole data are available in the production shaft footprint, σ^{*2}_B is again zero and Equation 6-15 becomes

$$\sigma^{*2}_L = 0.2\alpha_0\sigma^2 \tag{6-17}$$

Equation 6-14 is not affected other than that $m^*_B = m_B$, i.e., the mean strength at the boring in the shaft footprint only. The resulting CV_R (σ_L^{*2}/ m^*_L) leads to

$$CV_R \approx 0.60\sqrt{\alpha_0}\frac{\sigma}{m_B} \approx \sqrt{\frac{\alpha_0}{3}}\frac{\sigma}{m_B} \tag{6-18}$$

which for $m_B \approx m$ indicates a significant reduction in CV_R with respect to Equation 6-16 and also shows that CV_R increases as m_B decreases, i.e., as the mean local strength at a boring becomes smaller (provided that shaft dimensions and, hence, α_0 are kept constant).

6.7 Case Study – Jewfish Creek

6.7.1 Regression Analysis

Among data from several sites (Victory, Apalachicola-SR20, MIC People Mover, etc.) with load testing analyzed, Jewfish Creek was the only site with borehole data inside the load test footprints and at depths commensurate with load test instrumentation. For instance, Victory and Apalachicola-SR20 Bridges had data in the footprint of load tests, but at depths greater than

the tip of the shafts. A summary of the borehole data from Piers 1 through 38 from Jewfish Creek is contained in Appendix C resulting in the histogram and vertical variogram of Figure 6-7. The vertical variogram, however, may not be considered reliable, since vertical data spacing is too large (> 5 ft) and a few extreme data values dominate Figure 6-7(b). It will be used in the sequel with a vertical range av ≈ 15 ft for illustration purposes only. Note further that no

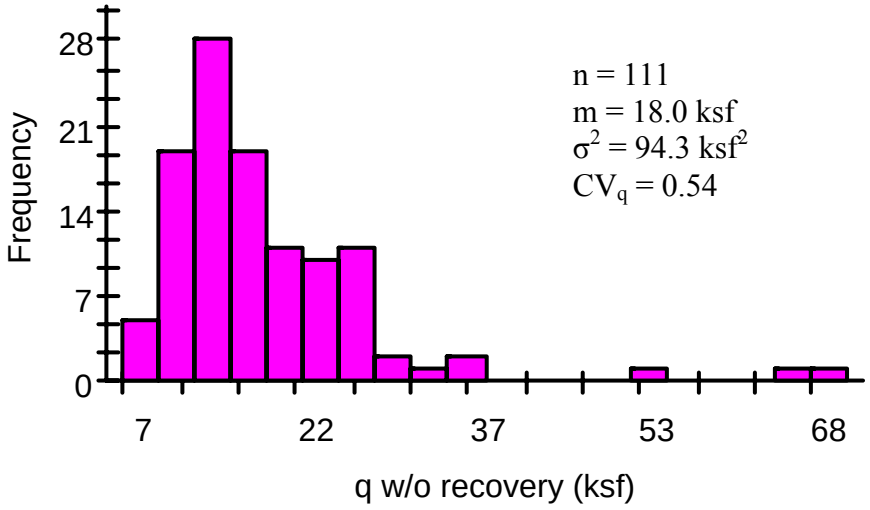

(a)

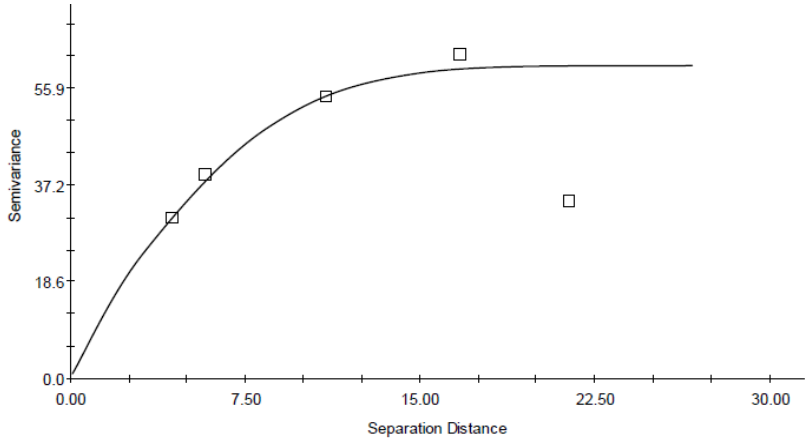

(b)

Figure 6-7. Jewfish Creek data (Appendix C): (a) Histogram with summary statistics; and (b) Vertical variogram. Note that the vertical variogram is not considered to be reliably inferred and is only used for illustrational purposes in the sequel.

recovery data was available for the borings in the footprints of the load tests. As a consequence, the regression model below is built with predicted borehole strengths that are not corrected for recovery and is only to be used with borehole prediction data which is not corrected for recovery either. If recovery data were available for borehole strength correction, it is expected that strength prediction would improve (i.e., different coefficients a and b, and smaller σ_ε^2). In theory, any parameter may be used as a predictor for unit load test side friction, however, its predictive power may be zero (i.e., b = 0 and large σ_ε^2) and the upscaling of the regression model would become questionable (high σ_ε^2 - low CV_R and Φ).

Shown in Figure 6-8 are the tabular reported unit skin frictions from statnamic load tests TS-1 and TS-2 at Jewfish Creek (shaft lengths L = 30 ft, diameters D = 48 and 60 in with strain gage intervals of 5 – 10 ft). Applied Foundation Testing, the company who conducted the testing, recommend in their report that the first values (51 and 32.2 ksf) in the tables be neglected due to construction issues (i.e., casing lip resulting in end bearing effects); also the last one or two values were neglected due to small axial displacements, i.e., failure to mobilize the ultimate skin friction. The remaining data are used herein, marked by red boxes and summarized in Figure 6-9(a) together with the corresponding local strength values from collocated core sample analysis, i.e., $q = 0.5(q_u q_t)^{1/2}$. Note that Figure 6-9(a) indicates a general tendency of the borehole data to over-estimate load test unit side friction ($m_{Li} = 17.4 < m_{Bi} = 21.1$ ksf). It may be further observed that both load tests were performed in areas of stronger ground than the site average ($m_{Bi} = 21.1 > m = 18.0$ ksf). The 6 data pairs are plotted in Figure 6-9(b) (red dots) to which a linear regression line is fitted (black line) resulting in parameters a = 1.55, b = 0.75 (CV_b = 0.23 from Equation 6-13) and $R^2 = 0.77$. These parameters define a (partially) random relationship between borehole and load test data, which is illustrated by the cloud of grey dots

Drilled Shaft Location	Segment Length (feet)	Segment Surface Area (ft²)	Maximum Mobilized Unit Side Shear (ksf)
Ground Surface +6.0 ft to –12.5 ft Perm Casing -12.5 ft to –15.3 ft (Segment 1)	2.8	35.2[1]	51.0[1]
-15.3 ft to –20.8 ft (Segment 2)	5.5	69.1	32.0
-20.8 ft to –26.2 ft (Segment 3)	5.4	67.8	16.8
-26.2 ft to –32.0 ft (Segment 4)	5.8	72.8	12.2
-32.0 ft to –37.4 ft (Segment 5)	5.4	67.8	4.9
Unit End Bearing @ Elevation -37.4 feet			11.2

Notes:
1) Assumed full load transfer to bottom of casing, with surface area calculated from the remaining 2.8 ft of limestone socket. Unit side shear in segment 1 likely elevated by "bearing lip" at casing bottom transition.
2) In calculation of estimated unit end bearing, we have subtracted out the side shear resistance from the 1.5 foot plug.

(a)

Drilled Shaft Location	Segment Length (feet)	Segment Surface Area (ft²)	Maximum Mobilized Unit Side Shear (ksf)	
Ground Surface +6.0 ft to –13.5 ft Perm Casing -13.5 ft to –18.5 ft (Segment 1)	5.0	78.59[1]	32.2[1]	⇐ DO NOT USE
-18.5 ft to –29.0 ft (Segment 2)	10.5	164.8	18.2	⇐ MAX
-29.0 ft to –39.1 ft (Segment 3)	10.1	158.5	7.2	
-39.1 ft to –49.9 ft (Segment 4)	10.8	169.5	2.2	
-49.9 ft to –59.5 ft (Segment 5)	9.6	150.7	2.6	
Unit End Bearing @ Elevation -59.5 feet			11.5	

Notes:
1) Assumed full load transfer to bottom of casing, with surface area calculated from the remaining 5.0 ft segment. Unit side shear in segment 1 likely slightly elevated by "bearing lip" at casing bottom transition.
2) In calculation of estimated unit end bearing, we have subtracted out the side shear resistance from the 1.5 foot plug.

(b)

Figure 6-8. Measured unit side friction from load tests over various intervals: (a) TS-1; and (b) TS-2. Red boxes indicate data used for regression model.

Depth interval		TS, q_{Li}	Boring, q_{Bi}
(ft)	(ft)	(ksf)	(ksf)
-15.3	-20.8	**32**	**37.5**
-20.8	-26.2	**16.8**	**14.3**
-26.2	-32	**12.2**	**19.5**
-18.5	-29	**18.2**	**16.8**
-18.5	-29	**18.2**	**27**
-29	-39.1	**7.2**	**11.3**
	Mean:	17.4	21.1
	Variance:	69.2	93.8

(a)

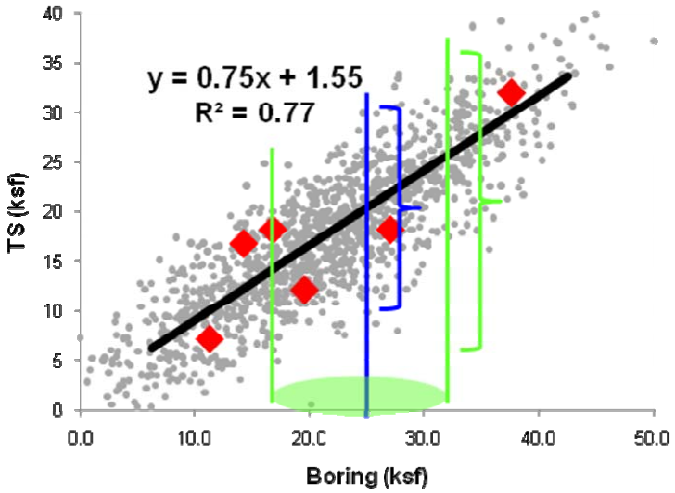

Red dots are data from (a) and black line is regression line with parameters a = 1.55, b = 0.75 and R^2 = 0.77. Small grey dots are many possible outcomes of this regression model. Blue sling brace symbolizes uncertainty in production shaft unit side friction when center boring is present (no uncertainty on x-axis). Green sling brace symbolizes increased uncertainty in production shaft unit side friction when center boring is not present (green ellipse symbolizes uncertainty on x-axis, i.e., in borehole data at production shaft location).

(b)

Figure 6-9. Data used from tests at Jewfish Creek: (a) Load test versus boring strengths; and (b) Regression model.

(i.e., the regression line of all grey dots is also equal to the black line with same R^2). From Equation 6-4, σ^2_ε = 15.9 ksf^2 where σ^2_{Li} = 69.2 ksf^2 from Figure 6-9(a). From Figure 3-2 (thick continuous line) or Equation B-5 (Appendix B) a_v = 15 ft from above, results in α_0 = 0.33 as the last parameter required for design.

6.7.2 Design without Boring in Footprint

According to Section 6.4 (and using parameters from Figure 6-7(a)), it is assumed that an exact production shaft location is not yet defined (or at a location where no borehole data are available) such that $m^*_B = m$ = 18.0 ksf and σ^{*2}_B = 33.0 ksf^2 from Equation 6-10 (with large $n_b \approx$ 20). Equation 6-7 further gives m^*_L = 15.1 ksf with CV_R = 0.32 from Equation 6-9 (symbolized

in green in Figure 6-9(b)) resulting in $\Phi_u = 0.47$ from Figure 6-4 and a design unit side friction $\mathbf{f_{des} = \Phi_u m^*_L = 7.1\ ksf}$. If no load test data are available, i.e., a, b, and σ^2_ε are not known for the particular site and the exemplary conservative values given above are adopted, then $m^*_B = m$ as before, however, $CV_R = 0.45$ from Equation 6-16 and $\Phi_u = 0.32$ from Figure 6-4. Term m^*_L = 13.5 ksf from Equation 6-14 leading to $\mathbf{f_{des} = 4.3\ ksf}$, which is smaller than 7.1 ksf for the presence of load testing. For comparison, if a value $\lambda_R = 0.8$ is adopted as the mean ratio of q_{Li}/q_{Bi} from Figure 6-9(a) with $CV_R = \alpha_0^{1/2} CV_q = 0.32$ (Equation 3-9) giving $\Phi_u = 0.47$ (Figure 6-4), then $\Phi = \lambda_R \Phi_u = 0.38$ and $\mathbf{f_{des} = \Phi m = 6.8\ ksf}$.

6.7.3 Boring in Production Shaft Footprint

According to Section 6.5, it is now assumed a production shaft is located at one of the previously sampled borings. Term m^*_B in this case is equal to the mean strength m_B at the boring in question and $\sigma^*_B = 0$. Assuming $m_B = m$ in a first example, m^*_L = 15.1 ksf as above with $CV_R = 0.15$ from Equation 6-11. Figure 6-4 indicates $\Phi_u = 0.74$ giving $\mathbf{f_{des} = 11.2\ ksf}$. For other hypothetical values of m_B = 15.5 and 20.3 ksf, respective values of f_{des} would be 9.2 and 12.6 ksf. In the absence of load testing, and adopting the examples of conservative regression parameters suggested above, $CV_R = 0.18$ from Equation 6-18 giving $\Phi_u = 0.68$ from Figure 6-4 and values of $\mathbf{f_{des} = 9.2}$, 7.2, and 10.7 ksf for m_B = 18.0, 15.5, and 20.3 ksf, respectively. These values of f_{des} are consistently smaller than for comparable cases (i.e., equal m_B) in combination with a regression model inferred from load test data.

6.7.4 Remarks

Values of f_{des} given above are strictly valid only for a production shaft diameter equal to the test shaft diameters. The same applies to shaft length, however, by adjusting the value of α_0 to production shaft length, production shaft length may differ from test shaft length. The

parameters of the upscaled regression model are theoretically not affected by different production and test shaft lengths. Evaluation of the possibility to extend the approach to multiple shaft foundations and situations where more than a single boring may be available in test and production shafts should also be considered. The same applies to a reliable definition of conservative (worst case) parameters of the regression model in the absence of load testing, where theoretical (geostatistical) considerations and upcoming field data from load tests with collocated boring data are combined. For practical implementation, it is again convenient to find a required shaft length, for example, from a given design load, which is the inverse calculation as performed above. The adoption of a procedure similar to the graphical quadrant chart iteration introduced in Chapter 3 appears viable and should be investigated as well. In general, it may be noted that results of previous chapters are consistent with the approach of the present chapter if the regression model $m^*_L = a + bm^*_B$ and $\sigma^{*2}_L = b^2\sigma^{*2}_B + \alpha_0\sigma^2_\varepsilon$ from Equation 6-7 and 6-8 is reduced to $m^*_L = \lambda_R m^*_B$ and $\sigma^{*2}_L = \lambda_R{}^2\sigma^{*2}_B$, i.e., $a = \sigma^2_\varepsilon = 0$ and $b = \lambda_R$.

CHAPTER 7
SUMMARY, CONCLUSIONS, AND RECOMMENDATIONS

7.1 Current Practice and Scope of Work

During the past five to ten years, the FDOT, as well as other DOTs and the FHWA, have moved away from allowable stress design (ASD) to load and resistance factored design (LRFD) based on probability for deep foundation design. For example, using their extensive database of load tests with adjacent borings/laboratory tests within Florida, the FDOT established LRFD resistance factors Φ based on assumed reliability (Figure 7-1). The LRFD resistance factors Φ for drilled shafts founded in Florida limestone were established for reliability of 2.5 to 3.0 and an expected pile/shaft coefficient of variation (CV_R) of 0.25 to 0.30. In addition, all limestone is generally treated as uniform and constant over a site, i.e., it is not broken into zones.

3.6.3 Resistance Factors [10.5.5] ***(01/06)***[33]

Delete ***LRFD*** Table 10.5.5-3 and substitute ***SDG*** Table 3.5 for drilled shafts.

Table 3.5 Resistance Factors for Drilled Shafts (Bridge Foundations)

Loading	Design Method	Construction QC Method	Resistance Factor,φ	
			Redundant	Non-redundant[6]
Compression	For soil: FHWA alpha or beta method[1]	Std Specifications	0.60	0.50
	For rock socket: McVay's method[2] neglecting end bearing	Standard Specifications	0.60	0.50
	For rock socket: McVay's method[2] including 1/3 end bearing	Standard Specifications	0.55	0.45
	For rock socket: McVay's method[2]	Statnamic Load Testing	0.70	0.60
	For rock socket: McVay's method[2]	Static Load Testing	0.75	0.65
Uplift	For soil: FHWA alpha or beta method[1]	Std Specifications	Varies[1]	Varies[1]
	For rock socket: McVay's method[2]	Std Specifications	0.50	0.40
Lateral[3]	FBPier[4]	Std Specifications Or Lateral Load Test[5]	1.00	0.90

1. Refer to FHWA-IF-99-025, soils with N<15 correction suggested by O'Neill.
2. Refer to ***FDOT*** ***Soils and Foundation Handbook***.
3. Extreme event.
4. Or comparable lateral analysis program.
5. When uncertain conditions are encountered.
6. As defined in SDG 3.6.9.

Commentary: LRFD resistance factors are based on the probability of failure (Pf) of an element or group of elements resisting structural loads. When resistance factors were calibrated, the state of practice utilized redundant drilled shaft

Figure 7-1. Table 3.5 of the *FDOT Structural Design Manual* for drilled shafts in limestone.

Unfortunately, typical rock strengths (unconfined and split tension) vary from site to site resulting in a range of coefficient of variation of rock strengths CV_q throughout Florida. Reducing the expected variation in axial shaft resistance CV_R over the measured rock strength variability CV_q, is the summation (i.e., mean or average) of rock strengths over the surface area of the shaft. Obviously, the length of shaft (e.g., L= 10 ft versus 30 ft) significantly affects the averaging process and the computed CV_R, which directly impacts the resulting LRFD Φ. Moreover, any rock strength which is correlated spatially as shown in Figure 7-2 (i.e., red→ yellow→green→blue indicating the range of strong-to-weak rock) may be represented by a spatial covariance function and correlation length and will result in less averaging and larger shaft variability CV_R, leading to smaller LRFD Φ. Also contributing to the uncertainty in addition to CV_R, are the number and locations of borings. Chapters 3 to 5 address all the issues related to estimating CV_R and the ensuing LRFD Φ for various boring scenarios, i.e., number of borings; location of borings relative to each other; and with respect to the design shaft through the principles of geostatistics which cumulate in a number of design charts.

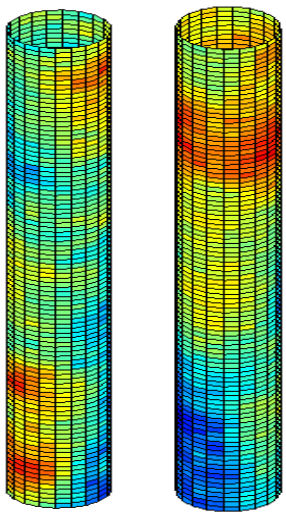

Figure 7-2. Variation of rock strength at 17th Street Bridge.

For this work, it was assumed that the relationship between the measured shaft resistance (e.g., skin and tip) and the borehole's estimate of resistance, based on insitu/laboratory properties (strength and modulus), is a known proportionality constant, i.e., bias (λ_R) (e.g., AASHTO's λ_R = 1.06). To address the issue of the uncertainty of the design method, as well as the use of load testing, Chapter 6 redevelops the relationships between measured load shaft variance σ^2_L and borehole predicted resistance variance σ^2_B plus a variance of a random residual σ^2_ε, which accounts for uncertainty in the shaft construction and the design methodology. A summary of the work follows.

7.2 Use of Geostatistics to Assess Shaft Resistance from Borehole Data

One of the major findings of this research is that typical Florida limestone has various levels of correlation in both the vertical and horizontal direction (e.g., 17th Street, Fuller Warren, and Jewfish Creek Bridges). Correlation may be established from a semi-variogram (frequently abbreviated to variogram) $\gamma(h)$, which may be assessed from strength data at multiple different distances (h) as

$$\gamma(h) = \frac{1}{2n_h}\sum_{n_h}\left(q_i - q_j\right)^2 \tag{7-1}$$

That $\gamma(h)$ is equal to half of the mean squared difference of n_h data pairs (q_i, q_j) separated by a distance h. The variogram is related to the spatial covariance function C(h) by

$$\gamma(h) = \sigma^2 - C(h) \tag{7-2}$$

where σ^2 represents the variance of the local strength data. Since the covariance function C(h) reaches zero at a distance **a**, the variogram will start small (e.g., 0) and rise exponentially or spherically, until the variance σ^2 is reached at a spacing of **a**. The correlation length a may be different in the vertical a_v, from the horizontal a_h, direction (e.g., 17th Street Bridge a_v = 5 ft, and

a_h = 12 ft). The vertical correlation a_v may be established readily from all borehole data which are considered similar. For instance, each of the six borings near Pier 10 at 17th Street Bridge had similar means and variance over the full depth and was consequently considered as a statistically homogeneous zone or region. In the case of Fuller Warren Bridge (Chapter 2), the differences in mean and variance were quite large over the depth. Subsequently breaking the depth into layers, the variance of each layer was greatly reduced, which resulted in a lower coefficient of variation CV_q of each layer and the ensuing CV_R of the whole shaft. Further discussion on anisotropy (zonal & geometric) is given in Chapter 2.

Having established the summary statistics (CV_q) as well as the relationship between point-to-point strength or modulus values C(h) as a function of correlation length a, the work focused on assessing the nominal shaft resistance R_n and its corresponding variability CV_R. Since the total side friction on a shaft is obtained from the average point-to-point rock strength (e.g., ½sqrt($q_u q_t$)), the ratio of the variance of the shaft resistance σ_s^2 to the rock σ^2 is given by (Equation 3-4),

$$\alpha = \frac{\sigma_s^2}{\sigma^2} = \frac{1}{A_s^2} \int_{A_s} \int_{A_s} C'(h) dA_1 A_2 \tag{7-3}$$

where C′(h) is the normalized covariance, i.e., C′(h) = C(h)/σ^2. Next, due to the simple linear relationship of the arithmetic averaging process for side friction, the mean rock strength (m) for all the borings will be the same as the mean shaft resistance (m_s). Consequently, the coefficient of variation of the shaft resistance (CV_R) is given by Equation 3-9 or

$$CV_R = \frac{\sqrt{\alpha \sigma^2}}{m} = \sqrt{\alpha} CV_q \tag{7-4}$$

Equation 7-3 was subsequently used to evaluate α for different assumptions on the covariance (e.g., spherical and exponential). For example, for a single shaft (solutions given for double, triple, and quadruple in Chapter 3) with an exponential covariance, α was given in Figure 3-2 and shown in Figure 7-3.

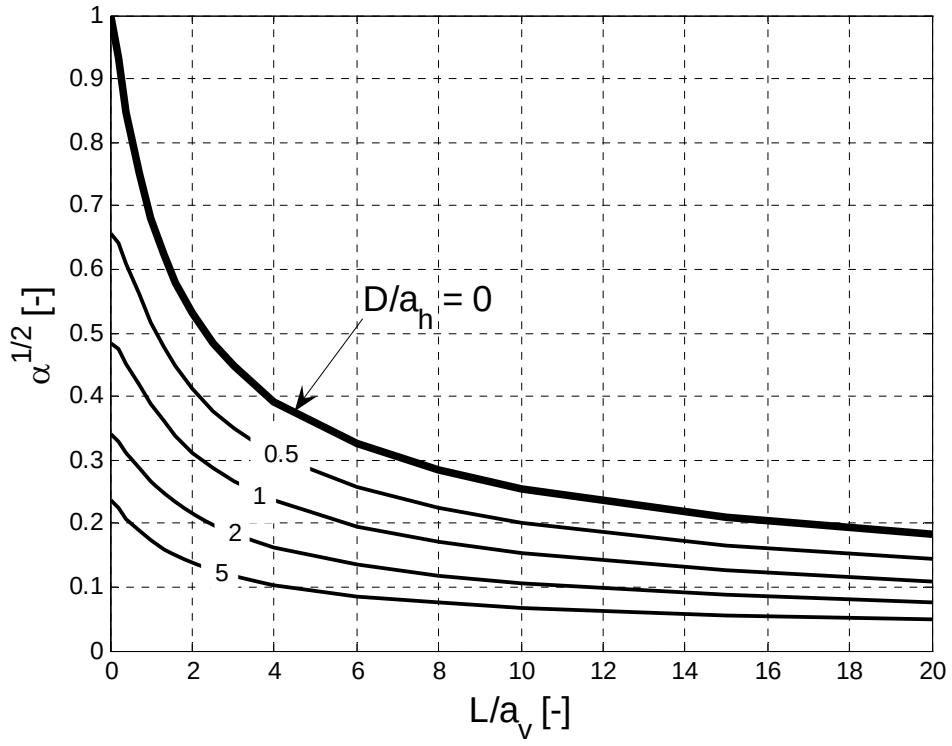

Figure 7-3. Integration $\alpha^{1/2} = \sigma_s/\sigma$ as a function of L/a_v and D/a_h for single shafts.

A number of important observations are evident from Figure 7-3. Firstly, the existence of large correlation lengths a_v or a_h, relative to shaft length and diameter, result in large $\alpha^{1/2}$ which result in larger CV_R and result in lower LRFD Φ. Secondly, assuming that the diameter of the shaft is small compared to a potentially unknown horizontal correlation length (a_h,) always results in a conservative estimate of CV_R.

Using AASHTO's First Order Second Moment Approach (i.e., assumed log-normal resistance and loads) with an assumed bias λ_R of 1.06, the LRFD Φ may be established (Figure

3-15). However in order to assess Φ for a given site, the physical dimensions of the shaft parameter are required based on a given design load. In an effort to find a practitioner-friendly solution to this problem, a graphical iteration method was developed in Chapter 3 based on the "quadrant chart" approach (see Figure 3-16, displayed in Figure 7-4). Four individual charts are arranged in a way that they share their axes with two neighboring charts such that when one chart is left at one axis, the respective neighboring chart is automatically entered. By prescribing a value for D, each chart possesses a series of curves whose parameters are known. The purpose of this is to perform a graphical iteration process to find L (starting from a guessed initial value) by "looping" through the quadrant chart in counter-clockwise direction. Each individual quadrant of the chart represents a fundamental relationship of the design process. Starting in the top-right corner and going counter-clockwise these relationships are:

- **1st quadrant**: $\Phi = f(CV_R)$ where β is a known parameter;
- **2nd quadrant**: $L/a_v = f(\Phi)$ using the LRFD design equation $Q_{des} = R_n\Phi = DL\pi m\Phi$ where $Q_{des}/(Da_v m)$ is a known parameter;
- **3rd quadrant**: $\alpha^{1/2} = f(L/a_v)$ where D/a_h is a known parameter; and
- **4th quadrant**: $CV_R = f(\alpha^{1/2})$ where CV_q is a known parameter.

While Figure 3-16 contains Figure 3-2(a) (variance reduction chart for single shafts) in the 3rd quadrant and, as a consequence, is limited to the design of single shaft foundations, substitution of the other multiple shaft configurations (double or quadruple) into the 3rd quadrant of Figure 7-4 results in respective quadrant design charts for triple or quadruple shafts. This type of quadrant chart is, thus, directly applicable to single and multiple shaft foundations within a single layer and neglecting end bearing with the only restriction that Equation 3-8 must be applied in the transition from the 3rd to the 4th quadrant in the presence of nested variogram structures

($n_v > 1$). Also, it should be noted that the LRFD Φ values obtained for multiple shaft foundations correspond to prescribed probabilities of failure for the whole pier (as opposed to individual piles, separately).

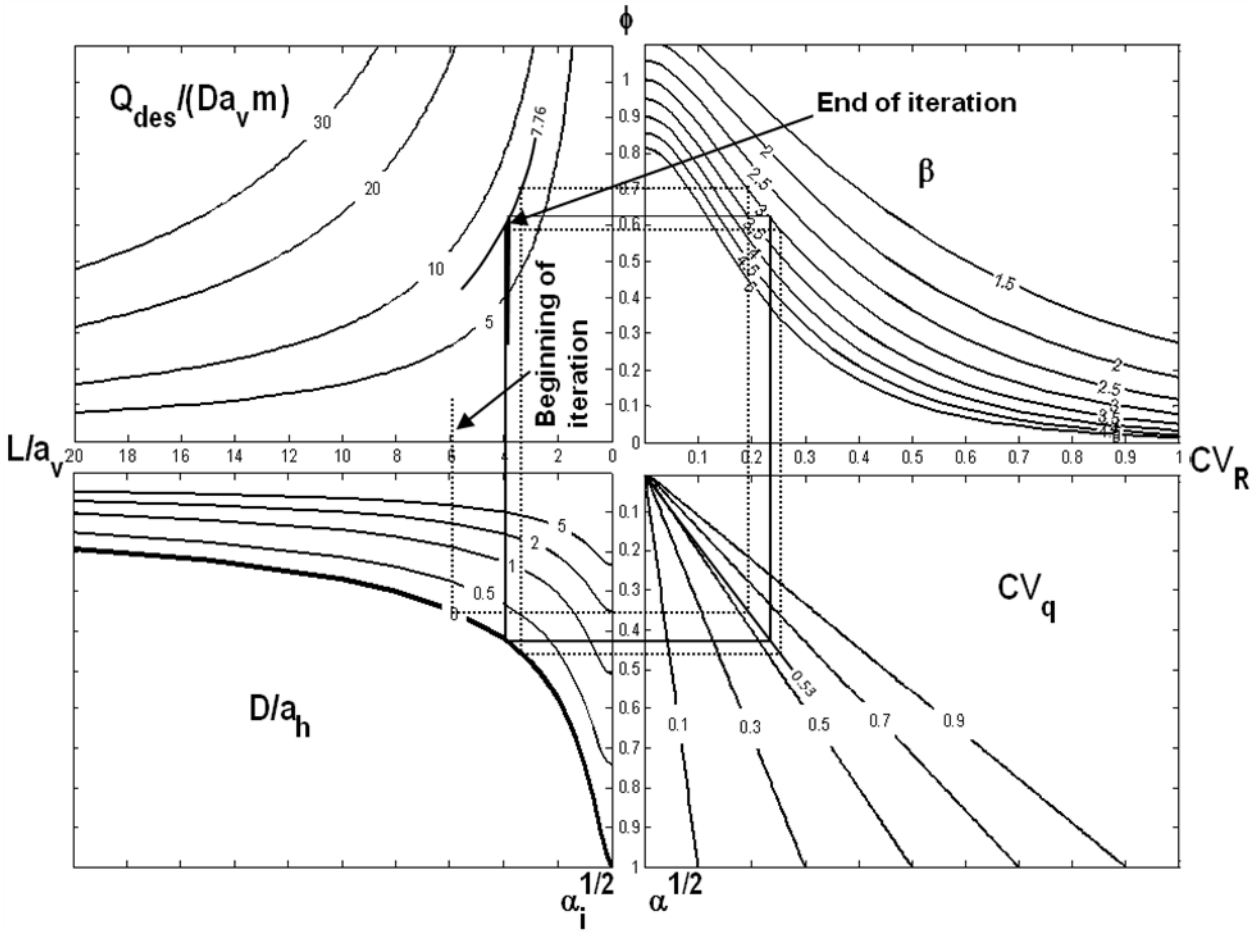

Figure 7-4. Dimensionless quadrant chart for single shaft design by graphical iteration.

Figure 7-4 illustrates the influence of each parameter involved on final Φ values. An increase in CV_q (larger variability in local strength) or β (lower probability of failure) leads to a reduction in Φ. An increase in Q_{des}/m (e.g., weaker rock → decrease in m) requires larger shaft dimensions, causing a higher degree of spatial averaging, and thus variance reduction, which increases Φ. The same is true for a decrease in a_v, as well as for a reduced D, which implies larger L to achieve the required resistance and, again, a larger degree of variance reduction (less

uncertainty in resistance; especially when spatial averaging in the horizontal direction is neglected). The third quadrant shows how $D/a_h = 0$, in fact, is the most conservative assumption for unknown a_h, since it leads to a minimum value of Φ for all L/a_v. Finally, it should be evident from Figure 7-4, **there does not exist a specific Φ** for a given site and rock strength (CV_q). Chapter 3 discusses the way Figure 7-4 may be used to handle layers, the inclusion of end bearing, as well as, multiple shaft designs.

The development of the variance reduction $\alpha^{1/2}$ given in Figure 7-3 for the estimate of CV_R, assumed that sufficient data were available to completely define the covariance function (C(h)) in both the vertical and horizontal direction. Chapter 4 addresses the issue of boring data at large lateral distances, as well as the possibility of having limited data. Specifically, for large spacing it was shown that the solution for $D/a_h = 0$ was conservative (solid line Figure 7-3), and the uncertainty associated with a few borings may be represented as Equation 4-1 which is shown as the dashed lines in Figure 4-1 as also displayed in Figure 7-5.

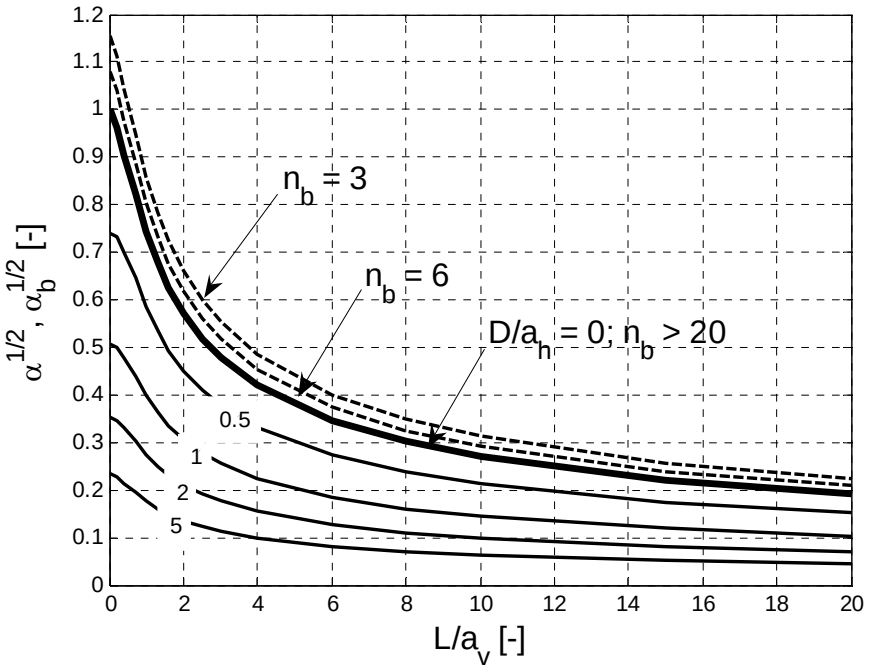

Figure 7-5. Modification of Figure 3-2 (Figure 7-3) to include number of borings.

Again, the dimensionless quadrant design chart given in Figure 7-4 (Figure 3-16) may be used with the third quadrant figure (bottom left) replaced with Figure 7-5. Evident from Figure 7-5, there is significant improvement between 3 and 20 borings at the site, but little improvement beyond that number. An example investigating the influence of number of borings (e.g., 6) is given in Chapter 4.

Finally, in the case of borings within the footprint of the pier/shafts (e.g., non redundant), which are still not close enough to one another to establish the horizontal correlation length (a_h) but are still at a sufficient proximity to allow for some variance reduction between the boring and the wall of the shaft, was presented in Figure 5-1. Interesting is the comparison of Figure 5-1 and Figure 4-1, which is given in Figure 5-4 and shown here in Figure 7-6. The reduction in the coefficient of variation in shaft resistance CV_R (= $\alpha^{1/2}$ CV_q) using borings within the footprint

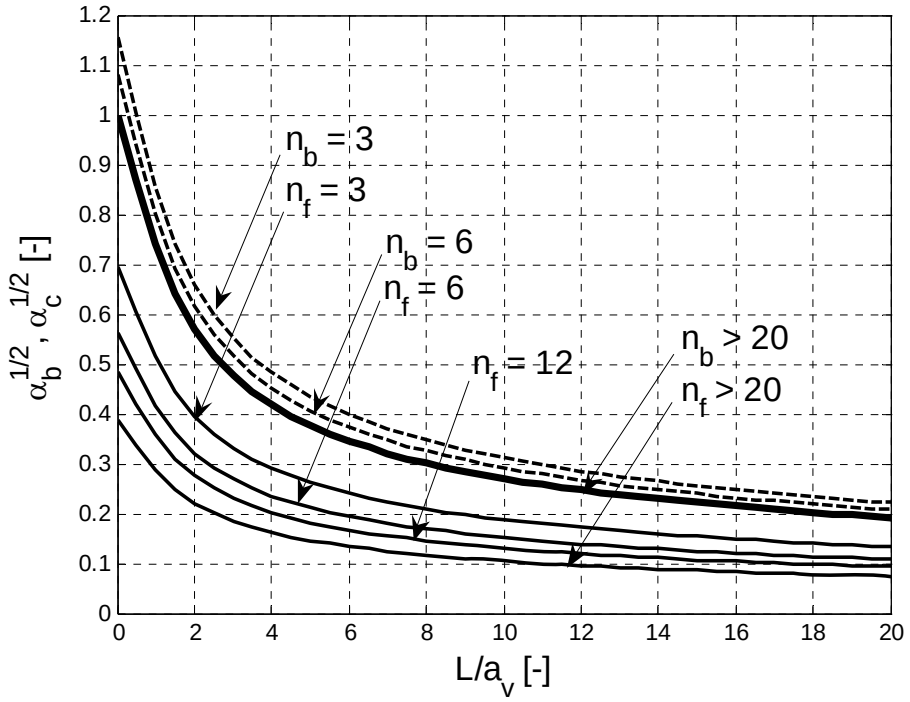

Figure 7-6. Comparison of CV_q reduction for borings in zone $\alpha_b^{1/2}$ versus within footprint $\alpha_c^{1/2}$ of design shaft.

($\alpha_c^{1/2}$) versus just within the zone ($\alpha_b^{1/2}$), is quite large. Increasing randomly the number of borings (n_b) does not have the same impact as increasing the number of borings within the footprints (n_f). Again, Figure 7-6 may readily replace the third quadrant chart in Figure 7-4 and be used for shaft design. Chapter 5 concludes with a nice example demonstrating the process.

7.3 Use of Both Load Test Data and Borehole Data to Estimate Shaft Resistance

For the work presented in Chapters 3 through 5, it was assumed that the ratio between the measured shaft resistance (e.g., skin and tip) and the borehole's estimate of resistance, i.e., bias (λ_R), was a known proportionality constant (e.g., AASHTO's $\lambda_R = 1.06$). However, since it is current practice to perform a few field load tests on a site (e.g., non redundant piles and shafts), it was decided to assess the variance of the design method σ^2_ε (referred to as random residual) in conjunction with the borehole predicted resistance variance (σ^2_B) to assess the expected design shaft resistance variance and associated CV_R.

The process involves obtaining borehole strength/modulus data within the footprint of the load tests (Figure 6-1) and performing a least square fit between the estimated shaft resistances from segments within the borehole (q_{Bi}) to the same segments obtained from the load test (q_{Li}, Figure 6-2 shown herein as Figure 7-7). The regression line was defined by the Equation 6-1 as

$$q_{Li} = a + bq_{Bi} + \varepsilon \tag{7-5}$$

where a and b are the intercept and slope of the regression line, respectively, and ε is a random residual of mean zero and minimized variance σ^2_ε. Variables a and b may be interpreted as parameters accounting for systematic prediction bias (e.g., consistent over- or under-estimation) and a larger degree of spatial averaging over the shaft intervals. Variable ε, in turn, represents

the **random prediction error** which includes spatial variability between borehole and shaft surface as well as random measurements errors, irregularities in test shaft surface, etc.

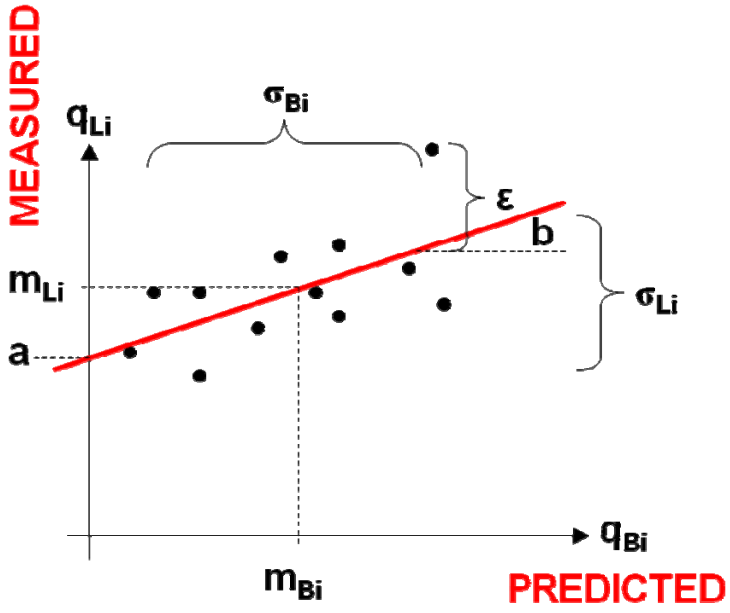

Figure 7-7. Data points of measured versus predicted strengths with linear regression line (red) and linear regression parameters.

Subsequently, Chapter 6 upscales the regression equation from intervals along the shaft to the whole shaft to arrive at the coefficient of variation of the complete shaft (i.e., Equation 6-9) as

$$CV_R = \frac{\sigma^*_L}{m^*_L} = \frac{\sqrt{b^2\sigma^{*2}_B + \alpha_0\sigma^2_\varepsilon}}{a + bm^*_B} \tag{7-6}$$

where m^*_B represents the predicted mean borehole strength over a depth L; σ^{*2}_B is the prediction uncertainty about m^*_B; and α_0 is the dark solid line found in Figures 7-3, 7-5, and 7-6. As discussed in Chapter 6, the variance of the borehole prediction, i.e., σ^{*2}_B depends on whether borehole data are available in the foundation footprint or not. For instance, in the case of borings not in the footprint of the shaft, Figure 4-1 (shown as Figure 7-5) may be used to assess $\alpha^{1/2}$

when multiplied by the rock strength variance (σ^2) gives σ^{*2}_B. In the case when borehole data are available in the footprint, $\sigma^{*2}_B = 0$ as borehole strength used for prediction is directly observed. The variance of the random residual (σ^2_ε) is given by Equation 6-4, and is related to the variance of the load test resistances and the correlation coefficient (r) from the least square fit of the data. Subsequently, the classic LRFD design equation $Q_{des} = \Phi R_n$ was reformulated as $Q_{des} = \Phi_u m^*_L A_s$ (A_s being the lateral shaft surface area) with the bias correction now being contained in m^*_L and Φ_u defined as Φ from AASHTO's FOSM equation with CV_R from Equation 7-6 and $\lambda_R = 1$. The design unit side friction is subsequently defined as $f_{des} = \Phi_u m^*_L$. Chapter 6 considers a real case (Jewfish Creek) which had two full-scale load tests and shows the improvements to the design resistance (Q_{des}) under different assumptions of borings locations. Finally, it should be noted that the combined use of load testing and boring data is quite an improvement over current AAHSTO practice of a fixed LRFD Φ based on a fixed number of load tests with rock coefficient of variation (CV_q).

7.4 Summary of Case Studies

For all the design scenarios discussed, case studies were presented based on data collected at three different sites (17^{th} Street, Fuller Warren and Jewfish Creek). Table 7-1 contains a summary of respective results in terms of resistance factors Φ and design shaft lengths L. However, as pointed out earlier, Φ has limited practical meaning since it is not a constant. Specifically, it is a function of the shaft's physical dimensions (length and diameter), as well as the geostatistical characteristics (CV and covariance, i.e., a_v, and a_h) of the soil/rock, the applied loads, and the target reliability β (equal to 3 in all of this work) of the foundation. This is illustrated, for example, by lines 7 and 8 in Table 7-1, where a 6% increase in Φ goes along with a 25% reduction in L, or even more so by lines 10 and 11 where a 5% increase in Φ is associated

with a 33% increase in L. For a given shaft length L, however (diameter D = 4 ft everywhere in Table 7-1), lines 1 and 2 show that separation into subzones and detrending of non-stationary data leads to increased Φ and, hence, increased Q_{des}. In the same way, lines 3 through 6 demonstrate the non-conservative effects of including a nugget variance or of not including a random areal trend in the variogram (increasing Φ and Q_{des}), as well as the conservative effect of the line shaft approximation for unknown horizontal correlation lengths a_h. Lines 7, 9, and 10 show how for a situation of equal Q_{des} and β, the shaft's design length L increases from 20 ft to 21 ft due to limited number of borings, and how L decreases to 15 ft (for equal mean strength m = 16.1 tsf), if data is available in the production shaft footprint. Lines 12 through 15 illustrate how Φ and, hence Q_{des}, behave under the design scenario of Chapter 6, inclusion of load testing. Performing load tests at a site with collocated core sample borings to establish a site specific bias relationship generally increases Φ (Q_{des}) for given shaft dimensions versus no load testing and assuming conservative bias correction coefficients. It is also seen that additional collection of core sample data in the footprint of production shafts may increase Φ (Q_{des}) substantially (here 57% with load testing). In the Jewfish Creek example, however, it turns out to be more favorable to not perform load testing and have data in the footprint of production shafts (Φ = 0.68) than performing load tests and not have borings in the footprint of production shafts (Φ = 0.47). Even though the latter is a reasonable result, it depends on site specific parameters, as well as, choice of the worst case regression parameters. Finally, note that it is not meaningful to directly compare Φ values of lines 1 through 11 to those of lines 12 through 15, since in the former case Φ contains the bias correction (resistance bias factor λ_R = 1.06 everywhere), while in the latter case bias correction (by the regression coefficients a and b) is not contained in Φ.

It is emphasized once more that Table 7-1 is a mere summary of design results from the case studies performed in this work and, as such, should not be used for drawing general conclusions about other sites or portions of sites not investigated here.

Table 7-1. Summary of Design Results for Case Studies Presented

Site	Scenario	Prescribed parameter	Φ [-]	L [ft]	Comments	Line #
Fuller Warren	Exhaustive data (Chapter 3)	L = 25 ft	0.80	25	Separate layers + detrended	1
			0.55		All data w/o treatment	2
17th Street			0.74		No nugget + a_h known	3
			0.80		40 % nugget + a_h known	4
			0.69		No nugget + a_h unknown	5
			0.51		No nugget + a_h unknown + 20 % random areal trend	6
		Q_{des} = 2500 t	0.62	20	No end bearing	7
			0.66	15	With end bearing	8
	Limited data (Chapter 4)		0.60	21	Data from 6 borings	9
	Data in footprint (Chapter 5)		0.78	15	m = 16.1 tsf	10
			0.82	20	m = 11.8 tsf	11
Jewfish Creek	No data in footprint (Chapter 6)	L = 30 ft	0.47	30	With load test data at site	12
			0.32		No load test data at site	13
	Data in footprint (Chapter 6)		0.74		With load test data at site	14
			0.68		No load test data at site	15

7.5 Recommendations

The work outlined in this report represents quite a departure from current practice, i.e., a fixed LRFD Φ. However, the proposed design has been developed from sound geostatistical theory which accounts for spatial correlation, i.e., covariance function, as well as upscaling from a simple borehole to a full-size shaft or multiple pile/shaft layouts. Unfortunately, even though the work investigated three sites (17th Street, Fuller Warren, and Jewfish Creek Bridges), it is

recommended that other sites be investigated, especially the inclusion of load testing and the evaluation of the random residual variance σ^2_{ε}. In addition, since geostatistics is relatively unknown to practicing geotechnical engineers, it is proposed that the FDOT develop a short course or set of tutorials on the topic (e.g., Chapter 2, scatterplots, variograms, covariance, etc.).

REFERENCES

Deutsch, C. V. (2002). *Geostatistical Reservoir Modeling*. Oxford University Press, New York, NY.

Deutsch, C. V., and Journel, A. G. (1992). *GSLIB – Geostatistical Software Library and User's Guide*. Oxford University Press, New York, NY.

Elkateb, T., Chalaturnyk, R., and Robertson, P. K. (2003). "An Overview of Soil Heterogeneity: Quantification and Implications on Geotechnical Field Problems." *Canadian Geotechnical Journal*, Vol. 40, pp. 1-15.

Fenton, G.A., and Griffiths, D.V. (2005). "Three-Dimensional Probabilistic Foundation Settlement." *Journal of Geotechnical Engineering*, Vol. 131, No. 2, pp. 232-239.

Goovaerts, P. (1997). *Geostatistics for Natural Resources Evaluation*. Oxford University Press, New York, NY.

Isaaks, E. H., and Srivastava, R. M. (1989). *An Introduction to Applied Geostatistics*. Oxford University Press, New York, NY.

Journel, A. G., and Huijbregts, C. J. (1978). *Mining Geostatistics*. Blackburn Press, Caldwell, NJ.

Kitanidis, P. K. (1997). *Introduction to Geostatistics: Applications to Hydrogeology*. Cambridge University Press, Cambridge, United Kingdom.

Menard, L., Baguelin, F., and Shields, D. (1972). *The Pressuremeter and Foundation Engineering,* Trans Tech Publications, Clausthal, Germany.

O'Neill, M. W., Townsend, F. C., Hassan, K. H., Buller, A., and Chan, P. S. (1996). "Load Transfer for Drilled Shafts in Intermediate Geomaterials," *Report No. FHWA-RD-95-172*, Federal Highway Administration, Washington, D.C., January.

Poulos, H. G., and Davis, E. H. (1972). *Pile Foundation Analysis and Design*. John Wiley and Sons, New York, NY.

Ueshita, K., and Meyerhof, G. G. (1967). "Deflection of Multilayer Soil System." *Journal of Soil Mechanics and Foundations Division, ASCE*, Vol. 93, No. SM5, pp. 257-282.

APPENDIX A
LOCAL STRENGTH DATA

A.1 17th Street Bridge

x, y are horizontal coordinates and z is elevation from bottom (in ft)
$q = 1/2 \times (q_u q_t)^{1/2} \times$ recovery (in tsf)

Boring 1			
x	y	z	q
9	24	40	11.95
9	24	39	16.15
9	24	38	9.95
9	24	37	7.6
9	24	36	25.05
9	24	35.5	20
9	24	35	9.25
9	24	34	7.7
9	24	33	13.01
9	24	32	10.98
9	24	31	14.49
9	24	30	16.7
9	24	27	16.36
9	24	26	6.72
9	24	25	12.63
9	24	24	7.79
9	24	23	6.96
9	24	22	4.96
9	24	20	6.05

Boring 2			
x	y	z	q
9	7	40	18.7
9	7	39	30.8
9	7	38	9.75
9	7	37	17.7
9	7	36	10.4
9	7	35	31.7
9	7	34.5	8.58
9	7	31	10.64
9	7	30	13.62
9	7	27	26.8
9	7	26	14.05
9	7	25	21.52
9	7	24	7.88
9	7	23	5.1
9	7	20	4.11
9	7	19	17.36
9	7	18	14
9	7	17	14.08
9	7	16	14.92
9	7	15.5	18.64
9	7	15	19.16
9	7	14	19.87
9	7	12	23.83
9	7	7	15

Boring 3			
x	y	z	q
9	0	40	14.2
9	0	39	17.45
9	0	38	25.95
9	0	37.5	13.05
9	0	37	16.45
9	0	36	9.3
9	0	35.5	20.9
9	0	34	11.38
9	0	32	7.96
9	0	31.5	19.44
9	0	30.5	11.7
9	0	30	12.2
9	0	29.5	17.68
9	0	29	12.32
9	0	28	6.44
9	0	27	7.56
9	0	26	7.28
9	0	25	5.52
9	0	23	4.66
9	0	22	3.88
9	0	21	4.39
9	0	20	13.09
9	0	19	24.6
9	0	17	10.36
9	0	15	9
9	0	14	11.74
9	0	10	10.63

Boring 4			
x	y	z	q
0	19	40	27.63
0	19	38	3.95
0	19	37	14.2
0	19	35	9.52
0	19	34	12.93
0	19	32	15.16
0	19	31	11.74
0	19	30	4.64
0	19	29	6.21
0	19	28	16.79
0	19	27	30.35
0	19	26	34.17
0	19	25	26.1
0	19	24	18.1
0	19	23	11.75
0	19	22	4.89
0	19	20	17.67
0	19	19	22.92
0	19	16	21.5
0	19	15	22.08
0	19	5	14.72

Boring 5			
x	y	z	q
0	10.5	40	13.52
0	10.5	39	14.95
0	10.5	38	21.36
0	10.5	37	20.97
0	10.5	36.5	44.54
0	10.5	35	26.71
0	10.5	33	16.93
0	10.5	31	15.16
0	10.5	30	20.49
0	10.5	29.5	34.45
0	10.5	28.5	35.32
0	10.5	27	18.18
0	10.5	25	17.27
0	10.5	24.5	19.21
0	10.5	23.5	9.28
0	10.5	23	12.55
0	10.5	22	3.74
0	10.5	20	4.62
0	10.5	19	22.76
0	10.5	17	26.04
0	10.5	16	29.84
0	10.5	12	19.04
0	10.5	10	18.33

Boring 6			
x	y	z	q
18	10.5	40	17.91
18	10.5	35.5	10.17
18	10.5	34	24.18
18	10.5	33	42.73
18	10.5	32	38.6
18	10.5	31	21.81
18	10.5	30	23.11
18	10.5	29	7.62
18	10.5	28	8.84
18	10.5	27	6.17
18	10.5	25	7.27
18	10.5	20	16.23
18	10.5	19	30.38
18	10.5	18	31.83
18	10.5	17	16.97
18	10.5	15	27.18
18	10.5	14	31.05
18	10.5	12	24.59
18	10.5	11	19.97
18	10.5	9	16
18	10.5	5	12.64
18	10.5	0	4.82

A.2 Fuller Warren Bridge

x, y are horizontal coordinates and z is elevation from bottom (in ft)
$q = 1/2 \times (q_u q_t)^{1/2}$ x recovery (in tsf)

Boring 1			
x	y	z	q
35	0	26	7.3
35	0	24	4.8
35	0	21	16.9
35	0	20	9.7
35	0	19	13.5
35	0	18	16.6
35	0	17	21.6
35	0	11	1.9
35	0	10	2.1
35	0	9	3.5
35	0	8	2.1
35	0	6	1.2
35	0	5	1.0
35	0	4	0.4
35	0	3	0.8
35	0	1	0.3

Boring 2			
x	y	z	q
35	40	26	6.5
35	40	25	8.9
35	40	21	4.8
35	40	20	10.0
35	40	19	11.6
35	40	18	13.8
35	40	17	5.0
35	40	15	1.5
35	40	14	2.5
35	40	13	1.6
35	40	11	2.5
35	40	10	3.2
35	40	9	2.7
35	40	7	1.3
35	40	6	1.5
35	40	5	1.9
35	40	4	1.8
35	40	3	0.9
35	40	2	0.6
35	40	1	0.7

Boring 3			
x	y	z	q
0	40	26	4.1
0	40	25	1.0
0	40	24	1.2
0	40	20	11.7
0	40	19	8.0
0	40	18	6.1
0	40	17	12.8
0	40	16	1.8
0	40	15.5	3.6
0	40	15	4.2
0	40	14	2.0
0	40	13	1.5
0	40	12	2.7
0	40	11	2.6
0	40	10.5	2.4
0	40	10	2.6
0	40	5	1.4
0	40	4	1.5
0	40	3	1.4
0	40	2	1.2
0	40	1	0.7

APPENDIX B
DERIVATION OF VARIANCE REDUCTION FACTOR
FOR $D/a_h = 0$ (LINE SHAFT)

In the appendix of Elkateb et al. (2003), a variance reduction factor Γ_T^2 (here α) is derived for a spherical correlation structure of range a and for averaging over a length T. By increasing T beyond a, their Γ_T^2 in equation A4 grows towards infinity, which is contrary to the requirement that Γ_T^2 approaches zero for averaging over an infinite multiple of correlation ranges. The variance reduction factor in Elkateb et al. (2003) is found to be correct only for the range $0 \le T \le a$, which is due to an error in their Equation A2 for the correlation function. Deriving the variance reduction factor based on Elkateb et al. (2003) with the correct Equation 3.6 from here and using α for Γ_T^2, L for T and a_v for a as in the present context leads to

$$\alpha = \frac{2}{L}\int_0^L \left(1-\frac{h}{L}\right) C'(h/a_v)\,dh \tag{B-1}$$

For $0 \le L \le a_v$ this gives

$$\alpha = \frac{2}{L}\int_0^L \left(1-\frac{h}{L}\right)\left[1-1.5\frac{h}{a_v}+0.5\left(\frac{h}{a_v}\right)^3\right]dh \tag{B-2}$$

and

$$\alpha = 1-\frac{L}{2a_v}+\frac{L^3}{20a_v^3} \quad \text{for} \quad 0 \le \frac{L}{a_v} \le 1 \tag{B-3}$$

as in Elkateb et al. (2003). However, for $L > a_v$ the integral in Equation B-1 needs to be split into one from 0 to a_v and another one from a_v to L according to Equation 3-6. The integrant of the latter is zero leading to

$$\alpha = \frac{2}{L}\int_0^{a_v} \left(1-\frac{h}{L}\right)\left[1-1.5\frac{h}{a_v}+0.5\left(\frac{h}{a_v}\right)^3\right]dh \tag{B-4}$$

and

$$\alpha = \frac{3a_v}{4L} - \frac{a_v^2}{5L^2} \quad \text{for} \quad \frac{L}{a_v} \geq 1 \tag{B-5}$$

Equations B-3 and B-5 can be seen to agree with the numerically obtained results for $D/a_h = 0$ (averaging over a vertical line of length L) in Figure 3-2(a).

DERIVATION OF EQUATION 6-8

By subtracting Equation 6-7 from Equation 6-6, an equation for the prediction error Δq_L is obtained as

$$\Delta q_L = q_L - m^*_L = b\Delta q_B + \sqrt{\alpha_0}\varepsilon \tag{B-6}$$

where $\Delta q_B = q_B - m^*_B$ is used as a random residual about the predictor. Squaring Equation B-6 gives

$$\Delta q_L^2 = b^2\Delta q_B^2 + \alpha_0\varepsilon^2 + 2b\sqrt{\alpha_0}\Delta q_B\varepsilon \tag{B-7}$$

Taking the expectation of the squared residual Δq^2_L is known to give the variance about m^*_L as

$$\sigma^{*2}_L = E[\Delta q_L^2] = b^2E[\Delta q_B^2] + \alpha_0 E[\varepsilon^2] + 2b\sqrt{\alpha_0}E[\Delta q_B\varepsilon] = b^2\sigma^{*2}_B + \alpha_0\sigma_\varepsilon^2 \tag{B-8}$$

which is identical to Equation 6-8. E[ ] hereby denotes the expectation (i.e., ensemble mean) operator knowing that $E[\Delta q^2_B] = \sigma^{*2}_B$ (variance of random residual about predictor), $E[\varepsilon^2] = \sigma^2_\varepsilon$ (variance of random residual about regression line) and $E[\Delta q_B\varepsilon] = Cov[\Delta q_B,\varepsilon] = 0$ (covariance between predictor and regression residuals), where the latter is based on the standard assumption of independence between predictor and regression residuals.

APPENDIX C
LOCAL STRENGTH DATA FROM JEWFISH CREEK (PIERS 1 – 38)

z is depth (in ft); horizontal coordinates not available
$q = 1/2 \times (q_u q_t)^{1/2}$ (in ksf)

Pier	z	q
2	-15.7	11.3
3	-35.8	17.4
3	-26.5	22.7
3	-11.8	15.6
4	-24.8	19.7
4	-19.8	12.5
4	-14.8	19.4
4	-10.8	17.9
5	-31.6	17.4
5	-11.6	19.3
5	-7.1	14.4
6	-26.9	13.8
6	-21.9	15.0
6	-16.9	9.4
6	-11.9	26.7
6	-8.1	20.0
7	-26.9	26.0
7	-21.9	11.3
7	-11.9	13.6
7	-7.4	15.7
8	-42.1	10.4
8	-37.1	12.1
8	-32.1	14.6
8	-27.1	14.7
8	-12.1	14.1
8	-7.6	15.6
9	-41.8	10.7
9	-36.8	24.2
9	-26.8	27.4
9	-21.8	8.7
9	-16.8	7.8
9	-11.8	23.1
9	-6.8	21.4
10	-36.6	11.5
10	-31.6	11.1
10	-26.6	19.4
10	-21.6	7.7

Pier	z	q
10	-16.6	11.9
10	-11.6	14.3
10	-7.1	7.4
12	-31.7	13.3
12	-26.7	22.0
12	-21.7	10.5
12	-16.7	10.0
12	-11.7	17.8
12	-6.7	14.2
13	-41.6	12.9
13	-36.6	17.9
13	-31.6	6.9
13	-26.6	13.6
13	-16.6	6.6
13	-11.6	14.1
13	-7.1	10.0
14	-26.6	11.6
14	-16.6	14.2
14	-11.6	15.4
14	-7.1	14.1
15	-61.9	25.0
15	-56.9	17.7
15	-31.9	30.0
15	-21.9	8.4
16	-27.4	16.6
16	-22.4	26.0
16	-17.4	23.5
16	-12.4	35.8
16	-7.9	27.1
17	-41.7	20.9
17	-26.7	11.0
17	-21.7	21.0
17	-16.7	27.2
17	-11.7	13.1
18	-26.7	14.5
18	-16.7	10.0
18	-11.7	14.6

Pier	z	q
18	-7.2	21.2
19	-31.8	10.1
19	-26.8	11.5
19	-21.8	18.4
19	-16.8	10.7
19	-11.8	16.9
19	-7.3	13.4
20	-9.5	11.1
21	-28.2	17.1
21	-8.7	12.9
22	-29.7	10.7
22	-10.2	17.4
23	-27.2	16.3
23	-15.2	25.3
24	-55.7	8.8
24	-10.7	27.2
25	-30.5	31.7
25	-11.0	23.2
26	-10.0	11.3
28	-30.6	24.1
28	-11.1	18.5
29	-31.1	20.3
29	-11.6	30.6
30	-11.8	24.8
31	-31.4	14.7
31	-18.4	25.7
32	-37.3	23.5
32	-11.8	19.9
33	-51.1	13.2
33	-25.1	36.8
33	-12.6	14.5
34	-26.8	52.1
34	-13.8	14.0
35	-31.2	68.0
35	-11.7	12.1
36	-16.8	15.0
38	-21.8	63.7